

CHARACTERIZATION OF CHEMICAL INTERACTIONS DURING CHEMICAL
MECHANICAL POLISHING (CMP) OF COPPER

By

SEUNG-MAHN LEE

A DISSERTATION PRESENTED TO THE GRADUATE SCHOOL
OF THE UNIVERSITY OF FLORIDA IN PARTIAL FULFILLMENT
OF THE REQUIREMENTS FOR THE DEGREE OF
DOCTOR OF PHILOSOPHY

UNIVERSITY OF FLORIDA

2003

To my parents, my wife, and my daughters, for their love and support.

ACKNOWLEDGMENTS

I would like to express my deepest appreciation to Dr. Rajiv K. Singh, my advisor, for his professional guidance, support, and encouragement. The open environment that he has provided over the years that I have worked with him has made for a very dynamic and rewarding graduate school experience. I would also like to thank Dr. Brij M. Moudgil, Dr. Stephen J. Pearton, Dr. Cammy R. Abernethy, and Dr. Dinesh O. Shah for kindly participating on my dissertation committee.

I would like to thank all the friends and coworkers who made graduate school such a memorable time. Dong-Gu, Kyu-Gong, Uday, Zhan, Mike, Wonseop, Sang-Yup, Jaeyoung, Joodong, Won-Seok, Hano, Sang-Hyun, Hyuk-Soo, Jeremiah, Karthik, Vishal, Nabil, Josh, Srinu, Chad, Joo-Han, Jin-Ki, Chad, Kyo-Se, Seemant, and others provided social perspective that is always necessary in life.

In addition, I truly thank my friends, who are in Korea, Kun-Chang, Hoo-Sung, and Nam-Jun for their encouragement and friendship thru the years.

I would like to acknowledge the financial support of the Particle Engineering Research Center (PERC) at the University of Florida, the National Science Foundation (NSF grant #EEC-94-02989), and the Industrial Partners of the PERC for support of this research.

I would like to thank Margaret and Greg for their kind support. I really appreciate their help for everything they did for me. I would also like to thank support staffs, Gary,

Gill, John, and Sophie in PERC for their dedication and technical support. I would like to thank Lance Khun for his tremendous help in the nanoindentation.

I would like to express my gratitude to my parents, Suk-Joo Lee and So-Ya Kim, my brother, Yoon-Ho, sister, Hee-Jung, parents-in-law, Sang-Hak Nam and Jung-Soon Lee, brothers-in-law, and the rest of my family for the love and support they have provided over the many years of my education.

Finally, without my wife, Jung-Lyun Nam, I would not have been able to persevere and sustain the long and hard years of study away from family and friends. My two daughters, Bora and Gah-Eun, and my wife have been and remain a constant source of strength, joy, and support for me through all these years. I would like to express my deepest gratitude to them.

TABLE OF CONTENTS

	<u>Page</u>
ACKNOWLEDGMENTS	iii
LIST OF TABLES	viii
LIST OF FIGURES	ix
ABSTRACT	xv
 CHAPTER	
1. INTRODUCTION	1
Objectives	4
Dissertation Outline	5
2. LITERATURE SURVEY	6
Interconnects on Circuit Performance	6
RC Time Delay	8
Power Consumption	14
Circuit Reliability	14
Multilevel Interconnection	15
Copper Metallization	17
Advantages of Copper Metallization	17
Lower resistivity	19
Electromigration resistance	19
Lower manufacturing cost	22
Challenge in Integrating Copper	26
Lack of volatile copper compound	26
Copper diffusion into dielectric layer	28
Low-k Materials	29
CMP	31
Planarity	33
Planarization Mechanism in Metal CMP Process	37
CMP Removal Models	43

3.	POTENTIODYNAMIC AND XPS STUDY OF THE CHEMICALLY MODIFIED SURFACE LAYER.....	48
	Introduction	48
	Experimental	50
	Sample Preparation	50
	Solutions of Various Chemical Additive Mixtures	52
	Electrochemistry	54
	X-ray photoelectron Spectroscopy	54
	Result and Discussion	55
	Electrochemical Behavior of Copper.....	55
	Chemical Composition of the Chemically Modified Surface Layer	66
	Summary	73
4.	THE KINETICS OF THE FORMATION OF THE CHEMICALLY MODIFIED SURFACE LAYER DURING COPPER CMP WITH <i>IN SITU</i> ELECTROCHEMISTRY	75
	Introduction	75
	Experimental	80
	Chronoamperometry	80
	Solution Chemistry	82
	Characterization of the Layer	85
	Results and Discussion.....	86
	Summary	113
5.	MECHANICAL PROPERTIES OF THE CHEMICALLY MODIFIED SURFACE LAYER ON THE COPPER SURFACE.....	115
	Introduction	115
	Experimental	116
	Nanoindentation	116
	Result	122
	pH Effect	124
	The Effect of the Concentration of an Oxidizer	131
	The Effect of the Concentration of BTA	136
	The Effect of the Concentration of Citric Acid	139
	Summary	142
6.	INTERPRETATION OF COPPER CMP PERFORMANCE BASED ON NANO AND MICRO SCALE INTERACTIONS	146
	Introduction	146
	Experimental	147
	Results and Discussion.....	147
	CMP Removal Model based on the Nano- and Micro-Scale Interactions....	147
	The contact area between pad and wafer (A_c)	148

The number of particles participating in the material removal (N_a) ..	153
Indentation depth of single particle into the wafer surface (δ_p)	154
Determination of copper removal rate	161
Evaluation of the Model	164
Effect of Chemical Interaction on Copper CMP Performance	167
Summary	170
 7. CONCLUSION	 172
LIST OF REFERENCES	175
BIOGRAPHICAL SKETCH	182

LIST OF TABLES

<u>Table</u>	<u>page</u>
1-1. Correlation of system level variables, with micro and nanoscale interactions and the output parameters in CMP [Sin02].....	3
2-1. Target values for Microprocessor (MPU) interconnect technology according to ITRS 2002 update [ITR02].	7
2-2. Low resistivity materials for interconnect conductor materials [Mur93, Ste97]....	20
2-3. The most promising candidates for low-k ILD materials in interconnect [Chi99].	30
3-1. Comparison of the potentiodynamic parameters.	62
3-2. Reference XPS parameters for copper and copper compounds [Der92, Mou95]. ...	67
4-1. Comparison of corrosion rate.	89

LIST OF FIGURES

<u>Figure</u>	<u>page</u>
1-1. Schematic diagram to depict micro and nanoscale phenomena occurring during CMP [Lee02, Sin02].	2
2-1. Time delay caused by interconnection and gate at different device sizes [Mur96]. Interconnect delay is being dominant in total time delay as the device is shrinking.	9
2-2. Schematic of the closed-packed IC interconnect.	11
2-3. Capacitances associated with metal lines. Line-to-line capacitance becomes dominant due to the scaling of the device size [Den74].	12
2-4. The relative size change in central processing unit (CPU) from http://www.intel.com .	16
2-5. The example of the multilevel interconnect (MLI) by dual damascene process.	18
2-6. Manifestation of electromigration damage in aluminum films: (a) Hillock formation, (b) whisker bridging between two conductor lines, and (c) mass accumulation and depletion [Vai80].	21
2-7. Copper and aluminum failure rates due to the electromigration [Cun00].	23
2-8. Expected interconnect RC time delay with copper and low-k ($k = 2.0$) device as well as aluminum and silica device [Pet98].	24
2-9. The reduction of the number of metal levels with copper and low-k material to achieve the same performance [Sin98].	25
2-10. Schematic diagram of the dual damascene process and two step copper CMP process.	27
2-11. Schematic illustration of a typical CMP tool.	32
2-12. Degrees of Planarity; (a) Unplanarized, (b) Surface Smoothing, (c) Local Planarization and (d) Global Planarization [Ols93].	34
2-13. A cumulative increase in topography by multi-level interconnection without using a planarization method [Vie01].	36

2-14. An example of the potentiodynamic scans for tungsten with 0.5M H ₂ SO ₄ [Bie98].	38
2-15. Current recorded for one stroke during the tribological experiments for anodic applied potential (+2 V) in 0.5M H ₂ SO ₄ for a sphere motion cycle of 0.2 second [Bie00].	40
2-16. Wear track volume vs. applied potential for experiments conducted by rubbing an alumina ball at 5 Hz with 5N load against a fixed flat tungsten sample immersed in 0.5M H ₂ SO ₄ for 25 minutes [Bie00].	41
2-17. Anodic current vs. time transients for tungsten measured in 0.5M H ₂ SO ₄ at several potentials [Bie00].	42
3-1. A cross-sectional SEM picture of as-received wafer (a); pre-existed oxide layer on the as-received copper wafer observed by TEM (b); and surface layer thickness by dipping copper samples in three etching solutions, measured by ellipsometry (c).	51
3-2. Potential-pH diagram of copper-nitric acid/ hydrogen peroxide-water system.	53
3-3. The typical potentiodynamic curve with passivated layer on the metal surface.	56
3-4. The potentiodynamic curves of copper in 5% hydrogen peroxide at different pH.	58
3-5. The potentiodynamic curves of copper in various concentration of hydrogen peroxide at pH 7.	59
3-6. BTA concentration effect on the anodic electrochemical behavior of copper in 5% hydrogen peroxide at pH 7.	60
3-7. The potentiodynamic curves measured in citric acid based solutions (a) and citric effect on the anodic electrochemical behavior of copper in 5% hydrogen peroxide and 10 mM BTA at pH 7.	61
3-8. The XPS spectra of the as-received and pre-treated copper surface: (a) surface analysis, (b) Cu Auger LMM line, and (c) O1s line on the copper samples.	68
3-9. XPS analyses on copper samples dipped in 3 different solutions at pH 7: (a) 5% hydrogen peroxide only; (b) 5% hydrogen peroxide and 10mM BTA; and (c) 5% hydrogen peroxide and 100 mM citric acid.	69
3-10. The XPS analysis on a copper sample, dipped in 5% hydrogen peroxide and 100 mM citric acid at pH 7 for 1 minute, with different sputtering time.	72
4-1. Schematic of metal CMP removal mechanism.	77

4-2. The contact area between the pad and wafer was measured by theoretical approach [Yu93] and experimental approach [Bas02]. These two results showed approximately 10^{-4} times the nominal area of the wafer.....	79
4-3. The typical curve of chronoamperometry with the passivation process.	81
4-4. A schematic illustration of the electrochemical measurement setup.....	83
4-5. Equivalence between the oxidizer action and the applying an anodic potential [Bie00].	84
4-6. The transient electrochemical behavior of the copper surface during 50 seconds when exposed to four slurry conditions: (i) BTA only; (ii) 5 wt.% H_2O_2 ; (iii) 5 wt.% H_2O_2 and 10 mM BTA; and (iv) 5 wt.% H_2O_2 , 10 mM BTA, and 200 mM citric acid.....	87
4-7. The XPS analyses on a copper sample, dipped in 5% hydrogen peroxide and 10 mM BTA at pH 7 for 50 seconds, before and after surface sputtering for 2 minutes.....	91
4-8. Comparison of atomic weight % of several elements before and after surface sputtering on a copper sample, dipped in 5% hydrogen peroxide and 10 mM BTA at pH 7 for 50 seconds.	92
4-9. The electrochemical response of copper during 65 millisecond as a function of different chemicals used in the slurry at pH 8.	95
4-10. The effect of pH on the transient behavior of the copper in 5% H_2O_2 solution.	97
4-11. Normalized void concentration in Cu_2O layer on the samples dipped in 5% hydrogen peroxide at different pHs.	98
4-12. Surface roughness (RMS) of the copper samples dipped in 5% hydrogen peroxide at different pHs.	100
4-13. XRR measurements ((a), (b), and (c)) and simulations (d) of the cuprous oxide layer on the copper surfaces that were dipped in 5% hydrogen peroxide at different pH: (a) pH 6, (b) pH 7, and (c) pH 8.....	101
4-14. The effect of H_2O_2 concentration on the transient behavior of copper at pH 7.....	103
4-15. Normalized void concentration in Cu_2O layer on the samples dipped in 2%, 5%, and 10% hydrogen peroxide at pH 7.....	104
4-16. XRR measurements ((a), (b), and (c)) and simulations (d) of the cuprous oxide layer on the copper surfaces that were dipped in solutions with various concentrations of hydrogen peroxide at pH 7: (a) 2%, (b) 5%, and (c) 10%.....	105

4-17. The effect of BTA concentration of the transient behavior of copper in 5% H ₂ O ₂ solution at pH 7.....	107
4-18. XRR measurements ((a) and (b)) and simulations (c) of the chemically modified surface layer on the copper surfaces that were dipped in solution: (a) 5 wt% hydrogen peroxide at pH 7 and (b) 5 wt.% hydrogen peroxide and 10 mM BTA at pH 7.....	108
4-19. The concentration effect of citric acid of the transient behavior of copper in various solutions at pH 7.....	110
4-20. Normalized void concentration in Cu ₂ O layer on the samples dipped in 5% hydrogen peroxide and 10 mM BTA solutions with different concentrations of citric acid at pH 7.....	111
4-21. XRR measurements ((a), (b), and (c)) and simulations (d) of the chemically modified surface layer on the copper surfaces that were dipped in solution of 5 wt.% hydrogen peroxide, 10 mM BTA, and various concentration of citric acid at pH 7: (a) 0 mM, (b) 10 mM, and (c) 100 mM.	112
5-1. Typical indentation load-displacement plot as a result of indentation	119
5-2. (a) SEM picture of Cube corner diamond indenter (www.hysitron.com), (b) in-situ image (1 by 1 μ m) of indent on the copper sample dipped in 5% hydrogen peroxide at pH 7 for 1 minute with Cube corner indenter, and (c)schematic diagram of the experimental apparatus. The maximum load was 60 μ N.	120
5-3. Load-time sequence during the nanoindentation experiments.	121
5-4. The typical load-displacement curves performed on an amorphous quartz substrate (a) and, as a result, calculated hardness and Young's modulus presented.	123
5-5. Selective load-displacement behaviors of copper samples subjected on 5% hydrogen peroxide solution at different pHs: (a) pH 5, (b) pH 6, (c) pH 7, and (d) pH 8. Arrows indicates the discontinuity on the loading curve.	125
5-6. <i>In situ</i> image of a copper sample, dipped in 5% hydrogen peroxide at pH 7 for 1 min, using the nanoindentation.	126
5-7. The mechanical properties – Young's modulus and hardness – of copper samples, extracted from Figure 5-5 using equation (5.1) and (5.2) as a function of the contact depth and the pHs of 5% hydrogen peroxide dipping solution: (a) pH 5, (b) pH 6, (c) pH 7, and (d) pH8.	127
5-8. Schematic diagrams and SEM pictures of two different indentation behaviors due to the substrate effect: (a) soft films on hard substrates (pile-up) and (b) hard films on soft substrates (sink-in) [Tsu99-a, Tsu99-b].	129

5-9. The hardness and Young's modulus of CuO and Cu ₂ O as a function of pH.	130
5-10. Selective load-displacement behaviors of copper samples subjected on various concentrations of hydrogen peroxide solution at pH 7: (a) 2%, (b) 5%, and (c) 10%. Arrows indicates the discontinuity on the loading curve.	132
5-11. The mechanical properties – Young's modulus and hardness – of copper samples, extracted from Figure 5-10 using equation (5.1) and (5.2) as a function of the contact depth and concentration of hydrogen peroxide dipping solution: (a) 2%, (b) 5%, and (c) 10%.	133
5-12. The hardness and Young's modulus of CuO and Cu ₂ O as a function of the concentration of hydrogen peroxide in the solution.	134
5-13. Selective load-displacement behaviors of copper samples subjected on various concentrations of BTA at 5% hydrogen peroxide solution at pH 7: (a) 0 mM, (b) 5mM, (c) 10 mM, and (d) 20 mM. Arrows indicates the discontinuity on the loading curve.....	137
5-14. The mechanical properties – Young's modulus and hardness – of copper samples, extracted from Figure 5-13 using equation (5.1) and (5.2) as a function of the contact depth and concentration of BTA in dipping solutions: (a) 0 mM, (b) 5 mM, (c) 10 mM, and (d) 20 mM.	138
5-15. Hardness and Young's modulus of the chemically modified surface layer as a function of the concentration of BTA in 5% hydrogen peroxide solution at pH 7.....	140
5-16. Selective load-displacement behaviors of copper samples subjected in 5% hydrogen peroxide solution with various concentrations of citric acid at pH 7: (a) 0 mM, (b) 10 mM, and (c) 100 mM	141
5-17. The mechanical properties – Young's modulus and hardness – of copper samples, extracted from Figure 5-16 using equation (5.1) and (5.2) as a function of the contact depth and concentration of citric acid in dipping solutions: (a) 0 mM, (b) 10 mM, and (c) 100 mM.....	143
5-18. The maximum hardness and Young's modulus of the chemically modified surface layer as a function of the concentration of citric acid in 5% hydrogen peroxide and 10 mM BTA solution at pH 7.	144
6-1. Schematic of the wafer-pad-particle interaction: (a) the micro-contact system and (b) the cross-sectional area of indentation.	149
6-2. The normalized contact area between the pad and the wafer as a function of applied pressure, measured by FTIP/ATP [Qin03].....	151

6-3. The applied pressure dependence on the contact pressure between the pad and the wafer using equation (6.2).	152
6-4. The relation between the substrate effect factor e and yield stress mismatch σ_f / σ_s for four different indentation depths, $\delta/h = 0.25, 0.5, 0.75$, and 1 [Che01].....	157
6-5. The hardness of layer with the normalized indentation depth can be estimated using the substrate effect factor.	159
6-6. The indentation depths with the applied pressure and various particle sizes using equation (6.12)	160
6-7. The load requirement with or without the soft substrate effect.	162
6-8. Comparison between the removal rates of copper, shown by the model (a) and measured by the CMP experiments.	166
6-9. Comparison between the experimental removal rate and the theoretical removal rate using the CMP removal model based on the micro- and nano-scale interactions. (a), (c), (e), and (g) present the effect of chemical additives in the copper removal rate and (b), (d), (f), and (h) shows the theoretical values obtained using the model.	168

Abstract of Dissertation Presented to the Graduate School
of the University of Florida in Partial Fulfillment of the
Requirements for the Degree of Doctor of Philosophy

CHARACTERIZATION OF CHEMICAL INTERACTIONS DURING CHEMICAL
MECHANICAL POLISHING (CMP) OF COPPER

By

Seung-Mahn Lee

August, 2003

Chair: Rajiv K. Singh

Major Department: Materials Science and Engineering

Chemical mechanical polishing (CMP) has received much attention as an unique technique to provide a wafer level planarization in semiconductor manufacturing. However, despite the extensive use of CMP, it still remains one of the least understood areas in semiconductor processing. The lack of the fundamental understanding is a significant barrier to further advancements in CMP technology.

One critical aspect of metal CMP is the formation of a thin surface layer on the metal surface. The formation and removal of this layer controls all the aspects of the CMP process, including removal rate, surface finish, etc. In this dissertation, we focus on the characterization of the formation and removal of the thin surface layer on the copper surface. The formation dynamics was investigated using static and dynamic electrochemical techniques, including potentiodynamic scans and chronoamperometry. The results were validated using XPS measurements. The mechanical properties of the surface layer were investigated using nanoindentation measurements.

The electrochemical investigation showed that the thickness of the surface layer is controlled by the chemicals such as an oxidizer (hydrogen peroxide), a corrosion inhibitor (benzotriazole), a complexing agent (citric acid), and their concentrations. The dynamic electrochemical measurements indicated that the initial layer formation kinetics is unaffected by the corrosion inhibitors. The passivation due to the corrosion inhibitor becomes important only on large time scales (> 200 millisecond). The porosity and the density of the chemically modified surface layer can be affected by additives of other chemicals such as citric acid. An optimum density of the surface layer is required for high polishing rate while at the same time maintaining a high degree of surface finish.

Nanoindentation measurements indicated that the mechanical properties of the surface layer are strongly dependent on the chemical additives in the slurry. The CMP removal rates were found to be in good agreement with the initial reaction kinetics as well as the mechanical properties of the chemically modified surface layer. In addition, the material removal model based on the micro- and nano-scale interactions, which were measured experimentally, has been developed.

CHAPTER 1 INTRODUCTION

As the copper interconnect was introduced to ultra large scale integration (ULSI) circuits in 1997, chemical mechanical polishing (CMP) has been widely recognized as the technology for eliminating topographic variations and achieving wafer-level global planarization [Sin02, Han02, Bey99]. However, despite its extensive utilization, process control in CMP remains at an empirical stage because the fundamental mechanisms underlying the polishing process have yet to be fully understood.

CMP combines the chemical and mechanical interactions to planarize metal and dielectric surfaces using a slurry composed of chemicals and sub-micron/nano sized particles. The understanding of the removal mechanism on CMP process can be achieved by studying the wafer-pad-slurry interactions that occur both at micro scale and nanoscale levels (Figure 1-1) [Mah99, Lee02, Sin02]. At the microscale level, the rough pad carrying particle based slurries interacts with the surface of the wafer. It is generally believed that the particles, which are between the wafer and the pad, participate in mechanical abrasion process that results in material removal. At the nanoscale level, the kinetics of formation and removal of the thin surface layer control the CMP output parameters such as removal rate, surface planarity, surface defectivity, and slurry selectivity (polishing rate of the top layer compared to the underlying layer).

Although the CMP process is intuitively quite simple to understand, a more detailed understanding has been limited primarily due to the large number of input variables in the polishing process. Table 1-1 lists the various systems level variables in a

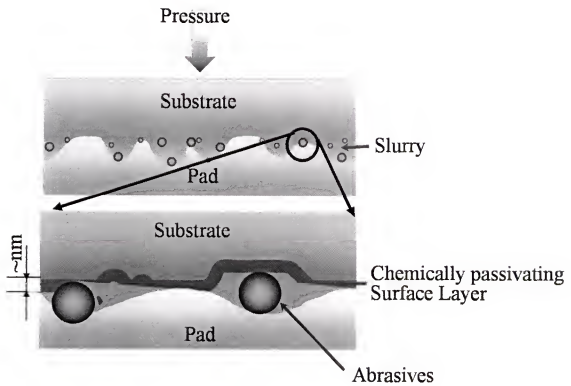
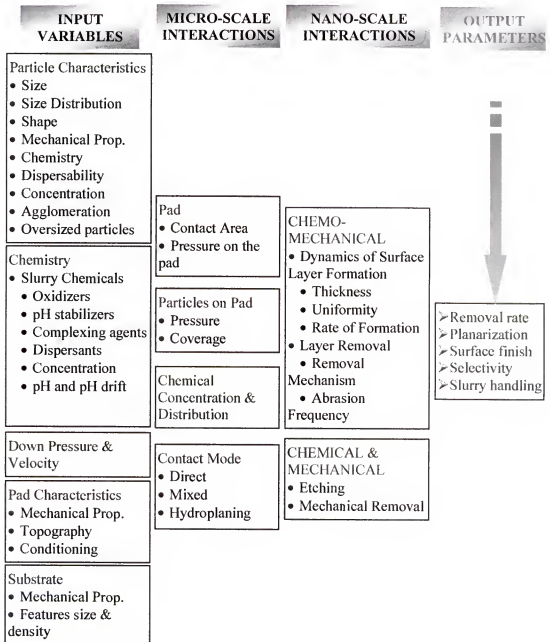


Figure 1-1. Schematic diagram to depict micro and nanoscale phenomena occurring during CMP [Lee02, Sin02].

Table 1-1. Correlation of system level variables, with micro and nanoscale interactions and the output parameters in CMP [Sin02].



CMP process. They include slurry variables such as particles and chemicals, pad variables, tool variables (down pressure and linear velocity) and substrate variables (pattern density, etc.) [Ste97, Sin02]. The total number of variables can exceed 20, making this process quite difficult to understand and control. Time dependent contributions by some of these variables cause further complexities in this process.

The majority of the CMP research to date has focused on empirical cause and effect relationships in which the effects of the process variables, such as pad type, applied pressure, and the platen and carrier speed on material polish rate, are determined [Pre27, Ste97, Ste99, Shi98, Zha99]. These empirical models allow for an adequate manufacturing process control, but they provide little information on the fundamental material removal mechanisms that occur during CMP. More importantly, they fail to include the chemical effects, which are synergistic with mechanical effects and cannot be excluded from any modeling work. Thus, both chemical changes at the surface and the removal of the chemically modified surface layer has to be considered to develop the principles and methodology of slurry design as well as a more precise and suitable removal mechanism in CMP.

Objectives

This investigation focuses on the chemical interactions between the chemical additives and the copper wafer, which is a critical issue to understand the removal mechanism on copper CMP. In this regard, the objectives of our work are as follows: (i) the characterization of the basic role of chemical additives using potentiodynamic measurements and XPS analysis; (ii) understanding the dynamic nature of the formation of the chemically modified surface layer on copper, which includes the rate of layer formation and passivation as a function of different chemistries; and (iii) measuring the

mechanical properties, such as hardness and Young's modulus, of the chemically modified surface layer, which is related to the polish rate and defectivity. Comparing all the results with the CMP performance (such as material removal rate and defectivity) led to a better understanding of the CMP removal mechanism and defectivity mechanism.

The information gathered from these experiments can be directly applied to develop the first principle and methodology of slurry design that, in turn, lead to an enhanced performance of the CMP process in semiconductor manufacturing.

Dissertation Outline

This dissertation consists of 7 chapters.

Chapter 1 introduces the necessity, objectives, and outline of this study

Chapter 2 gives a general review on the subject of the chemical mechanical polishing (CMP) process in the manufacturing of integrated circuits with copper interconnection lines. This includes the historical background and the basic concept of CMP. The removal mechanism and models on the copper CMP removal are also discussed. Chapter 3 presents the characterization of the basic role of chemical additives using potentiodynamic measurements and XPS analysis, followed by the dynamic nature of the formation of the chemically modified surface layer on copper as results of *in situ* electrochemistry described in Chapter 4. Chapter 5 presents the results of the nanoindentation on the chemically modified surface layer formed under various chemical conditions. Chapter 6 presents the material removal model, based on the micro- and nano-scale interactions, and the correlation of copper CMP performance to all the results. Finally, Chapter 7 summarizes the conclusions drawn from this investigation.

CHAPTER 2 LITERATURE SURVEY

Interconnects on Circuit Performance

Today's state-of-the-art integrated circuits (ICs) contain numerous device elements including tens of millions of transistors, capacitors and resistors on a single chip. According to Moore's law [Moo65], the market demand for functionality per chip doubles every 1.5 to 2 years. Moore also observed that microprocessor (MPU) performance (clock frequency (MHz) x instruction per clock) doubles every 1.5 to 2 years. With this trend, interconnect becomes a critical technology. The target values for MPU interconnect technology from the ITRS (International Technology Roadmap for Semiconductors) 2002 update are presented in Table 2-1[ITR02]. The transistor density is, now, around hundred million per cm^2 , and it will increase to approximately billion per cm^2 in the near future. Achieving these ambitious goals necessitates a substantial modification to the current interconnect technology. As it is projected that the MPU half pitch - so called the technology node - is smaller and smaller, a larger scale of integration, a higher device density, lower power consumption, and faster clock speed are required to produce ICs. There is also an enormous impetus to reduce process complexity and cost. However, these goals must be achieved without compromising reliability. The scaling down of the device size has several negative effects on the MPU performance: the interconnect RC time delay, power consumption, and circuit reliability.

Table 2-1. Target values for Microprocessor (MPU) interconnect technology according to ITRS 2002 update [ITR02].

Year	2002	2003	2006	2010	2013
MPU $\frac{1}{2}$ pitch (nm)	130	107	70	32	22
Number of metal levels	8	8	10	11	11
Chip size (mm ²)	310	310	310	310	310
Transistor density at high-performance MPU (Mtransistor/cm ²)	112	142	283	714	1427
Power supply voltage range (V)	1.0-5.5	Same as left	0.6-3.3	Same as left	Same as left
Clock frequency (MHz)	2317	3088	5631	11511	19348
Total interconnect length (m/cm ²)	4843	5788	10022	16063	22695
Jmax (A/cm ²)-wire (at 105 °C)	1.1E+06	1.3E+06	1.9E+06	3.3E+06	3.9E+06
Conductor effective resistivity ($\mu\Omega$ -cm)	2.2	Same as left	Same as left	Same as left	Same as left
Interlevel metal insulator (minimum expected) effective dielectric constant (κ)	3.0-3.6	Same as left	2.6-3.1	1.9	1.8

RC Time Delay

Reductions in semiconductor device dimensions provide higher densities and improved performance for integrated circuits. Ryan *et al.* [Rya95] reported that most high-performance systems must accommodate increased current density, decreased wire width, increased chip size, increased tolerance to noise, and minimized power variations across the chip, and reduced resistance (R) and capacitance (C) interconnection schemes to maintain chip performance. Due to an increase in device density provided by scaling of semiconductor processes to improve circuit performance, decrease of the total delay times is strongly demanded. The total delay times consist of two major delays: the gate delay and the interconnect delay. According to scaling theory, the small dimension of a MOS (metal-oxide semiconductor) transistor enhances its switching speed, resulting from the lower gate delay. However, the scaling of interconnect increases the parasitic resistance and capacitance associated with the interconnect system. Therefore, today, major contribution to the total delay is not due to the gate delay, but is because of the delays in the interconnection system (Figure 2-1). The delay in interconnects is characterized by the so-called RC (Resistance x Capacitance) time constant. This is the time taken for the voltage at one end of a metal line to reach 63% of its final value when a step input is presented at the other end of the line. The lower the RC is, the faster is the operation speed in the interconnection system. As can be seen from the Figure 2-1, the role of RC time delay becomes more significant in the total delay time as the size of the device becomes smaller [Liu99].

The total line capacitance is composed of line-to-line capacitance (C_{ln-ln}) and line-to-substrate capacitance (C_{ln-sub}). The schematic of the closed-packed IC interconnect is

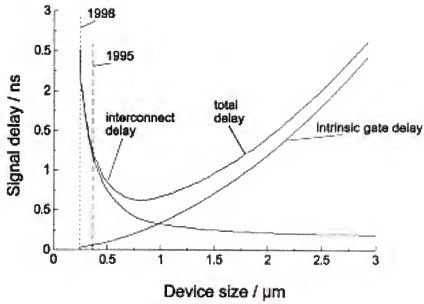


Figure 2-1. Time delay caused by interconnection and gate at different device sizes [Mur96]. Interconnect delay is being dominant in total time delay as the device is shrinking.

illustrated in Figure 2-2. $C_{\text{ln-ln}}$ between two adjacent interconnect lines separated by a distance, d , is given by

$$C_{\text{ln-ln}} \propto \epsilon \epsilon_o \frac{t_{\text{metal}} L}{d} \quad (2.1)$$

where t_{metal} and L are the metal thickness and metal line length, respectively. ϵ and ϵ_o are the dielectric constant and the permittivity of free space. $C_{\text{ln-sub}}$ between an interconnect line and the silicon substrate is

$$C_{\text{ln-sub}} \propto \epsilon \epsilon_o \frac{WL}{t_{\text{dielectric}}} \quad (2.2)$$

where W is the metal line width, $t_{\text{dielectric}}$ is the dielectric thickness.

Therefore, the total line capacitance can be expressed as follows [Dan81]:

$$C_{\text{total}} = K_l (C_{\text{ln-ln}} + C_{\text{ln-sub}}) \quad (2.3)$$

where K_l is a factor that takes into account the fringing field.

With the scaling of devices, the metal line width (W) and spacing (d) become smaller. As a result, line-to-line capacitance increased exponentially and it becomes a dominant factor, whereas the line-to-substrate capacitance becomes a marginally factor in the total capacitance as shown in Figure 2-3 [Den74].

On the other hand, the resistance in the interconnect line is given by

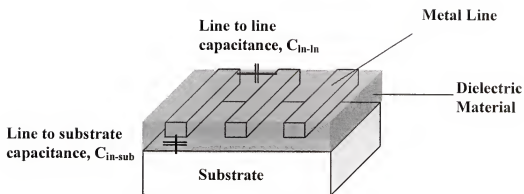


Figure 2-2. Schematic of the closed-packed IC interconnect.

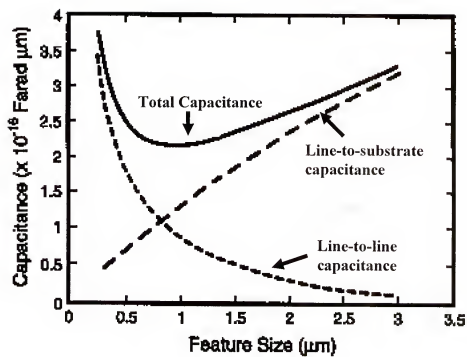


Figure 2-3. Capacitances associated with metal lines. Line-to-line capacitance becomes dominant due to the scaling of the device size [Den74].

$$R = \rho \frac{L}{W t_{\text{metal}}} \quad (2.4)$$

where ρ is the resistivity of the interconnect metal. Therefore, combining (2.2) and (2.4) gives the expression of the interconnect RC time delay:

$$RC \propto \rho \epsilon \epsilon_o L^2 \left(\frac{1}{Wd} + \frac{1}{t_{\text{metal}} t_{\text{dielectric}}} \right) \quad (2.5)$$

The first term becomes dominant in the case of the smaller device size being less than 0.25 μm , whereas the second term is the dominant factor in the device size of more than 1.0 μm . This equation (2.5) suggested that the interconnect RC time delay does not depend on either the metal line thickness or the oxide thickness in the device whose size is less than 0.25 μm . From this equation, it is known that the reduction in ρ , ϵ or L , or an increase in d or W will decrease the interconnect RC time delay. However, because of increasing the chip complexity, the metal line width and the space between two adjacent metal lines are scaled down, resulting in an increase of the RC time delay. Thus, the importance of enhancing the interconnection performance has led to the adoption of multilevel interconnection (MLI) technologies, a low resistivity metal and a low dielectric material. Decreasing L has the most significant effect because interconnect delay is proportional to the square of L , forming the basis of the multilevel interconnection technique. The new interconnect metal also needs to be a better conductor than Al or its alloys, and an ILD with lower dielectric constant (commonly referred as low-k materials) than SiO_2 is needed. It should be noted that the materials,

whose dielectric constants are less than 3.0, are called low-k materials. Since the main reliability problem with the Al interconnection is the electromigration at higher current densities, new interconnect material should also have a superior electromigration (EM) resistance.

Power Consumption

The scaling of the device size has negative impacts – not only in the interconnect RC time delay, but also on the power consumption – of the interconnect system. The power consumed by interconnects ($P_{interconnect}$) at a certain operating frequency, f , and voltage, V , is described by Weste and Eshraghian [Wes85] as follows:

$$P_{interconnect} = C_{total} V^2 f \quad (2.6)$$

As shown in equation (2.6), the power consumed by the interconnect system is proportional to the total capacitance (C_{total}). Thus, reducing the line-to-line capacitance in the smaller device is required to reduce the power consumption.

Circuit Reliability

As the interconnect line becomes thinner and narrower, the current density through the line is increased. This high current density can cause the failure in the metal interconnect due to the electromigration. Generally, the mean-time-to-failure (MTTF) of an interconnect line due to the electromigration is derived from an empirical relation, which is known as Black's law:

$$MTTF^{-1} = B j_e^n \exp\left(-\frac{E_a}{kT}\right) \quad (2.7)$$

where B is a constant, E_e is the activation energy for electromigration, n depends on the interconnect material, and j_e is the current density [Bla69]. At a certain operating current, the thinner the interconnect metal line is, the higher current density is in the metal line. Therefore, if the resistance of the electromigration is not high enough, a shorter lifetime of the interconnect metal line can be expected. The detail of the electromigration will be explained in the following section.

Multilevel Interconnection

Interconnects in a chip are the conductor lines, which connect these discrete elements with each other to form a circuit. In order to meet the stringent requirements of future ICs (see Table 2-1), the first choice is the multilevel interconnect (MLI) technique. The MLI technique is usually accomplished by increasing the capacity and reducing RC time delay in the smaller chip size. For example, the chip size was decreased from the Intel Pentium I processor to the Intel Pentium II processor in Figure 2-4. In the past thirty years, interconnects have evolved from a single layer of aluminum to several levels of copper interconnects, resulting in the multilevel interconnects (MLI).

The multilevel interconnect technology brings several advantages in the circuit's performance and reliability. First, the use of the MLI reduces the total length of the interconnect metal lines, resulting from the direct routing of metal lines. Second, the multilevel scheme enables the use of the wider interconnect metal lines with a reduced packing density. Consequently, as can be seen from equations (2-1) to (2.5), the resistance and the capacitance of the interconnect technology are significantly reduced, resulting in the decrease of the interconnect RC time delay. The power consumption is also minimized by reduction of the total capacitance. Finally, the use of the wider interconnect metal lines decreases the current density of the lines, leading to an

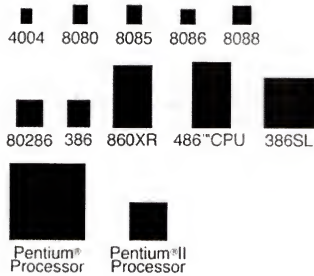


Figure 2-4. The relative size change in central processing unit (CPU) from <http://www.intel.com>.

improved circuit reliability. With an increasing number of metal layers and shrinkage of interconnection dimensions, requirements placed on the interconnect system have vastly increased, such as the global planarization. In the MLI scheme (Figure 2-5), the first layer of interconnection is reserved for making ohmic contacts to the silicon devices or components. An insulating interlevel dielectric (ILD) layer separates the silicon or local interconnection lines from the metal interconnect layer. In the following metal layers, the linkage from one layer of interconnects to another is provided by vias, metallic conductors in holes between the surrounding ILD [Wil93]. As more and more layers are built on the silicon surface, surface planarity begins to have a greater impact on yield and performance than depth of focus of high performance photolithography tools. The residual material after dry etching is also the limiting parameters for the technique developed in the single level interconnect technology [Mur00].

Copper Metallization

For the better performance of ICs, a low resistivity material as well as MLI technology is required. The conventional conductive material for the interconnect is aluminum and its alloy. However, as the device becomes smaller and smaller, these materials have severe drawbacks such as the low electromigration resistance and relatively high resistivity.

Advantages of Copper Metallization

Copper, as the new interconnect material, has become an increasingly popular choice for interconnect metal and has begun replacing aluminum in the semiconductor industry, while the search for the low-k ILD continues. Copper has several properties that make it very attractive for an interconnect metal.

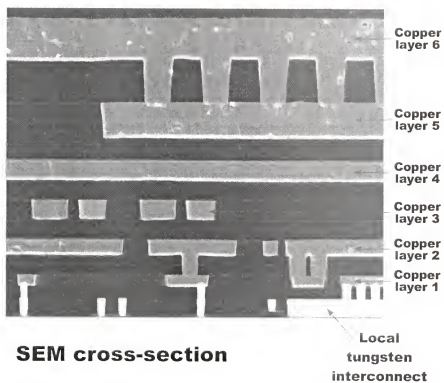


Figure 2-5. The example of the multilevel interconnect (MLI) by dual damascene process.

Lower resistivity

Table 2-2 lists the possible candidate materials for the interconnect metal with lower resistivities [Mur93, Ste97]. Among the candidates, only silver, gold, and copper have lower resistivities than aluminum. These three materials need the diffusion barrier due to the diffusion into silica and silicon, resulting in the deep level defects. However, a diffusion barrier for gold and silver has been proven difficult to be fabricated [Ste97]. Moreover, gold has a higher resistivity than copper. On the other hand, tantalum and tantalum nitride are conventionally used as a copper diffusion barrier in the interconnect technology. Therefore, copper with a lower resistivity ($1.7 \mu\Omega\text{-cm}$) compared to aluminum ($2.65 \mu\Omega\text{-cm}$) allows finer line having lower resistive losses. This lower resistance is critical in high performance ICs because it enables signals to move faster by decreasing RC time delay as shown in equation (2.5).

Electromigration resistance

Copper lines can be made thinner because copper has a superior resistance to electromigration. Electromigration (EM) is defined as the atomic diffusion in an electric field created by high current densities in a conductor. EM damage results from the occurrence of electromigration flux divergences at grain boundary triple points [Mur00]. It can significantly create the reliability problems of the IC through the generations of hillocks on film surfaces, bridges between two conductor lines or discontinuity (voids) in a conductor line as shown in Figure 2-6 [Vai80]. In silicon technology involving Al interconnects, EM resistance can be increased by using a so-called bamboo structure (which reduces the possibility of grain boundary triple points) and alloying (addition of 1 to 4% Cu to Al) [Mah98]. However, even with these enhancements, Al-alloys do not

Table 2-2. Low resistivity materials for interconnect conductor materials [Mur93, Ste97].

Metal	Bulk Resistivity ($\mu\Omega\text{-cm}$)	Thin Film Resistivity ($\mu\Omega\text{-cm}$)
Ag	1.6	
Cu	1.7	1.8-2.1
Au	2.4	4.1
Al	2.65	2.7
Mo	5.2	7.5-12
W	5.6	10-14
WSi ₂	12.5	26-100
TiSi ₂	16.7	17-25
MoSi ₂	21.6	40-100
TaSi ₂	38	35-60

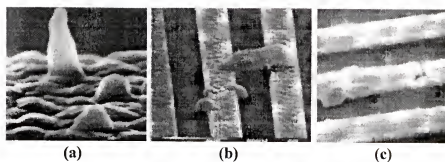


Figure 2-6. Manifestation of electromigration damage in aluminum films: (a) Hillock formation, (b) whisker bridging between two conductor lines, and (c) mass accumulation and depletion [Vai80].

address the concerns regarding reliability because the current densities in interconnects increase with the scaling of ICs (more than 10^6 A/cm²). Since metals with higher melting points are less prone to EM and copper has a higher melting point (1083 °C) than aluminum (660 °C), copper has a greater EM resistance. The reports of EM lifetime testing of Cu interconnect show one and two order-of-magnitude greater lifetime for Cu as compared to Al-alloys [Fra98, Cun00] as shown in Figure 2-7. In essence, high electromigration resistance of copper means that it can reliably handle higher current densities with thinner lines reducing power consumption. This also enables it to replace tungsten in the high aspect-ratio vias, thus eliminating the necessity for using two different metals.

Lower manufacturing cost

In reality, the most important benefit of copper interconnection, beyond the ability to increase chip speed and reliability and reduce power consumption, is that it can actually lead to lower manufacturing costs compared to aluminum. There are two reasons for these reduced costs. The first one directly relates to achieving tighter packing densities with copper, which is a natural result of using smaller lines. Figure 2-8 shows the expected interconnect RC time delay for copper and low-k ($k = 2.0$) device as well as aluminum and silica device [Pet98]. As the RC time delay is significantly decreased with copper and low-k material, improved performance can be achieved. In addition, since higher packing densities can be achieved per level, fewer levels of metallization are needed for the same performance with aluminum and silica device, resulting in significantly lowered manufacturing costs as shown in Figure 2-9 [Sin98]. The decline in the number of levels of metallization also results in a decrease in complexity. The second

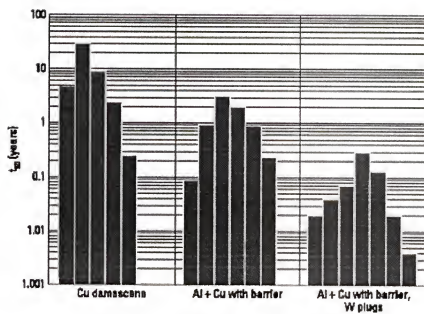


Figure 2-7. Copper and aluminum failure rates due to the electromigration [Cun00].

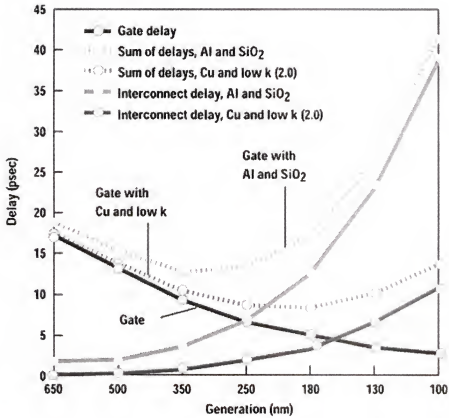


Figure 2-8. Expected interconnect RC time delay with copper and low-k ($k = 2.0$) device as well as aluminum and silica device [Pet98].

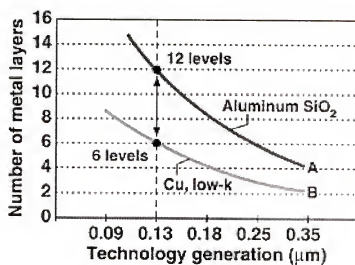


Figure 2-9. The reduction of the number of metal layers with copper and low-k material to achieve the same performance [Sin98].

reason for cost reduction has to do with the advantages brought by the damascene architecture, which is the new process to form copper interconnect lines. The damascene process requires 20-30 % fewer steps than the traditional subtractive patterning [Mur93, Sin98, Jac98]. This is especially seen in the dual damascene process, in which the vias and trenches are both etched into the dielectric (such as silicon dioxide (SiO_2)), and then metal is deposited (Figure 2-10). Metal CMP is then carried out, leaving only the recessed metal in the dielectric. The details are explained in the following section. As the dual damascene process is introduced in the MLI, the CMP process continues to become more attractive to the semiconductor industry. The advantages of this process are no metal etching required, no interface resistance between the vias and lines, single step deposition of copper, and the global planarized surface after CMP. This means that the subsequently deposited dielectric will also be planarized, and thus will not have to undergo CMP. As a result, the number of process steps is reduced. The dual damascene process steps and two-step copper CMP process are schematically shown in Figure 2-10.

Challenge in Integrating Copper

Although, copper provides crucial advantages over aluminum, it has two major disadvantages: non-volatile copper compound in dry-etching process and poisonous copper diffusion into silicon dioxide.

Lack of volatile copper compound

The traditional subtractive patterning method, which has been used for aluminum, is not currently feasible for copper interconnection because the volatile copper compounds do not form at the relatively low temperatures (less than 100 °C) normally used for reactive ion etching (RIE) [Ste97]. Copper etch processes necessitate

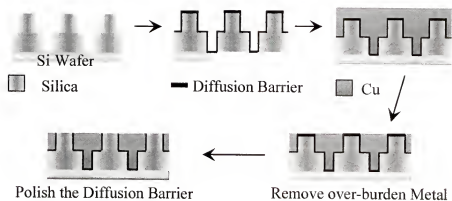


Figure 2-10. Schematic diagram of the dual damascene process and two step copper CMP process.

temperatures in excess of 250 °C, which leads to significant manufacturing problems such as the stability of the etch mask [Ste95]. Accordingly, when copper and its alloys are used instead of conventional aluminum or aluminum alloys as an interconnection material, the lack of dry etching processes is overcome by using the damascene process. For example, a damascene process together with chemical-mechanical polishing (CMP) can be used to define copper lines. In a damascene process, trenches are etched in a dielectric material, such as silicon dioxide (SiO_2). A barrier material is then deposited, generally by sputtering. Very thin seed copper layer (~ 30 nm) is then deposited by sputtering. Finally, thick copper is then deposited typically using electrochemical deposition (ECD) techniques (*e.g.*, electroplating) to fill the barrier lined trenches. The overburden regions of the copper film are then removed by CMP to define the copper lines.

Copper diffusion into dielectric layer

There are other challenges in integrating copper into the IC fabrication process: copper diffusion through SiO_2 and its poor adhesion to SiO_2 . Copper is poisonous to silica and silicon since it readily diffuses into silica and silicon, causing deep-level defects, which degrades the electrical performance of the devices in the chip. Copper impurities in the dielectric also lead to significant leakage currents. The poor adhesion of copper to SiO_2 also results in the delamination or peel-off of the copper layer. Therefore, copper must be isolated from silicon and silica, usually through use of a diffusion barrier/adhesion promoter before depositing the Cu. Tantalum or tantalum nitride are usually used for these reasons [Ste97]. Tantalum is an attractive barrier metal because of its high melting point and its immiscibility with copper. It is also highly reactive and forms strong metal-metal bonds, much like titanium does for aluminum interconnects.

Thus, it should provide a low-resistance ohmic contact with good adhesion to copper. In addition, doping the Ta film with nitrogen blocks grain boundary diffusion pathways, resulting in a better diffusion barrier [Ste97]. Alternative materials under consideration include tungsten nitride and titanium silicon nitride [Jac98].

Low-k Materials

As the last effort to reduce the RC time delay in high speed circuits, the need for new interlevel dielectric (ILD) materials arises from the relatively high dielectric constant (k) of silica. Capacitance is directly proportional to k , so high- k values lead to a high capacitance (see equations (2-2) to (2-4)), and thus to unacceptable RC delays in smaller technology node (e.g., 32 nm in year 2010). As shown in Table 2-1, as the technology node is projected to be smaller and smaller in the near future, the reasonable dielectric constant of the interlevel dielectrics is less than 2.0. With low- k dielectric materials, the total capacitance can be lowered, resulting in the decrease of the RC time delay in the interconnect system and the reduction of the power consumption (see equation 2.6)).

With this regard, a large variety of low- k dielectric materials has been proposed for use as ILD materials. To utilize the low- k dielectric materials as new ILD materials, the important requirements should be fulfilled: the dielectric constant lower than 3, the thermal stability in the range 400–450 °C, moisture adsorption less than 1%, good adhesion to metal, mechanical stability, planarization behavior, plasma etching behavior, etc. The details are well described in Ref [Mai01]. Table 2-3 lists the most promising candidates for low- k ILD materials in interconnect [Chi99]. Low- k ILD materials are either organic or inorganic, and can be applied by spin-on or chemical vapor deposition (CVD) methods. Among them, Black Diamond, SiLK, BCB, poly(arylene) ether, and

Table 2-3. The most promising candidates for low-k ILD materials in interconnect [Chi99].

Application method	4.	3.	3.	k 2	2	1.	1.
CVD	SiO ₂ k 4.1	FSG F ₂ SiO _x silicon oxyfluoride k 3.4-4.1	Methyl-doped SiO ₂ k 2.6-3.0 Trikon Technology	Applied Materials, Black Diamond k 2.7-2.2			
Organic				Parylene AF4 k 2.25 Novellus (Alpha) DuPont	PTFE k 1.9		
Spin-on							
Organic			HSQ hydrogen silsesquioxane k 2.9-3.1 Dow Corning FOX, Hitachi, EKC & Ashian		Nanoglass k 1.3-2.5 AlliedSignal, etc.		
			MSQ methyl silsesquioxane k 2.7 Dow Corning				
Organic		Silicon-based polymer k 2.8-3.0 AlliedSignal T-23		BCB, SiLK k 2.65 Dow Chemical		PTFE k 4.9 W.L. Gore Speedfilm	
				Poly(arylene) ether k 2.6-2.8 AlliedSignal Flare 2 Schumacher Velox		Porous organosilicates k 2.2 and lower IBM, Dow Chemical	

Flare are favored low-k dielectric materials, and extensive works are concentrated on these new materials.

CMP

Chemical Mechanical Polishing (CMP) is being used extensively in the semiconductor industry. Since Beyer applied the concept of CMP to semiconductor processes at IBM, the CMP process has been receiving an interest due to its great advantages: global planarization, less defectivity, lower cost of ownership, better step coverage, applicability to variable materials, simple technique, etc. [Bey99, Sho00, Ste97].

Chemical Mechanical Polishing, as the name suggests, is a polishing process in which the surface topography on a wafer is removed by smoothing and planarizing, both through chemical reactions and mechanical abrasion to polish surfaces. As schematically illustrated in Figure 2-11, a typical rotary CMP tool consists essentially of a polishing pad affixed to a circular polishing plate, a carrier to hold a wafer against the pad, and a slurry. Both the carrier and the plate are rotated as the front of the wafer is pressed down against the pad which is soaked with the polishing slurry. The polishing slurry provides the means by which both chemical and mechanical actions are used to remove and subsequently planarize the wafer surface.

Mechanical interaction is accomplished by the use of abrasive particles included in the slurry, and thus it is enhanced by down pressure and velocity. Chemical interaction is achieved by the incorporation of chemical agents into the slurry that aid in planarization [Car90]. Typical slurry is water-based and contains both abrasive and chemical additives. Sub-micron or nano sized SiO_2 , Al_2O_3 , or CeO_2 particles are commonly used as abrasive

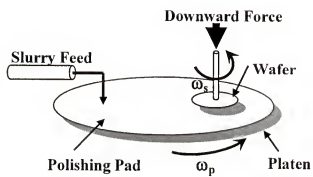


Figure 2-11. Schematic illustration of a typical CMP tool.

particles in slurries. The chemical component of the slurry, which acts isotropically on the wafer surface, is necessary to enhance the mechanical action of the slurry. The chemical components that may be present include oxidizing agents, complexing agents, corrosion inhibitors, dispersion agents, pH buffers, etc. These chemicals have specific roles in creating an easily removable surface layer on the material – such as the formation of an oxide layer on the metal surface in order to achieve the planarization while increasing the removal rate; dissolution of the abraded materials; passivation to maintain a low chemical removal (etching) rate from the recessed area; and stabilization of the slurry. The combination of mechanical interaction with the chemical interaction causes material to be easily removed from the surface of the wafer with less defectivity. Planarization could only be achieved if removal rates obtained are higher at the protruding areas than at the recessed areas of the wafer surface. When a rigid pad with low compressibility such as IC-1000 stacked by Suba IV (manufactured by Rodel®) is used, most of the mechanical abrasion concentrates on the protruding areas, resulting in higher mechanical removal rate of the high features. When the mechanical and the chemical additives are tailored appropriately and their contributions to the removal of the material are adjusted properly, the topography of the thin film can be removed effectively due to different removal rates of low and high regions on the wafer surface.

Planarity

Wafer surfaces can be categorized into three degrees of planarity, as illustrated in Figure 2-12 [Ols93]:

(1) surface smoothing, where feature corners are smoothed and high aspect ratio holes are filled.

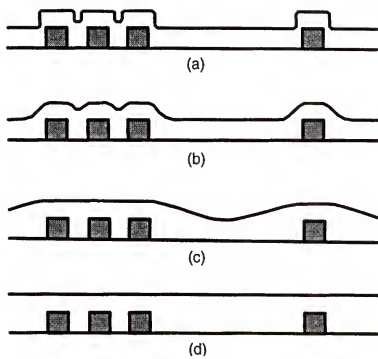


Figure 2-12. Degrees of Planarity; (a) Unplanarized, (b) Surface Smoothing, (c) Local Planarization and (d) Global Planarization [Ols93].

(2) local planarity, where surfaces are locally flat but the surface height varies across the die.

(3) global planarity, where the surface is flat across the entire wafer.

Surface smoothing and local planarity are important for ensuring proper metal step coverage. However, with additional metal levels being added, global planarization is becoming a more critical issue because non-planarity on the surface becomes cumulative, and severe topography can be developed even with surface smoothing. This results in poor step coverage and electromigration [Ols93]. In addition, as circuit dimensions are shrunk below the sub-0.5 μm regime, lithography tools require a topographic variation of less than 150 nm across the stepper field. Finally, with multiple metal layers, even surface smoothing will lead to a cumulative increase in topography towards the final metal level, further reducing process yield as illustrated in Figure 2-13 [Ste97, Mur93, Lan92, Vie01]. This figure clearly shows that the final level has a severe topography due to the accumulated small topography from previous levels, resulting in a failure in the device. Thus, one more planarization process is required to reduce the topography through the entire wafer. This additional process also causes the poisonous effects - such as cost, interlevel dielectric loss, and interconnect metal thinning. All the above factors clearly illustrate the need for global planarization in present day semiconductor manufacturing technology. Thus, in order to fabricate high-performance multilevel devices, planarization of the interlayer connection metals as well as the interlayer dielectric materials is essential. For this reason, CMP has emerged as the most effective and widely accepted technique for achieving global planarization of thin metal layers and dielectric materials simultaneously in these multilevel metallization schemes [Ste97].

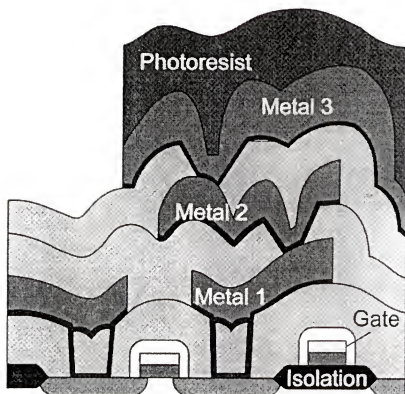


Figure 2-13. A cumulative increase in topography by multi-level interconnection without using a planarization method [Vic01].

Planarization Mechanism in Metal CMP Process

Since copper was introduced in the semiconductor industry as a new inlaid metal, numerous researchers have begun focusing on copper CMP. They have made a significant progress in developing slurry chemistries for copper CMP [Kau00-a, Kau-b, Kon00-a]. However, the mechanisms of material removal are still unclear, and the process is not yet fully optimized.

The most commonly accepted planarization mechanism in metal CMP is Kaufman's tungsten CMP removal mechanism [Kau91]. In this model, the removal mechanism of tungsten during CMP is the formation of the blanket passivation layer on the surface of tungsten due to the oxidizing nature of the slurry and then its mechanical abrasion from the slurry. The polishing pad subsequently removes the abraded material. The bare metal, when immediately exposed to the oxidizer, is repassivated. This mechanism has also been applied to explain the processes for metal removal and planarization for copper [Her01] and aluminum [Kuo00]. Obviously, as indicated by this mechanism, the passivation of metal in the slurry plays a very important role in CMP performance, by either forming native metal oxides on the surface using oxidizers such as H_2O_2 [Mue99, Gru00], KIO_3 [Kne97, Lee99], $\text{K}_3\text{Fe}(\text{CN})_6$ [Lan92, Bie99, Car01] etc. or by forming chemically adsorbed layers (e.g. Cu-BTA polymeric layer) using organic inhibitors. For example, benzotriazole (BTA), a common corrosion inhibitor for copper, could be utilized in copper CMP slurries [Ste97, Gru00, Lee00]. However, there have been several papers published by respected CMP groups, showing that the oxidation rate of tungsten during polish in iodate, ferric, and persulfate based slurries is too low to account for the higher polish rates [Ste99-a, Ste99-b, Kne96, Ste98, Elb98, Kne97]. Thus,

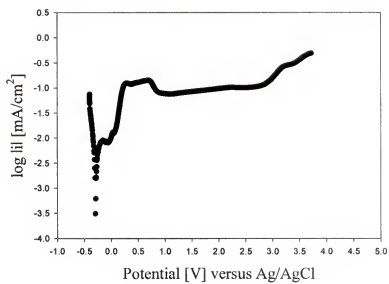


Figure 2-14. An example of the potentiodynamic scans for tungsten with 0.5M H₂SO₄ [Bie98].

they concluded that the passivation layer might not exist on the metal surface during CMP. These conclusions were based on static and dynamic potentiodynamic electrochemical measurements, a well-known standard electrochemical technique used to select the chemicals included in the slurries and characterize the metal CMP slurries. An example of the potentiodynamic scans (for tungsten in presence of 0.5 M oxidizer at pH 4) is shown in Figure 2-14 [Bie98]. This figure shows the formation of the passivation layer in tungsten and also indicates that the rate of formation of the passivated layer is approximately 1-2 nm/min, which is 200 times less than the removal rate of tungsten during CMP. Thus, the potentiodynamic measurements present that the oxidation rates are two to three orders of magnitude lower than the experimentally observed CMP removal rates. These experimental measurements and conclusions have thus questioned the validity of the oxidation-abrasion Kaufmann model, and suggest that other non-oxidation mechanisms may play an important role in controlling the removal rate [Ste98, Ste99-b, Kne97]. It should be noted that the low oxidation rate of metal compared to its CMP removal rate may represent one of the most controversial CMP fundamental issues. However, this large discrepancy between the oxidation rate and the removal rate of metal is a strong indication of the formation of a passivation layer on the metal surface.

According to Yu's model [Yu93] and Basim's experimental results [Bas02], it was shown that the contact area between the pad and wafer was approximately 10^{-4} times the nominal area of the wafer. Thus, it has been estimated that the time interval between consecutive particle interactions at a particular point on the surface is in the range of 10 to 400 milliseconds [Sin02]. It depends on the particle concentration, size, the pad contact

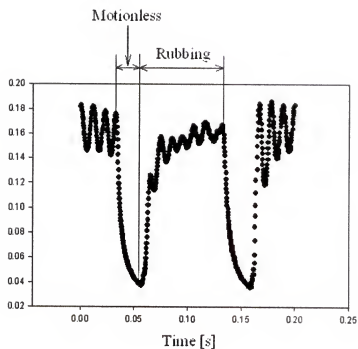


Figure 2-15. Current recorded for one stroke during the tribological experiments for anodic applied potential (+2 V) in 0.5M H_2SO_4 for a sphere motion cycle of 0.2 second [Bie00].

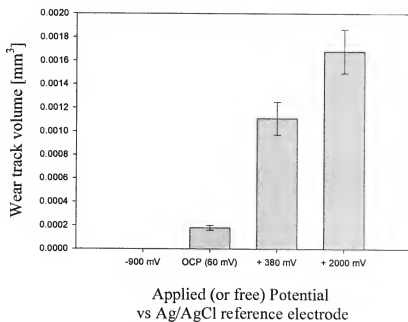


Figure 2-16. Wear track volume vs. applied potential for experiments conducted by rubbing an alumina ball at 5 Hz with 5N load against a fixed flat tungsten sample immersed in 0.5M H_2SO_4 for 25 minutes [Bie00].

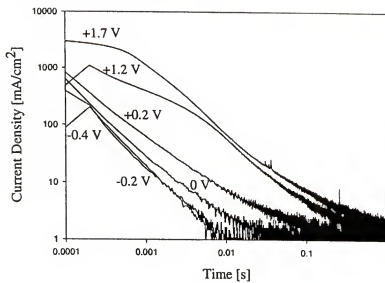


Figure 2-17. Anodic current vs. time transients for tungsten measured in 0.5M H₂SO₄ at several potentials [Bie00].

area, and the nature of particulate dispersions. Biemann [Bie98, Bie00], have also hypothesized that due to the high frequency of particle-surface contacts taking place in a CMP process, the CMP process is essentially a transient phenomena, and thus chemical changes occurring on the surface of tungsten (or any material being polished) should be measured in very short time-scales (with microsecond sensitivity). Thus, he developed a unique set of electrochemical measurements for CMP simulation, which have proven that the passivation of the tungsten surface plays an important role in the removal of tungsten (Figure 2-15) and the tungsten wear rate is indeed equal to the oxidation rate (Figure 2-16) in tribological experiments. Moreover, he observed that the tungsten surface is fully passivated by the tungsten oxide layer in millisecond range (Figure 2-17), conducted by in-situ electrochemistry. The static and dynamic potentiodynamic measurements used by all the other groups are essentially steady-state measurements with the time scale ranging from several seconds to several minutes, and thus are unable to measure the transient changes which are occurring at the surface of the polished material, resulting in the non-oxidation mechanism [Ste98, Ste99-b, Kne97, Kuo00]. Therefore, the thickness formed between consecutive abrasion interactions and the dynamic nature of this layer are key issues in understanding the CMP removal mechanism and factors of performance, such as polish rate, planarity, and defectivity. With this regard, more detailed studies are required to understand the transient phenomena of metal during CMP process.

CMP Removal Models

In the CMP process, the passivation layer is removed by mechanical action of the abrasive slurry. Researchers have taken four approaches in modeling material removal mechanisms and material removal rates in the CMP processes in terms of mechanical interaction.

The first is a phenomenological approach based on the results of the CMP process. Preston [Pre27] presented the first mechanical model, which empirically relates the removal rate to pressure and velocity:

$$MRR = K_p PV \quad (2.8)$$

where MRR is the material removal rate, K_p is the Preston coefficient, P is the pressure, and V is the velocity. The Preston equation states that the material removal rate is proportional to the product of the polish pressure, P , and the velocity, V . Originally proposed for glass polishing, the Preston equation is of empirical nature and lacks scientific basis. As it is well known, the CMP polish rate depends on several factors such as slurry characteristics (*e.g.*, particle size, concentration, oxidizers, and other additives), pad condition (*e.g.*, degradation), and other factor (*e.g.*, nature of the polishing surface), and thus the usefulness of the Preston equation is limited. There have been several attempts carried out by various researchers to modify the model so that better wafer level modeling can be developed [Bro81, Bur91, War91, Shi93, Zha99, Tse97, Tse99, Luo98]. These approaches were physically reasonable, but failed to reveal insights into the material removal mechanism.

The second approach is based on the theory of fluid hydrodynamics. During fluid-based wear, abrasive particles impinge on the surface at some velocity and angle. The mechanism is virtually same with the erosion-corrosion process. The energy imparted to the surface from the collisions with the abrasive particles results in strain, weakened bonds and eventually material removal [Ste97]. Runnels and Eyman [Run94] studied the

lubrication and material removal rate of the CMP process. Sundararajan *et al.* [Sun99] estimated the slurry film thickness and hydrodynamic pressure in CMP. This approach assumes slurry erosion to be the main material removal mechanism and negated mechanical abrasion by particles embedded in the surface of the polishing pad.

The third approach makes use of the theory of contact mechanics based on Hertzian indentation. During Hertzian indentation, the abrasive particles are dragged across the surface and act as cutting tools. Yu *et al.* [Yu93] measured the surface roughness of the polishing pad and explored the material removal mechanism based on the distribution of surface asperity heights using the Greenwood and Williamson elastic model [Gre66]. Larsen-Basse and Liang [Lar99] studied possible material removal mechanisms based on experimental data, simple calculations and logical reasoning. They concluded that models, which include synergistic combination of both the chemical effects and the mechanical effects, using a fundamental particle-wafer interactions approach may be more suitable to develop models for CMP polishing. Liu *et al.* [Liu96] analyzed the material removal mechanism based on the rolling kinematics of abrasive particles between the pad and the wafer. Liang and Xu [Lia02] observed that the hydrodynamic lubrication regime was never reached in copper CMP process, thus proposed the contact-polishing mode in copper CMP. Moreover, as the CMP removal mechanism (the chemistry-assisted mechanical abrasion) postulated by Kaufman [Kau91] becomes the basis for recent modeling and analysis of material removal in CMP process, the synergistic effects of mechanical and chemical interactions are formulated into the model [Luo01, Fu01, Luo03, Zha02, Zha03]. However, these are regarded as preliminary due to the challenging issues such as the experimental proofs of microscale and nanoscale

interactions (the wafer-pad-abrasive contact area, chemical kinetics, mechanical properties of the chemically modified surface layer, molecular bonding energy, etc.).

The fourth approach builds on the theories of contact mechanics and fluid hydrodynamics. Yu *et al.* [Yu94] developed a physical CMP model that combines the effects of pad roughness and slurry hydrodynamic pressure. Tichy *et al.* [Tic99] presented a one-dimensional deterministic model to predict the magnitude of measured sub-ambient hydrodynamic pressure in the CMP process. In this approach, mechanical abrasion in CMP occurs in two modes: Hertzian indentation and fluid-based wear. Fluid layer thickness between the wafer and the pad determines whether mechanical removal occurs as Hertzian indentation or fluid-based wear. If fluid layer thickness is low, Hertzian indentation dominates while fluid-wear becomes the main material removal mechanism when the fluid layer thickness is large. Since the thickness of fluid layer varies vastly across the wafer, both mechanisms play a role in different regions of the wafer [Moo99]. However, the roles of slurry particles and chemical reactions in the CMP process were not modeled in this approach. Almost all models mentioned above have several critical limitations: (i) simplifying assumptions without experimental proofs, (ii) fitting parameters to match experimental data, (iii) no measurements of micro and nano-scale effects, (iv) no predictability of slurry performance and (v) no correlation between various output parameters such as surface finish, planarity and selectivity except the material removal rate.

As seen from this brief discussion, chemical mechanical planarization is an extremely complex process. Although a fundamental understanding of the process still does not exist, several studies and patents have demonstrated that satisfactory levels of

planarization of various films can be achieved using well-tailored slurries that are usually prepared empirically at present.

Recently, extensive investigations – abrasive-free polishing (AFP), electro-chemical polishing (ECP), and spin-etch planarization (SEP) – are being conducted to reduce the defectivity (*e.g.*, scratches, dishing, and erosion) during CMP and to remove the drawbacks (*e.g.*, abrasive contamination and cost) of CMP process [Kon00-a, Kondo00-b, Sat01, Fur99, DeB00]. Moreover, in alternative polishing methods, the thickness and the mechanical properties of the chemically modified surface layer play more critical roles in the material removal rate, defectivity, planarization, etc., because the mechanical interaction by abrasives is reduced. Thus, understanding of the change in the mechanical properties of the layer due to the chemical additives as well as the nanoscale interaction between the wafer and chemicals is a stringent requirement for the further enhancements of CMP process.

CHAPTER 3 POTENTIODYNAMIC AND XPS STUDY OF THE CHEMICALLY MODIFIED SURFACE LAYER

Introduction

Copper is poised to replace aluminum as the interconnect conductive material in integrated circuits (ICs). Due to inappropriateness of the reactive ion etching (RIE) for copper, chemical mechanical polishing (CMP) now becomes a critical process in the semiconductor manufacturing [Ste97]. Copper CMP has now been recognized and accepted as the process that is capable of providing the global planarization with a dual-damascene technology to build multilevel interconnects schemes with below quarter-micron lines.

One of the key issues in copper CMP is the development of slurries which can provide high removal rates, good planarity and high selectivity [Rut95]. A number of slurry chemistries have been studied to optimize copper CMP conditions: nitric acid (HNO_3) and hydrogen peroxide (H_2O_2) as oxidizers [Car95, Car01, Kau00-a, Kau00-b], benzotriazole (BTA, $\text{C}_6\text{H}_5\text{N}_3$) as an inhibitor [Kau00-a, Kau00-b, Luo98], citric acid ($\text{HO}_2\text{CCH}_2\text{C}(\text{OH})(\text{CO}_2\text{H})\text{CH}_2\text{CO}_2\text{H}$) as a complexing agent [Kau00-a, Car01, Gru00], etc. It is well known that H_2O_2 being used in all copper CMP slurries as an oxidizer in order to make the stable oxide passive layer on the copper surface. However, it was reported that the copper oxide layer by H_2O_2 forms a non-passive film on the surface [Uhl85, Ogl75, Noy76]. Thus, a corrosion inhibitor is necessary to form the passivated layer and then prevent the surface from further chemical attacks. In addition, a

complexing agent, a surface film forming agent, an organic amino compound and other additives are required to achieve high removal rate and low surface roughness as well as high selectivity.

The passivation layer, the most important key parameter in the metal CMP removal mechanism, is formed on the metal surface as discussed by Kaufman et al. [Kau91]. Biemann et al. [Bie00] have also proved experimentally that a passive layer is necessary to obtain high removal rate as well as low surface roughness in tungsten CMP. In copper CMP, a number of studies have been reported on the oxide layers formed on the copper surface [Mil95, Car95, Her01]; however, a systematic study on the chemical additive effects in case of copper CMP is still necessary to delineate the copper CMP removal mechanism.

In an effort to better understand the copper CMP removal mechanism and further develop the optimal slurry design guideline, initial studies were performed in this Chapter to examine the chemical additive effects on the formation of the chemically modified surface layer on the copper by electrochemistry and x-ray photoelectron spectroscopy (XPS). Copper samples were exposed to various slurry mixtures of H_2O_2 , BTA, and citric acid at different pH. The electrochemistry was used to determine how the different components of the slurry modified the passivity of the copper surface. As chemical additives interact with the copper surface to form the chemically modified surface layer, electrochemical testing of the chemical effects is critical to determine its characteristics. On the other hand, the chemical composition of the layer on the copper surface was determined by XPS measurements. The passivity and chemical composition of the

chemically modified surface layer are the most important parameters to control the CMP performance by balancing the chemical additives.

Experimental

Sample Preparation

For all of the electrochemical experiments, high purity copper foils (Aldrich, 99.9985%) were mechanically polished (grade 2000), dipped in 3% hydrochloride acid (HCl) solution for 1 minute to remove any oxide and organic materials from the copper surface before experiments, and then rinsed for 5 seconds in de-ionized water. Without air drying, samples were immersed immediately into the solution including various chemical additives. The sample was also kept at a cathodic potential in the solution to prevent the formation of the chemically modified surface layer before the measurements. Figure 3-1(a) shows a cross-sectional SEM picture (1.5 μ m Cu/50nm Ta/500nm SiO₂ on silicon wafer) and Figure 3-1(b) shows the existence of the copper oxide layer on the as-received copper wafer observed by TEM. The thickness of the oxide layer is around 45 Å. The result of ellipsometry presented that its thickness was reduced by dipping the samples in the etching solutions as shown in Figure 3-1(c). Among three different etching solutions (0.5% HF, 3% HCl, and 3% HNO₃), it was known that 0.5% HF and 3% HCl solutions are effective to etch the copper oxide layer. But, due to the safety concerns, a 3% HCl etching solution was used in this experiment.

XPS measurements were performed on 1.2 cm by 1.2 cm samples cleaved from an 8 inch diameter copper wafer. All the pre-cleaning processes mentioned above were carried out for all the copper samples except the mechanical polishing to maintain the smooth surface. Samples were dipped for one minute in the solutions of various chemical additive mixtures. Then, they were rinsed for 5 seconds in de-ionized water and dried

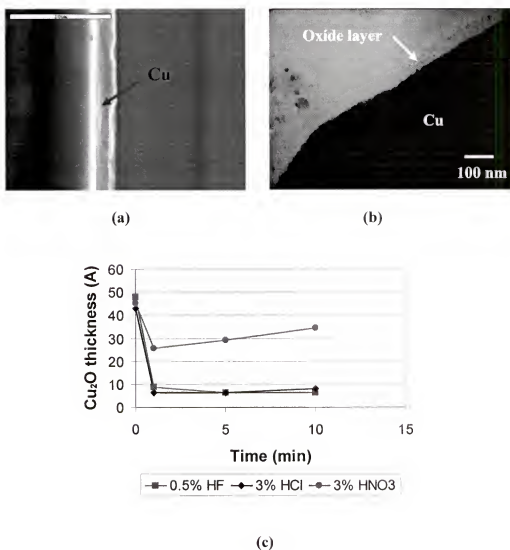


Figure 3-1. A cross-sectional SEM picture of as-received wafer (a); pre-existing oxide layer on the as-received copper wafer observed by TEM (b); and surface layer thickness by dipping copper samples in three etching solutions, measured by ellipsometry (c).

with compressed nitrogen gas for 5 seconds. After drying the sample, it took about 30 seconds to place it into the load-lock chamber of XPS.

Solutions of Various Chemical Additive Mixtures

The chemically modified surface layer on the copper surface is strongly dependent on the chemical additives in the slurry. The chemical additives used to activate the chemical reaction on the surface in this experiment are pH, hydrogen peroxide (H_2O_2) (as an oxidizer for copper), benzotriazole (BTA) (as a copper corrosion inhibitor), citric acid as a complexing agent of copper) and their various combinations. For the concentration experiments, the concentration of hydrogen peroxide was varied between 2 to 10 wt.% by diluting 30 wt.% hydrogen peroxide with de-ionized water; the concentration of BTA was between 0 to 20 mM; and the concentration of citric acid was from 0 to 200 mM. For the pH experiments, the pH was adjusted from 6 to 8 by adding 0.1M nitric acid and 0.1M potassium hydroxide (KOH). Figure 3-2 shows the potential-pH (Pourbaix) diagram of copper-nitric acid/ hydrogen peroxide-water system using Nernst equation.

The reactions with these chemicals are as follows:



It was observed that nitrate ion does not act as an oxidizer of copper for pH values above 4. Therefore, 0.5M potassium nitrate (KNO_3) was used as a supporting electrolyte in the range of pH between 6 and 8 for the electrochemistry measurements.

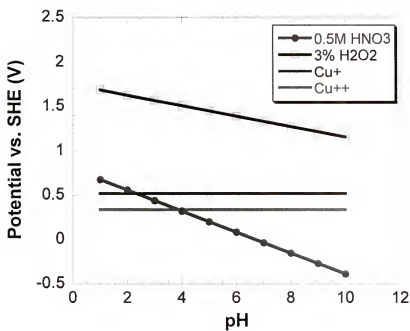


Figure 3-2. Potential-pH diagram of copper-nitric acid/ hydrogen peroxide-water system.

Electrochemistry

In order to characterize the chemical reaction between chemical additives and the copper surface, potentiodynamic polarization measurements, as an electrochemical technique, were used with an Autolab® PGSTAT 30. The potentiodynamic scans were performed at a rate of 1 mV/s, beginning at -0.75 V (vs. SCE) and ending at 0.5 V (vs. SCE). The three-electrode cell was used for the electrochemical experiments. Copper was used as a working electrode with 1 cm² surface area, embedded in a chemically inert resin. A saturated calomel electrode (SCE) was used as a reference electrode. All the potentials reported in this Chapter are related to the SCE potential value (0.2412 V vs. SHE (standard hydrogen electrode) at 25 °C). Also, a spiral wire of a platinum counter electrode was used to increase the surface area of the counter electrode.

X-ray Photoelectron Spectroscopy (XPS)

In order to determine the chemical composition of the chemically modified surface layer on the copper surface after dipping in the solutions, XPS experiments were performed. The XPS technique is highly surface specific due to small mean free path of the photoelectrons that are excited from the solid [Mou95]. Photoelectrons were excited by using non-monochromatized Mg K α x-ray irradiation (1253.6 eV), and the detection angle was normal to the sample surface. The pressure in the ultra high vacuum (UHV) chamber was less than 10⁻⁸ Torr during the measurements. The spectrometer was calibrated against Carbon 1s at 285 eV that is always on the sample surface due to the environmental contamination.

Result and Discussion

The slurry composition is an important factor in the CMP process. Depending on the choice of the oxidizer, the abrasive, and other useful additives, the polishing slurry can be tailored to provide an effective polishing of metal layers at desired polishing rates while minimizing surface imperfection, defects, corrosion, dishing, and erosion. Furthermore, the polishing slurry may be used to provide controlled polishing selectivities to other thin-film materials used in current integrated circuit technology such as an diffusion barrier/ adhesion layer (Ta, Ti, TaN, TiN, WN) of copper [Mue99].

Electrochemical Behavior of Copper

The chemically modified surface layer formation plays a key role in metal CMP removal mechanism. In this regard, as an initial study, the potentiodynamic measurements were carried out in the various chemical environments. Figure 3-3 shows the typical potentiodynamic curve with passivated layer on the metal surface [Wil81]. Region A in Figure 3-3 is the active region in which the metal specimen corrodes as the applied potential is made more positive. At B, further increase in the rate of corrosion ceases and the onset of passivation begins. The loss of chemical reactivity under certain environmental conditions – probably due to the formation of a film on the metal surface – is referred to as specimen passivation. In region C, the current decreases rapidly as the passivation film grows on the metal surface. Region D is the passivation region where the current density is stabilized even though the applied potential is increased due to the stable passivation film in this region. The passivation film begins to break down in region E, the transpassive region. Therefore, it is well known that the potentiodynamic curve, so called Tafel curve, indicates surface film formation and whether the surface film is passive or porous [Ste97]. These two important parameters can be obtained from the

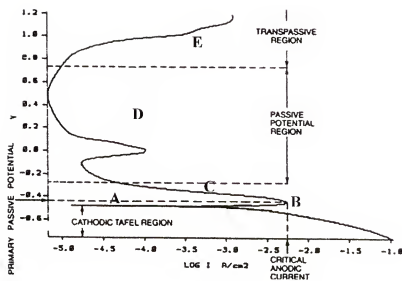


Figure 3-3. The typical potentiodynamic curve with passivated layer on the metal surface.

anodic electrochemical behavior of copper in the polarization curves: open-circuit potential (OCP) value changes and level-off (or decrease in the current density in anodic behavior of the copper) region.

Copper samples were immersed in hydrogen peroxide based solution with various chemical components – pH, hydrogen peroxide, BTA, and citric acid – to characterize the chemical interaction between the chemical additives and the copper surface. Figures 3-4, 3-5, 3-6, and 3-7 show the anodic electrochemical behavior of the copper in these solutions. The corrosion potential and corrosion rate are listed in Table 3-1. The pH effect was presented in Figure 3-4. At pH 6, the corrosion potential (E_{corr}) of copper in the testing solution was 0.178 V, and narrow passivation region was observed in the anodic potentiodynamic curve. However, since the current density was slightly increased with the potential in this region, it is the evidence of the formation of the porous oxide layer on the copper surface. The layer also breaks down at about 0.4 V. According the Pourbaix diagram of copper-water system [Pou74], the cuprous oxide (Cu_2O) is the stable phase at pH between 5 and 12. However, the anodic electrochemical behavior of copper is not in agreement with this observation. As the pH increased, the corrosion potential of the copper was decreased, and the passivation region became narrower and had lower currents. Thus, it indicates the less porous layer formation on the surface at higher pH. Also, these curves did not exhibit the typical peak-shaped active to passive transition because the copper samples have already been passivated. However, relatively higher dissolution rate should be improved to reduce the defect during copper CMP. Moreover, the corrosion potential values measured are in good agreement with the theoretical estimated ones reported by Tamilmani *et al.* [Tam02]. It infers that the

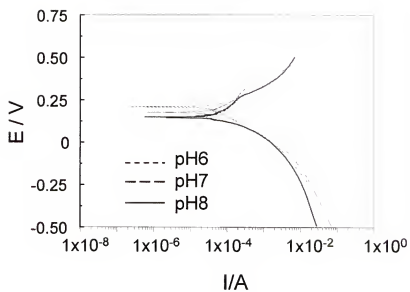


Figure 3-4. The potentiodynamic curves of copper in 5% hydrogen peroxide at different pH.

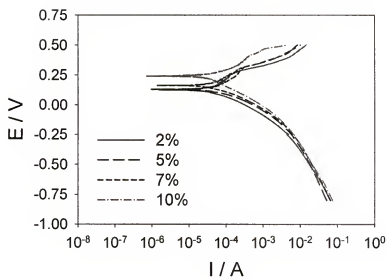


Figure 3-5. The potentiodynamic curves of copper in various concentration of hydrogen peroxide at pH 7.

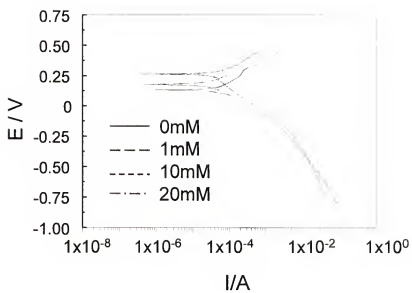


Figure 3-6. BTA concentration effect on the anodic electrochemical behavior of copper in 5% hydrogen peroxide at pH 7.

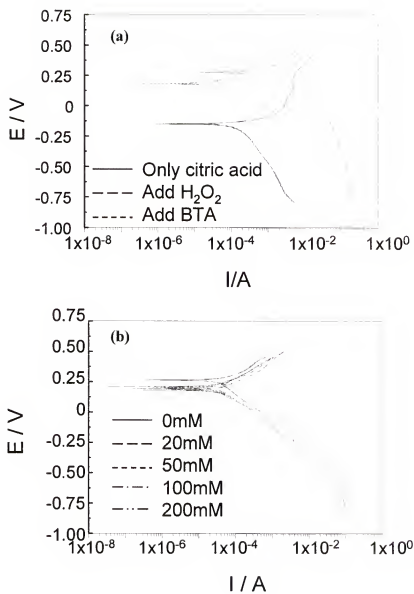


Figure 3-7. The potentiodynamic curves measured in citric acid based solutions (a) and citric effect on the anodic electrochemical behavior of copper in 5% hydrogen peroxide and 10 mM BTA at pH 7.

Table 3-1. Comparison of the potentiodynamic parameters.

Solution Chemistry		E _{corr} (V)	Corrosion Rate (A/min)
5% H ₂ O ₂	pH 6	0.178	15.30
	pH 7	0.13	21.46
	pH 8	0.095	20.26
H ₂ O ₂ at pH 7	2%	0.127	28.61
	5%	0.13	21.46
	7%	0.179	19.75
	10%	0.235	12.17
5% H ₂ O ₂ and BTA at pH 7	1mM	0.193	11.21
	10mM	0.264	7.52
	20mM	0.266	6.45
200mM Citric acid at pH 7		-0.144	69.37
DI Water at pH 7		-0.149	49.60
5% H ₂ O ₂ and 200mM Citric acid at pH 7		0.251	403.92
5% H ₂ O ₂ , 10mM BTA and Citric acid at pH 7	20mM	0.191	13.96
	50mM	0.204	15.52
	100mM	0.208	19.73
	200mM	0.179	18.20

reaction kinetics between the hydrogen peroxide and copper is high to form the oxide layer in the quasi-steady-state potentiodynamic measurements. It should be noted that the passivation region, break-down potential, and corrosion rate (Table 3-1) are wider, higher, and lower at lower pH, respectively. A possible explanation of pH effect is that as the porous layer was formed on the surface at lower pH, the thicker oxide layer was formed in the passive region. It results in charge transfer limitations of reactants or products even though the layer is porous. Thus, lower corrosion current and higher passivation current were observed at lower pH. The detail will be explained in the next Chapter.

Hydrogen peroxide, a commonly used oxidizer in copper CMP slurry, oxidizes the copper surface, and then the copper surface has a reaction with oxygen, resulting in the oxide layer formation (equation (3.2) and (3.4)). Therefore, the concentration of hydrogen peroxide plays a critical role in the slurry chemistry as shown in Figure 3-5. Potentiodynamic curves clearly show the effect of hydrogen peroxide: the corrosion potential was increased, and the corrosion current was decreased, which can infer the formation of the more noble layer on the surface. A similar observation on the decrease in the corrosion current with the concentration of hydrogen peroxide has been described by Hernandez et al. [Her01]. The interesting observation is that the passivation region was not changed by the concentration of hydrogen peroxide. Generally, since the noble layer passivates the metal surface from the chemical attacks, the passivation region is extended [Fis96]. However, the chemically modified surface layers formed during experiments already passivate (but, not fully) the copper surface, resulting in the similar passivation region in the anodic electrochemical behavior of copper. It may result from the fast

reaction kinetics in the transient time regime. Details of this behavior were explained in Chapter 4 using a dynamic electrochemical technique.

To passivate the copper surface, a corrosion inhibitor is necessary as shown in Figure 3-6. BTA, a well-known copper corrosion inhibitor, is chemically adsorbed on the copper surface where it forms a stable and inert layer: Cu-BTA layer at acidic pH and Cu_2O -BTA layer at neutral pH [Ste97]. Another corrosion inhibitors of copper are typically tolytriazole (TTA), imidazole, 5Mercapto-1-Phenyl-Tetazole, α -Benzoinoxime, etc. The corrosion inhibitors have more efficiency in protecting the surface from the chemical attacks when they have asymmetric structure and larger molecular weight. Thus, TTA and BTA are the best inhibitors for copper. As BTA was added in 5 wt.% hydrogen peroxide solution at pH 7, the corrosion rate was reduced from 21.5 Å/min to 6.5 Å/min. Even 1 mM BTA has a remarkable efficiency to reduce the corrosion current by forming Cu_2O -BTA layer. Potentiodynamic curves of 10 mM and 20 mM BTA in 5% hydrogen peroxide are almost identical, indicating that the adsorption of BTA on the copper surface is saturated at around 10 mM BTA. Altura and Nobe discussed that the copper surface coverage of BTA is a linear dependence with the BTA concentration [Alt72]. Their result suggests that in the decrease in the corrosion rate results from a linear adsorption on the copper surface with the concentration of BTA. The corrosion potential was, also, increased with BTA concentration. Thus, higher corrosion potential and significantly lower dissolution rate indicate that the Cu_2O -BTA layer formed uniformly and was protective.

The role of a complexing agent is significant in the CMP performance. A complexing agent enhances the material removal rate, reduces the defectivity, and

controls the selectivity. Moreover, in the nanoscale and microscale interactions in the CMP removal mechanism, a complexing agent plays an important role in the modification of the mechanical properties of the chemically modified surface layer (*e.g.*, density, hardness, and Young's modulus), passivity of the layer, etching of the copper from the surface, and dissolution of abraded materials. Several complexing agents were tested on copper CMP: ammonium hydroxide (NH_4OH) [Car95], citric acid [Kau00-a, Kau01, Watt99], tartaric acid [Kau00-c], ethylenediaminetetraacetic acid, acetic acid, Glycine [Kau00-b], etc. Among them, ammonium hydroxide and citric acid are commonly used in CMP application. Figure 3-7(a) shows the potentiodynamic curves measured in citric acid based solutions. As shown Figure 3-7(a) and Table 3-1, the potentiodynamic curve of copper in citric acid solution was almost matching to DI water. Due to the etching of copper with citric acid, the dissolution rate was slightly increased from 50 Å/min to 69 Å/min. When hydrogen peroxide was added into a solution including citric acid, the dissolution rate was dramatically increased to 404 Å/min. The corrosion potential was also increased due to the formation of the oxide layer. Moreover, as BTA was added to hydrogen peroxide and citric acid solution, the dissolution rate was decreased to 18 Å/min and the corrosion potential remained at the similar range. From these curves, it was clearly shown that citric acid is more effective to etch the oxidized copper than bare copper, whereas BTA can control the citric acid effect by reducing the dissolution rate of copper. Viet [Vie01] discussed that the optimal CMP performance can be achieved by the balance between the passivation due to BTA and the dissolution of abraded material by a complexing agent. Thus, control of the concentration of BTA and citric acid can be a key parameter to perform the optimal CMP condition. In this regard,

various concentrations of citric acid were added into 5% hydrogen peroxide and 10mM BTA solution. Figure 3-7(b) presents the potentiodynamic curves of copper in these mixture solutions. Corrosion potential was marginally changed with the concentration of citric acid. Moreover, the corrosion rate was linearly increased with citric acid until 100 mM. From the result, it can be estimated that even though BTA was presented in the solution, citric acid enhanced the dissolution of copper from the surface. Due to the dissolution of copper with citric acid, no passivation region was observed in the potentiodynamic curve.

Chemical Composition of the Chemically Modified Surface Layer

In order to establish the chemical composition of the chemically modified surface layer, copper samples were exposed to the chemical mixture solutions and analyzed using XPS. XPS analysis allows a valuable distinction between cuprous and cupric species. Data on the Cu 2p_{3/2} line, the Auger line, and O 1s line are listed in Table 3-2 [Der92, Mou95]. A clear distinction between Cu₂O and CuO is also possible due to the satellite line [Kim74, Bru92].

In this experiment, XPS analyses were performed on an as-received copper sample, a 3% HCl pre-treated sample, and samples dipped in 3 different solutions at pH 7 – 5% hydrogen peroxide only; 5% hydrogen peroxide and 10mM BTA; and 5% hydrogen peroxide and 100 mM citric acid – as shown in Figures 3-8 and 3-9. The XPS spectra of the as-received copper surface (Figure 3-8) shows that Cu2p_{3/2} consists mainly of CuO as indicated by the satellite line at a binding energy of 943.2 eV. The presence of this satellite line has been attributed to charge transfer transitions from the ligands (O²⁻ ions for CuO) into the unfilled (*d*⁹) valence level of Cu⁺² ion [Kim74]. For Cu₂O, which have a filled (*d*¹⁰) ground state configuration of Cu⁺¹ ion, such transition cannot occur and no

Table 3-2. Reference XPS parameters for copper and copper compounds [Der92, Mou95].

Oxidation State	Cu2p _{3/2} Binding Energy (eV)	Cu Auger LMM Energy (eV)	O1s Binding Energy (eV)
Cu	932.6	334.9	
Cu ₂ O	932.6	336.8	530.4
CuO	933.7	335.7	529.4
Cu(OH) ₂	935.1	337.0	531.3

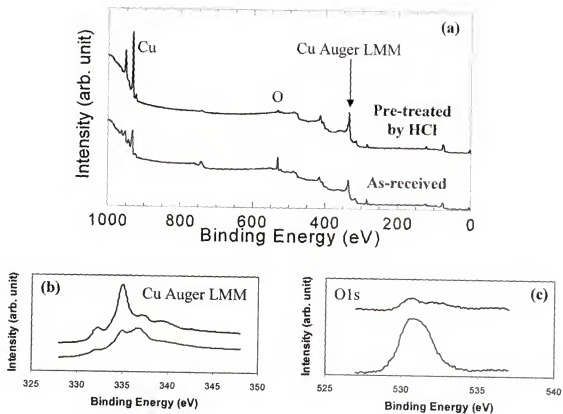


Figure 3-8. The XPS spectra of the as-received and pre-treated copper surface: (a) surface analysis, (b) Cu Auger LMM line, and (c) O1s line on the copper samples.

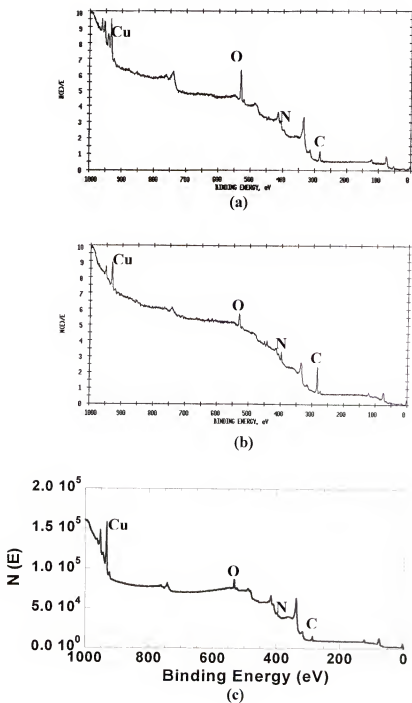


Figure 3-9. XPS analyses on copper samples dipped in 3 different solutions at pH 7: (a) 5% hydrogen peroxide only; (b) 5% hydrogen peroxide and 10mM BTA; and (c) 5% hydrogen peroxide and 100 mM citric acid.

satellite is observed. Moreover, Cu_2O was characterized by the shift of the copper Auger LMM energy of 336.6 eV and by O1s binding energy of 530.6 eV. $\text{Cu}(\text{OH})_2$ on the surface was absent in XPS spectra, indicated by O1s binding energy. The oxide layer on the copper surface has been commonly described as a dual film [Spe85, Mil69]. CuO is formed by the precipitation mechanism on the Cu_2O surface. Therefore, the result indicates that the surface layer on the as-received copper wafer consists of Cu_2O and CuO dual layer. To remove the initial oxide layer on the surface, pre-treatment was performed: dipping a sample into 3% HCl solution for 1 minute. From the XPS spectra of a pre-treated sample, no satellite line was observed, indicating no CuO layer on the surface. Because the $\text{Cu}2p_{3/2}$ binding energies and peak widths of Cu^0 and Cu_2O are very similar (see Table 3-2), the analysis of the Cu Auger LMM line and O1s line is necessary. In the Auger line, two peaks were observed at 334.9 eV and 337.1 eV, representing metallic copper and Cu_2O , respectively. On the other hand, in O1s line, Cu_2O was characterized by the binding energy of 530.6 eV and its intensity was very weak. Moreover, the adsorbed water was found at the binding energy of 531.9 eV. The observation of Cu_2O and water on the copper surface showed either that the air exposure of the sample before XPS measurement caused the oxidation of copper or that the oxide layer was formed when the sample was rinsed by DI water after HCl dipping. Thus, it was found that 3% HCl solution is good etchant of copper oxide layer. In further experiments, HCl pre-treatment of the samples was always conducted to eliminate the artifacts from the initial oxide.

At first, a copper sample was dipped in 5% hydrogen peroxide solution. The XPS spectra of Figure 3-9(a) shows that CuO was formed on the surface that was indicated by

the satellite line of $\text{Cu}2p_{3/2}$ at 943.2 eV with high intensity. Also, Cu_2O was characterized by O1s binding energy of 530.4 eV and by Cu Auger LMM binding energy of 336.8 eV. Thus, it was observed that the oxide structure formed in hydrogen peroxide solution is the same as one on the as-received copper sample. On the other hand, from the intensity of the satellite line of $\text{Cu}2p_{3/2}$ and O1s, it could be inferred that the CuO layer formed in the hydrogen peroxide solution is thicker than the as-received sample. Speckmann *et al.* [Spe85] suggested that as CuO forms, Cu_2O underneath also grows simultaneously at a different rate. Thus, the copper oxide layer has the dual-structure with thicker thickness in hydrogen peroxide solution.

When BTA was added to the solution of hydrogen peroxide, XPS spectra obviously shows no satellite line of $\text{Cu}2p_{3/2}$, indicating that no CuO was present on the surface due to the effect of BTA, shown in Figure 3-9(b). As O1s binding energy was observed at 530.6 eV, Cu_2O was characterized on the surface. Its intensity was very weak, inferring that the thickness of Cu_2O was very thin. Moreover, the peak of N1s binding energy of 299 eV and relatively high intensity of C1s clearly indicated that BTA was chemically adsorbed on the copper oxide surface. As a result, we can infer that the thin Cu_2O -BTA layer was formed on the copper surface.

As citric acid acts as a complexing agent of copper, it increased the corrosion rate significantly with hydrogen peroxide (see Table 3-1). From Figure 3-9(c), the $\text{Cu}2p_{3/2}$ line and its satellite were observed at 933.6 eV and 943.3 eV with the very weak intensity, indicating thin CuO on the surface. Cu_2O and $\text{Cu}(\text{OH})_2$ was also revealed from O1s binding energy of 530.4 eV and 531.3 eV, respectively. Moreover, C1s of carboxylic acid group ($-\text{COOH}-$) was found at 288 eV, indicating citric acid on the surface. After surface

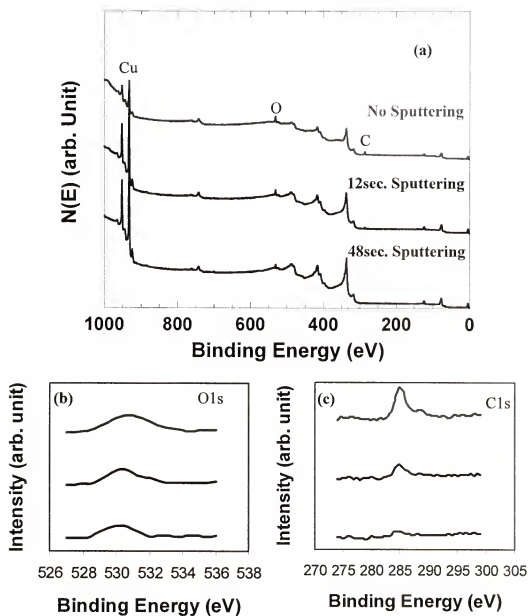


Figure 3-10. The XPS analysis on a copper sample, dipped in 5% hydrogen peroxide and 100 mM citric acid at pH 7 for 1 minute, with different sputtering time.

sputtering with Ar^+ ions for 12 seconds, $\text{Cu}(\text{OH})_2$, and citric acid were vanished as shown in Figure 3-10. If the sputtering rate of a copper oxide layer is assumed to be similar to one of Ta_2O_5 (sputtering rate is 1.6nm/min [Vie01]), sputtered thickness is around 3 Å where $\text{Cu}(\text{OH})_2$ and citric acid existed. Interestingly, CuO still existed after 48 sec sputtering (Figure 3-10(a)), indicating that the thick CuO was formed on the surface with an assistance of citric acid. Hence, CuO/Cu₂O is the main component of an oxide layer exposed to 5% hydrogen peroxide and 100 mM citric acid solution. Also, citric acid was not adsorbed on the surface. The data of XPS analysis suggested that citric acid etches not only the pristine copper, but also the copper oxide layer – especially, cuprous oxide – that was formed by the reaction with hydrogen peroxide. After copper oxide is formed on the surface by hydrogen peroxide, it reacts to citric acid in the solution, resulting in the very high corrosion rate (see Table 3-1) when a corrosion inhibitor is not presented in the solution. From the result, we can infer that the role of the complexing agent in the slurry for copper CMP is not only the dissolution of abraded materials, as known, but the etch on the copper oxide.

Summary

The chemical additive effects on the formation of the chemically modified surface layer on the copper surface have been investigated. As a result of the electrochemistry and XPS analysis, the basic roles of the chemical additives were verified. At first, hydrogen peroxide is an effective chemical to oxidize the copper. Also, when hydrogen peroxide is used in the solution, the copper surface is easily covered by thick Cu₂O/CuO dual layer and low corrosion rate. On the other hand, BTA enhances the passivity of the surface by the formation of Cu₂O-BTA layer on the surface, indicated by lower corrosion rate. Finally, the corrosion rate and XPS analysis of a sample subjected in the solution

with citric acid showed that pristine copper and copper oxide reacts to citric acid, and then copper-citric acid complex is formed in the solution (not on the copper surface). As seen in the summary of the results, the synergistic effect by the interaction of individual chemical additives plays an important role in the electrochemical behavior of copper. In the next Chapter, the more detail experiments were conducted by chronoamperometry with respect to the transient kinetics when the chemically modified surface layer is formed. Chapter 5 presents the mechanical properties of the oxide layer measured by the nanoindentation. The correlation of the CMP performance with the results of the electrochemistry and the nanoindentation would be described in Chapter 6.

CHAPTER 4

THE KINETICS OF THE FORMATION OF THE CHEMICALLY MODIFIED SURFACE LAYER DURING COPPER CMP WITH *IN SITU* ELECTROCHEMISTRY

Introduction

Chemical mechanical polishing (CMP) has been recognized as the only technology to eliminate topographic variation and achieve wafer level global planarization for ULSI circuits. However, despite its extensive utilization, process control in CMP remains at an empirical stage because the fundamental mechanisms underlying the polishing process have yet to be fully understood. Since Preston presented the first empirical mechanical model, researchers have devoted their efforts to modify the standard Preston equation [Pre27, Bro81, Ste97].

To delineate the CMP removal mechanism and to further develop more quantitative and predictive models, it is necessary to understand the mechanical and chemical interactions encountered during CMP. For example, the wafer-pad contact area, the thickness and physical properties of a chemically modified surface layer, and the fractional surface coverage of abrasives in the wafer-pad-abrasive interface, etc.

The mechanical interactions have been investigated extensively [Yu93, Bas02, Cho01]. The wafer-pad contact area during CMP was calculated theoretically [Yu93] and measured by Fourier Transform Infrared Spectroscopy (FTIR) [Bas02]. The fractional surface coverage of abrasives in the wafer-pad-abrasive interface was also determined by *in situ* friction force measurements [Cho01]. Based on the contact mechanics and abrasive wear, Zhao *et al.* [Zha99] reported the contact based CMP removal model.

However, the chemical interaction has not been discussed due to its complexity. More importantly, models fail to include the chemical effects, which are synergistic with mechanical effects and cannot be excluded from modeling work. Recently, several approaches have been done to include the chemical interactions into the model [Luo01, Fu01, Luo03, Zha02, Zha03] as described in Chapter 2. However, these are regarded as preliminary due to the challenging issues such as the experimental proofs of microscale and nanoscale interactions.

The investigation of the chemical interaction between the substrate (e.g., copper) and chemicals included in the slurry has been carried out in two aspects: the formation of the chemically modified surface layer on the surface of metal typically by x-ray photoelectron spectroscopy (XPS) [Her01, Xu00] and the passivation study by potentiodynamic electrochemical measurements [Kne97, Ste98, Bie98] as also examined in Chapter 3. These measurements can provide the static information such as the passivity, corrosion rate, and chemical composition of the chemically modified surface layer, which are very important to screen the candidates of chemical additives; however, the results from these measurements cannot be correlated to the CMP performance due to a limitation of thickness resolution and time-resolved information.

The removal mechanism of metal during CMP involves the formation of a passivation layer on the metal surface due to the oxidizing nature of the slurry, and its mechanical abrasion from the abrasives included in the slurry. The polishing pad subsequently removes the abraded material. Simultaneously, the pristine metal, immediately exposed to the slurry, is repassivated [Kau91, Vie01]. Figure 4-1 shows the

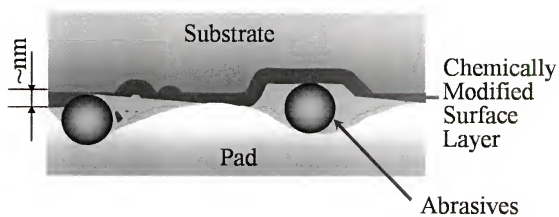
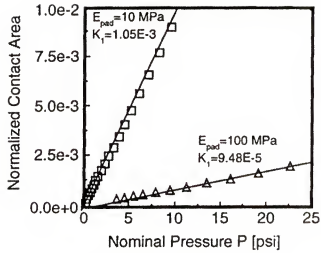


Figure 4-1. Schematic of metal CMP removal mechanism.

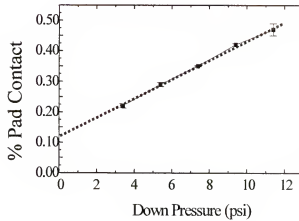
schematic of the CMP removal mechanism in the nano-scale interaction scheme.

Obviously, as indicated by this figure, the passivation of metal in the slurry plays a very important role in CMP performance, either by forming native metal oxides on the surface using oxidizers such as H_2O_2 , KIO_3 , $\text{K}_3\text{Fe}(\text{CN})_6$, etc., or by forming chemically adsorbed layers (e.g., Cu-BTA layer) using organic corrosion inhibitors. As a proof of the formation of the passivation layer on the metal surface, the static potentiodynamic measurements showed that the static oxidation rates of metal are one to three orders of magnitude lower than the experimentally observed CMP removal rates [Ste98, Bie98, Ste99, Kne97]. This large discrepancy between the static oxidation rate and the removal rate of metal is a strong indication of the formation of a passivation layer on the metal surface.

To achieve a high removal rate of copper, the surface layer formation should be relatively fast because of the time scale of the particles interacting with surfaces. According to Yu's model [Yu93] and Basim's experimental results [Bas02] in Figure 4-2, it was shown that the contact area between the pad and wafer was approximately 5×10^{-4} to 4×10^{-3} times the nominal area of the wafer. Thus, it has been estimated that the time interval between consecutive particle interactions at a particular point on the surface is in the range of 10 to 400 milliseconds [Sin02]. It depends on the particle concentration, size, the pad contact area, and the nature of particulate dispersions. Therefore, the dynamic nature of the chemically modified surface layer and the thickness formed between consecutive abrasion interactions are key issues to understand CMP removal mechanism and performance such as polish rate, planarity, and defectivity. As shown in Figure 4-1, a thin chemically modified surface layer is formed in millisecond range and then removed



(a)



(b)

Figure 4-2. The contact area between the pad and wafer was measured by theoretical approach [Yu93] and experimental approach [Bas02]. These two results showed approximately 10^{-4} times the nominal area of the wafer.

by abrasives. The kinetics and thickness of this layer strongly depends on the chemicals included in the CMP slurry.

In this regard, the objective of this chapter is to understand the dynamic nature of the formation of the chemically modified surface layer on copper, which includes the rate of layer formation and passivation as a function of different chemistries. As the kinetics of the chemically modified surface layer is strongly dependent on the electrochemical behavior of the copper, electrochemical measurements (chronoamperometry) were conducted. Moreover, *in situ* measurements are necessary because the transient behavior of CMP taking place in less than one second can be correlated to the CMP performance. Other instruments, XPS, XRR, VASE, TEM, etc., are usually using to measure the thickness of the layer. However, they cannot provide information of the kinetics of the layer formed in less than one second without any artifact. Based on the results of the *in situ* electrochemistry, the formation kinetics and the thickness of the chemically modified surface layer were observed with various chemicals and their respective concentrations.

Experimental

Chronoamperometry

The chemical interactions with copper were measured and analyzed using chronoamperometry. Figure 4-3 shows the typical curve of chronoamperometry with the passivation process. Chronoamperometry is a technique that measures the decrease in current with time at a given anodic potential (Figure 4-3(a)) due to the formation of the passivated layer on the surface as shown in Figure 4-3(b). Thus, this technique can provide valuable time-resolved information such as the rate of passivation from the current decrease with time and the layer thickness that is related to the area below current curve. In this study, chronoamperometry as an electrochemical technique was used *in situ*

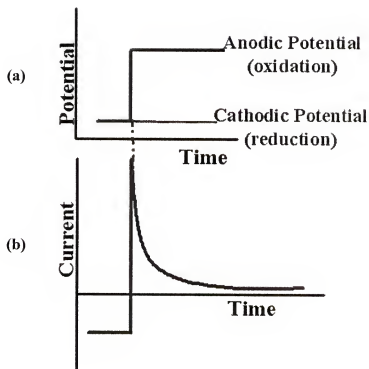


Figure 4-3. The typical curve of chronoamperometry with the passivation process.

with a short rise-time (< 2 microsecond) potentiostat instrument (Autolab[®] PGSTAT 30 with FRA2 modules) to investigate the formation and kinetics of the chemically modified surface layer on the copper surface in the millisecond time range.

A schematic illustration of the electrochemical measurement setup is shown in Figure 4-4. A three-electrode cell was used. High purity copper foils (99.9985%) were employed as a working electrode. Copper samples were pre-polished mechanically and dipped in 3% HCl solution to remove any oxide and organic materials from the copper surface before experiments. The sample was also kept at a cathodic potential in the solution to prevent the formation of the chemically modified surface layer before applying an anodic potential. Since the magnitude of the current depends on the applied potential, it is critical to choose a potential that can simulate the condition of the CMP process. Biemann *et al.* [Bie00] observed that the electrochemical polarization can be used to simulate the oxidizing action of a corrosive environment by applying open circuit potential (OCP) as shown in Figure 4-5. Thus, the OCP obtained from the potentiodynamic measurements was applied in this experiment. As a reference electrode, a saturated calomel electrode (SCE) was used during electrochemical measurements, and all values reported were referred to the SCE potential (0.2412 V vs. SHE (standard hydrogen electrode) at 25 °C). In addition, as current plays a critical role in this study, a spiral wire of a platinum counter electrode was used to increase the surface area of the counter electrode.

Solution Chemistry

The chemically modified surface layer on the copper surface is strongly dependent on the chemical additives in the slurry. For example, Cu₂O and CuO dual oxide layer is

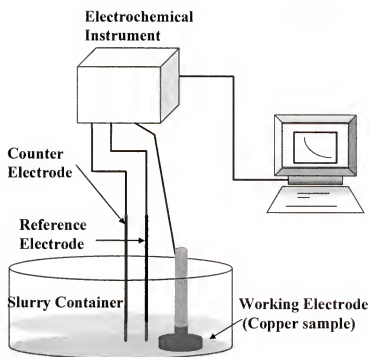


Figure 4-4. A schematic illustration of the electrochemical measurement setup.

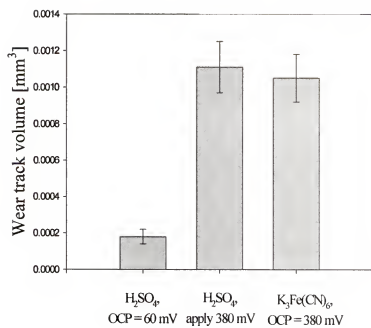


Figure 4-5. Equivalence between the oxidizer action and the applying an anodic potential [Bic00].

formed on the copper surface in hydrogen peroxide (H_2O_2) solution, while cuprous oxide-benzotriazole (BTA) layer is formed by adding BTA in H_2O_2 solution (details in Chapter 3). The chemical additives used to activate the chemical reaction on the surface in this experiment are hydrogen peroxide (H_2O_2) (as an oxidizer for copper), benzotriazole (BTA) (as a copper corrosion inhibitor), pH, citric acid (as a complexing agent of copper), and their variable combinations. All are typical of the chemicals used in the copper CMP. A supporting electrolyte, 0.5M potassium nitrate (KNO_3), was also used in the range of pH between 6 and 8. The pH was adjusted using 0.1M nitric acid and 0.1M potassium hydroxide.

Characterization of the Layer

Potentiodynamic measurements were also used to measure the dissolution rate of copper in the various chemical solutions. In addition, to characterize the chemically modified surface layer formed in the different chemical conditions, variable angle spectroscopic ellipsometry (VASE) and x-ray reflectometry (XRR) were used.

VASE is a very sensitive measurement technique by nondestructive means that uses polarized light to characterize thin films, surfaces, and material microstructures. It determines the thickness and optical properties in multilayered structure from the determination of the relative phase change, Psi and Delta, in a beam of reflected polarized light. All measurements were made with a J. A. Woollam M-88® variable angle ellipsometry, with the angle of incidence set of 35°.

XRR measurement is a non-destructive and non-contact technique for thickness determination between 2 – 200 nm with a precision of about 1 – 3 Å. In addition to the thickness measurement, density and roughness of films are also characterized by XRR.

Philips X'Pert[®] x-ray diffraction system was used for XRR measurements in this experiment. The details in the principle of VASE and XRR have been report in ref [Woo99, Joh99, Rus02].

Results and Discussion

The chemically modified surface layer formation plays a key role in metal CMP removal mechanism (formation of a passivation layer, mechanical abrasion of this layer, then re-formation of a passivation layer). Thus, the material removal rate and surface defects are a function of the kinetics and thickness of the chemically modified surface layer on the metal surface. In this regard, the copper samples were subjected to various chemical environments (oxidizers, inhibitors, and complexing agents) used in CMP to measure the formation kinetics and the thickness of this layer using chronoamperometry. Typically, oxidizers such as H_2O_2 , potassium iodate (KIO_3), etc. are added to metal slurries to form a thin oxide passive layer. The thin oxide surface layer can be naturally passivating, as in the case of tungsten that forms a thin passive layer without the aid of passivating agents [Bie98]. However, in the case of copper, chemical additives such as benzotriazole (BTA) have to be added to the slurry to passivate the growing oxide layer.

Figure 4-6 shows the transient electrochemical response of the copper surface during 50 sec when exposed to four slurry conditions: (i) BTA only; (ii) 5 wt.% H_2O_2 ; (iii) 5 wt.% H_2O_2 and 10 mM BTA; and (iv) 5 wt.% H_2O_2 , 10 mM BTA, and 200 mM citric acid. In the absence of any secondary reaction, the current delivered from a conductive surface during experiments is directly proportional to the quantity of the formation of the chemically modified surface layer. Table 4-1 shows the static etch rates that were measured from the potentiodynamic measurements (recalled from Chapter 3).

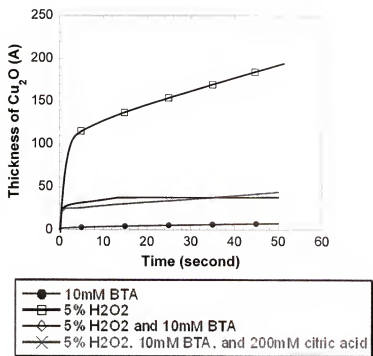


Figure 4-6. The transient electrochemical behavior of the copper surface during 50 seconds when exposed to four slurry conditions: (i) BTA only; (ii) 5 wt.% H_2O_2 ; (iii) 5 wt.% H_2O_2 and 10 mM BTA; and (iv) 5 wt.% H_2O_2 , 10 mM BTA, and 200 mM citric acid.

Most of the chemical compositions induced the low static etch rates (around 1 nm/min).

These low static etch rates indicate that the dissolution of the copper can be negligible in terms of the kinetics and thickness of the chemically modified surface layer. Therefore, to measure the thickness from the integrated current, it was assumed that the current went towards the formation of the chemically modified surface layer. Thus, thickness was calculated using the Faraday's law of electrolysis [Fon86], which is as follows:

$$I = Q/t \quad (4.1)$$

$$Thickness = [Q/n \cdot F] \frac{M}{\rho \cdot A} \quad (4.2)$$

where I is the current, Q is total charge, t is time, n is the electrochemical equivalent, F is the faraday coefficient (96400 Coulomb), M is the molecular weight of the surface layer, ρ is the density of the surface layer, and A is area of the working electrode.

The figure shows that when only BTA was used, the passivation kinetics of the chemically modified surface layer – copper-BTA layer [Car95] – was the fastest among variable slurry conditions, resulting in very thin surface layer formation (less than 10 Å). When only hydrogen peroxide was used in solution, a relatively thicker layer ($\text{Cu}_2\text{O}/\text{CuO}$ dual oxide layer) was formed. However, it was not completely passivating the copper surface and grew with time. When BTA was further added to hydrogen peroxide solution, a passivating thin layer (thickness of around 38 Å) was formed on the surface, resulting in lower dissolution rate shown in Table 4-1. Moreover, when citric acid was introduced in the mixture solution of hydrogen peroxide and BTA, the passivation kinetics and the

Table 4-1. Comparison of corrosion rate.

Solution Chemistry		Corrosion Rate (A/min)
5% H ₂ O ₂	pH 6	15.30
	pH 7	21.46
	pH 8	20.26
H ₂ O ₂ at pH 7	2%	28.61
	5%	21.46
	7%	19.75
	10%	12.17
5% H ₂ O ₂ and BTA at pH 7	1mM	11.21
	10mM	7.52
	20mM	6.45
200mM Citric acid at pH 7		69.37
DI Water at pH 7		49.60
5% H ₂ O ₂ and 200mM Citric acid at pH 7		403.92
5% H ₂ O ₂ , 10mM BTA and Citric acid at pH 7	20mM	13.96
	50mM	15.52
	100mM	19.73
	200mM	18.20

thickness of the copper surface layer are almost identical to the results of the mixture of hydrogen peroxide and BTA. The copper surface was, however, not passivated with this layer, resulting in a slight increase in the thickness of the layer. This behavior was also observed in potentiodynamic measurements in Chapter 3: lower corrosion potential and higher corrosion current, indicating that less noble layer was formed with citric acid.

To verify the result of the electrochemical chronoamperometry measurement, x-ray photoelectron spectroscopy (XPS) was carried out. As a dipping solution, the mixture of 5 wt.% hydrogen peroxide and 10mM BTA was used. The passive layer is formed on the copper surface in this solution, thus it could minimize the further oxidation of the copper surface in the air exposure. Figure 4-7 shows XPS analyses on a copper sample, dipped in 5% hydrogen peroxide and 10 mM BTA at pH 7 for 50 seconds, before and after surface sputtering for 2 minutes. In $\text{Cu}2p_{3/2}$ line, no satellite line was observed, indicating no CuO layer on the surface. Cu_2O and nitrogen-oxygen bonding were characterized by $\text{O}1s$ binding energy of 530.3 eV and 532.5 eV, respectively. Interestingly, adsorption of BTA on the surface was revealed by $\text{C}1s$ carbon-nitrogen binding energy of 285.3 eV and by $\text{N}1s$ binding energy of 400.7 eV. After surface sputtering for 2 minutes, $\text{O}1s$ nitrogen-oxygen bonding and $\text{N}1s$ from BTA were abruptly diminished, whereas $\text{Cu}2p_{3/2}$ and LMM Auger lines showed higher intensities. Accordingly, when BTA was added in hydrogen peroxide solution at pH 7, BTA was adsorbed on Cu_2O surface by the reaction between nitrogen in BTA and oxygen in the oxide layer. Figure 4-8 shows that comparison of atomic weight % of several elements before and after sputtering. Atomic sensitivity factors of copper, carbon, oxygen, and nitrogen were used to estimate the atomic wt.% [Wag81]. After the surface sputtering with Ar^+ for 2 minutes, atomic

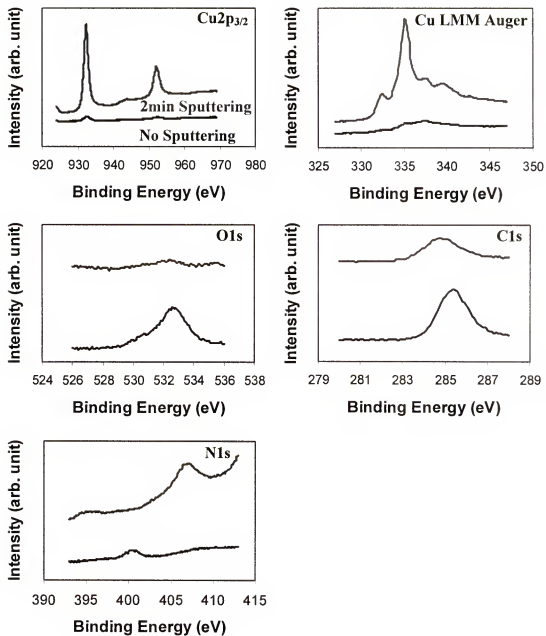


Figure 4-7. The XPS analyses on a copper sample, dipped in 5% hydrogen peroxide and 10 mM BTA at pH 7 for 50 seconds, before and after surface sputtering for 2 minutes.

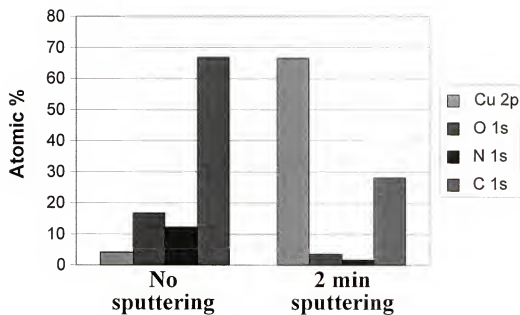


Figure 4-8. Comparison of atomic weight % of several elements before and after surface sputtering on a copper sample, dipped in 5% hydrogen peroxide and 10 mM BTA at pH 7 for 50 seconds.

weight % of oxygen and nitrogen were decreased by a factor of six. Also, sputtering rate of cuprous oxide was assumed to be similar to that of tantalum(V) oxide (Ta_2O_5), which is 1.6 nm/min [Vie01]. From a result, it was estimated that the thickness of the chemically modified surface layer was approximately between 32 Å and 50 Å, which was in agreement with the thickness (38 Å) estimated from the electrochemical measurement. This concurrence shows that chronoamperometry is an accurate technique to simulate the thickness of the surface layer formed during CMP, as well as to resolve the time information.

The dimension of the surface layer, which interacts with the mechanical component of the slurry, should be maintained at an optimal value. Too thin a layer will lead to mechanical polishing, while a thick layer ($> 2\text{-}10$ nm) will lead to loss of planarization capability of the slurry [Vie01]. Moreover, it should be kept in mind that the time to reach surface passivation should be kept as short as possible (typically, in the millisecond range). To achieve a high removal rate (compared to a purely mechanical action of particles), the surface layer formation should be relatively rapid because of the time scale of the particle interactions with surfaces. It has been estimated that the time interval between consecutive particle interactions at a particular point on the surface is in the range of 0.01 to 0.4 seconds, depending on the particle concentration, size, pad contact area, and the nature of particulate dispersions. Under optimum conditions, the surface passivation time should be much less than the average interaction time between the particles. As the thickness of this layer has to be kept in the nanometric dimensions, a high surface reaction rate followed by rapid passivation is needed. Chemicals such as oxidizers and other additives have to be adjusted to control this reaction rate and the

surface passivation. Figure 4-9 shows the rate of surface layer formation in copper during 0.065 sec as a function of different chemicals used in the slurry. The same *in situ* electrochemical chronoamperometry technique with the microsecond resolution was used to study the reaction kinetics on the surface. The figure shows that depending on the chemicals used, the formation rate of the chemically modified surface layer on the surface was varied. If only water at pH 8.0 was used, a thin layer was formed. However, the slope of the curve was not consistent, but changed with time. It is indicated that the decrease in current was controlled by at least two chemical reactions such as the oxide formation on the surface and the dissolution of copper. Moreover, from the slope of current decrease in Figure 4-9(a) and the static etch rate of water in Table 4-1, it was found that the reaction kinetics on the copper surface was primarily controlled by the dissolution of copper. Therefore, the thickness obtained in water includes the dissolved copper thickness. The actual thickness of the chemically modified surface layer is thinner than an estimated value. With 10 mM BTA only, very thin layer (less than 2 Å) was formed due to the fast passivation kinetics. CMP with this layer was expected to show mechanical polishing behavior (direct interaction of particle with the copper surface, which can cause the low removal rate and high defectivity) because the thickness of this layer is thinner than the indent depth of the abrasive particles. On the other hand, if using hydrogen peroxide, the reaction kinetics of the oxide layer was much faster (Figure 4-9(a)). With 5% hydrogen peroxide, the initial reaction kinetics exceeded 120 nm/sec (Figure 4-9(b)), thus it is high enough to achieve the desired polish rates. When BTA was added in 5% hydrogen peroxide solution, the initial reaction kinetics was not changed; however, it made a significant difference in longer time scale of the process as shown in

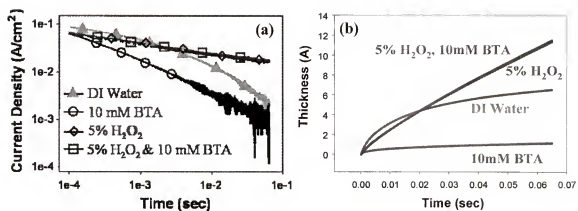


Figure 4-9. The electrochemical response of copper during 65 millisecond as a function of different chemicals used in the slurry at pH 8.

Figure 4-6. Accordingly, it was clearly known that when hydrogen peroxide was used in the solution, the chemically modified surface layer in millisecond range was not $\text{Cu}_2\text{O}/\text{CuO}$ dual layer, but just Cu_2O . CuO layer on Cu_2O is formed by precipitation mechanism after the critical thickness of Cu_2O , which limits the current flow from the surface in the solution, is reached. Thus, the thickness value shown is of the cuprous oxide layer. It should be noted that the thickness of the cuprous oxide layer could not represent the CMP removal rate even though the entire layer was removed by abrasives during CMP. It is due to the volume difference between the copper ($\rho = 8.92 \text{ g/cm}^3$) and the cuprous oxide ($\rho = 6.0 \text{ g/cm}^3$). The actual reacted copper thickness is 0.67 times lower. Figures 4-6 and 4-9 also show that during CMP, the thickness of the surface layer has to be optimized to ensure the optimum removal, good planarity, and scratch-free.

In regard to the chemical effect on the passivation kinetics and thickness of the chemically modified surface layer, the concentration effect of the individual chemical additives – the pH of the slurry, hydrogen peroxide, BTA, and citric acid – was also investigated as shown in Figures 4-10, 4-14, 4-17, and 4-19.

Even though the oxide layer is the stable phase between pH 6 and 8 in Pourbaix diagram [Pou74], the kinetics of the formation of the oxide layer was varied in this pH range. As shown in Figure 4-10(a), the passivation kinetics at higher pH was slightly faster than at lower pH, resulting in slower reaction kinetics on the copper surface. Figure 4-10(b) shows that the thinner oxide layer was caused from the faster passivation rate and the slower reaction rate. To characterize the oxide layers formed at various pH conditions, variable angle spectroscopic ellipsometry (VASE) and x-ray reflectometry (XRR) were used. The result of VASE in Figure 4-11 shows that the lower void concentration in the

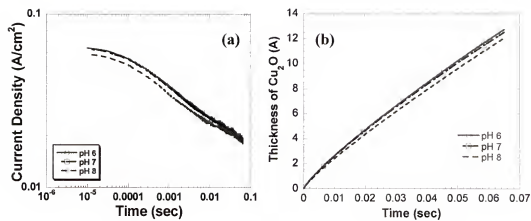


Figure 4-10. The effect of pH on the transient behavior of the copper in 5% H_2O_2 solution.

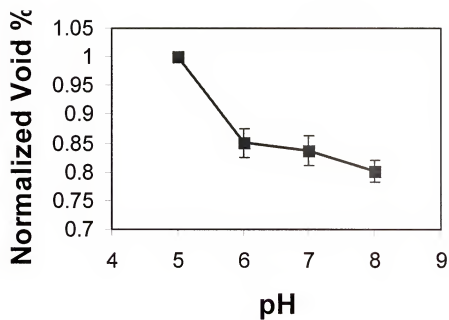


Figure 4-11. Normalized void concentration in Cu_2O layer on the samples dipped in 5% hydrogen peroxide at different pHs.

oxide layer was observed on the copper sample dipped in the solution of high pH. This result may indicate faster passivation kinetics in high pH. However, this information was measured by ignoring the surface roughness. Even though the same surface layer was formed on the rough and smooth copper surface, the rough surface can show the more void content than the smooth surface. To verify the hypothesis, surface roughness was measured by the surface profilometer (Tencor Alpha-Step[®]). The scan size was 100 μm and the roughness values were average of 10 scans. As observed in Figure 4-12, surface roughness (Rms) of the copper samples was slightly changed due to the various reaction kinetics when the oxide layer was formed at different pHs. Because of the deviation of the surface roughness, the origin of the different void concentration on the oxide layer could not be clearly defined. XRR was also conducted to further understand the characteristics of the oxide layer without the artifact of the surface roughness. All the layer parameters, such as the thickness and roughness from the results of *in situ* electrochemical chronoamperometry measurements and the surface profilometer, were used to simulate the experimental results. Figure 4-13 shows the XRR measurements and simulations of the cuprous oxide layer on the copper surface. The oxide layer was formed in 5 wt.% hydrogen peroxide solution at different pH conditions. A shift in the total reflection edge (so called the critical angle, θ_c) is apparent, which implies a change in density. By applying Snell's law and small angle approximations, the critical angle can be expressed as

$$\theta_c \approx \sqrt{C \cdot \rho} \quad (4.3)$$

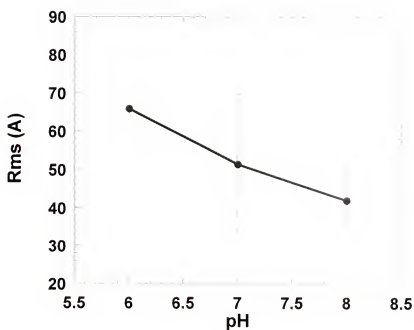


Figure 4-12. Surface roughness (RMS) of the copper samples dipped in 5% hydrogen peroxide at different pHs.

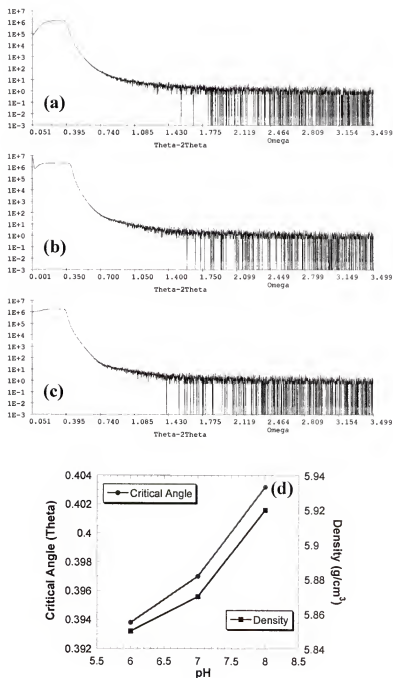


Figure 4-13. XRR measurements ((a), (b), and (c)) and simulations (d) of the cuprous oxide layer on the copper surfaces that were dipped in 5% hydrogen peroxide at different pH: (a) pH 6, (b) pH 7, and (c) pH 8.

where C is the constant as a function of x-ray wavelength, the number of electrons per atom and atomic weight and ρ is the density of the surface layer. This equation expressed that the higher critical angle results from the higher density of the layer as represented in Figure 4-13(d). From the result, it was observed that the oxide layer formed at higher pH is denser than that formed at lower pH. It was also indicated that lower dissolution rate and faster passivation kinetics at higher pH was induced from the denser surface layer on the copper surface. Therefore, it is expected that copper removal during CMP at higher pH would be lower than at lower pH due to the formation of the thinner and denser oxide layer on the copper surface.

Hydrogen peroxide is one of the chemicals widely used in copper CMP as an oxidizer. Figure 4-14 shows the effect of hydrogen peroxide concentration on the formation kinetics of the cuprous oxide layer in short time regime. From Figure 4-14(a), it was observed that the passivation rate was increased with the concentration of hydrogen peroxide. On the other hand, the growth of the Cu_2O layer was linear with time in all concentrations of hydrogen peroxide solution as shown in Figure 4-14 (b). Also, higher concentration of hydrogen peroxide in the solution leads to thinner oxide layers, resulting in possibly lower removal rate of copper during CMP. The result of VASE showed no change in the void concentration in Figure 4-15(a), whereas the surface roughness was slightly increased with the concentration of hydrogen peroxide. Moreover, the XRR measurements showed that the total reflection edge shifted due to a change of the oxide layer density in Figure 4-16. This observation indicates that higher concentration of hydrogen peroxide induces the formation of the denser oxide layer on the copper surface. As hydrogen peroxide acts as an oxidizer on copper, it is generally

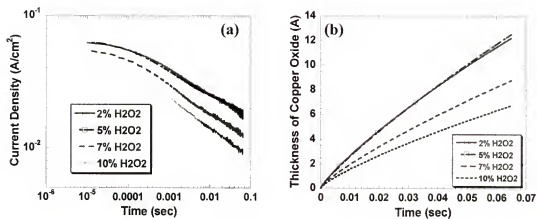


Figure 4-14. The effect of H_2O_2 concentration on the transient behavior of copper at pH 7.

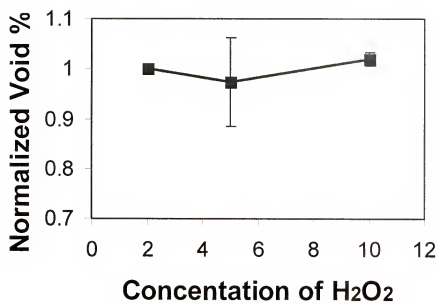


Figure 4-15. Normalized void concentration in Cu_2O layer on the samples dipped in 2%, 5%, and 10% hydrogen peroxide at pH 7.

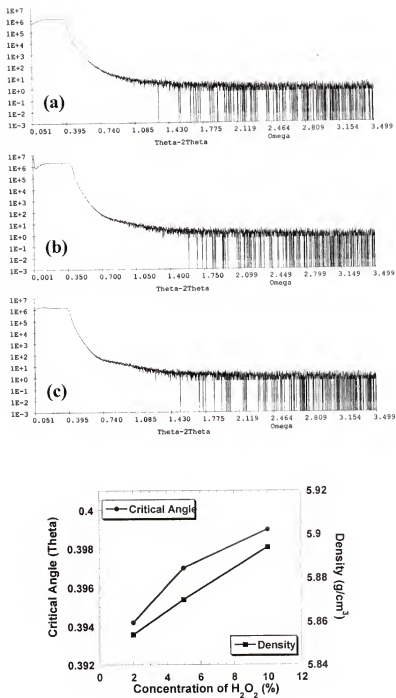


Figure 4-16. XRR measurements ((a), (b), and (c)) and simulations (d) of the cuprous oxide layer on the copper surfaces that were dipped in solutions with various concentrations of hydrogen peroxide at pH 7: (a) 2%, (b) 5%, and (c) 10%.

believed that higher concentration of hydrogen peroxide leads to higher removal rate as in the case of tungsten CMP [Bie98]. However, this belief has been in conflict with the several investigations [Her01, Lee99]: higher removal rate of copper was observed when lower concentration of oxidizer was used. The phenomenon observed in Figure 4-14 can explain why higher concentration (above 7%) of H_2O_2 slurry showed lower copper removal rate on copper CMP unlike tungsten.

As already shown in Figures 4-6 and 4-9, adding just BTA in solution caused the lowest reaction kinetics among the additives on copper CMP. The mixture solution of higher concentration of BTA with 5% H_2O_2 shows decreased reaction kinetics and relatively faster passivation kinetics than lower concentration of BTA with 5% H_2O_2 as shown in Figure 4-17(a) and 4-17(b). Moreover, the reaction kinetics did not change when relatively lower concentration (1 and 5 mM) of BTA was added into 5% H_2O_2 solution. Even though the initial reaction kinetics was decreased with the concentration of BTA (especially, 10 mM and 20 mM BTA), the growth of the chemically modified surface layer was still linear with time in the short time regime. On the other hand, in the long time regime (Figure 4-17(c)), the reaction kinetics was changed considerably without BTA. These figures indicate that the copper surface was passivated with higher concentration of BTA in less than 1 second. In Figure 4-18, XRR measurements clearly showed that the chemically modified surface layer (Cu_2O -BTA layer) having lower density was formed in BTA based solution. As described in Chapter 3, the surface layer formed in hydrogen peroxide solution has a dual layer structure of $\text{CuO}/\text{Cu}_2\text{O}$. On the other hand, when BTA was added in hydrogen peroxide solution, CuO layer could not be precipitated on the Cu_2O surface due to the adsorption of BTA on the Cu_2O surface. Thus,

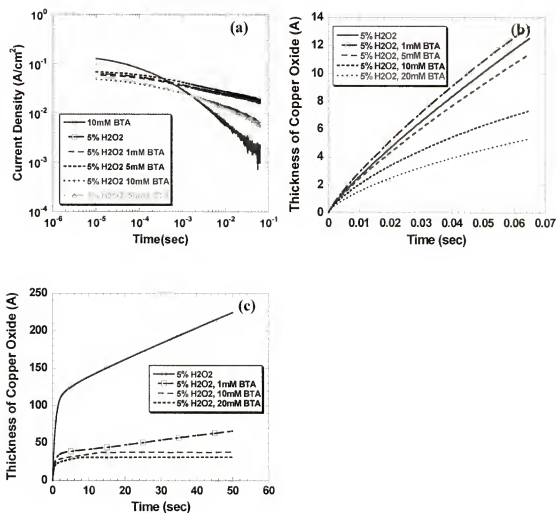


Figure 4-17. The effect of BTA concentration of the transient behavior of copper in 5% H_2O_2 solution at pH 7.

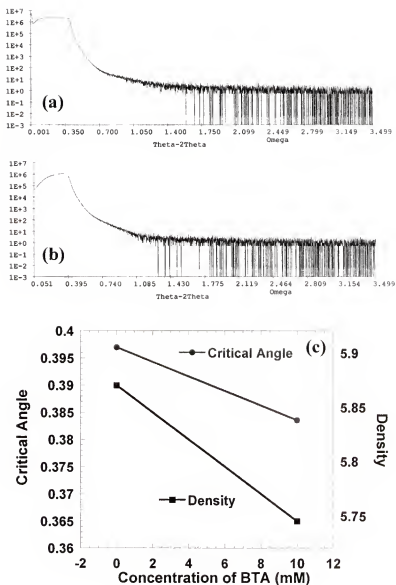


Figure 4-18. XRR measurements ((a) and (b)) and simulations (c) of the chemically modified surface layer on the copper surfaces that were dipped in solution: (a) 5 wt% hydrogen peroxide at pH 7 and (b) 5 wt.% hydrogen peroxide and 10 mM BTA at pH 7.

when the density of the layer was measured using XRR, CuO layer takes into account the density of layer when hydrogen peroxide is only chemical in the solution. Since the density of CuO (6.31 g/cm^3) is higher than that of Cu_2O (6.00 g/cm^3), the overall density of the dual layer on the surface was higher than one of Cu_2O -BTA layer. Based on this analysis, it cannot be expected whether higher removal rate could be achieved by adding BTA into hydrogen peroxide based slurry or not with respect to the density of the layer; however, relatively high concentration of BTA can cause lower removal rate due to the formation of the thinner layer. Therefore, optimal concentration of BTA plays a key role in the material removal and planarity.

Figure 4-19 shows the effect of citric acid in the mixture solution of hydrogen peroxide and BTA. As citric acid is an organic complexing agent of copper, adding citric acid was expected to increase the amount of copper reacted with chemicals and then to lead to higher copper removal. As a result, the reaction kinetics was enhanced by adding citric acid. Figure 4-19(a) indicates that complexing agent alone is not enough to achieve optimal removal of metal. Using citric acid with an oxidizer showed the chemically synergistic effect so that thicker copper was reacted. Also, more copper was reacted when higher concentration of citric acid was added (Figure 4-19(b)). When citric acid was added in the mixture solution of hydrogen peroxide and BTA, the initial reaction rate was increased in this investigation window. In addition, the slope of the curve was slightly changed with time. This result indicates that citric acid as a copper complexing agent enhances the reaction kinetics by dissolving the copper oxide layer. As the reaction kinetics increased, the results of VASE (Figure 4-20) and XRR (Figure 4-21) shows that the porosity of the cuprous oxide layer was considerably increased and density of the

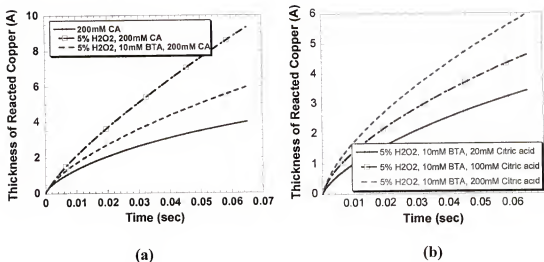


Figure 4-19. The concentration effect of citric acid of the transient behavior of copper in various solutions at pH 7.

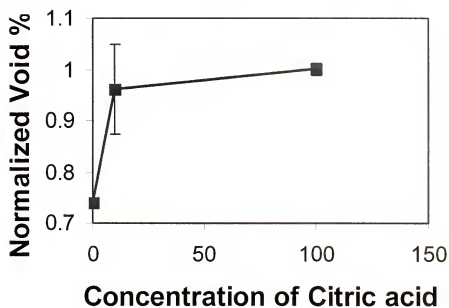


Figure 4-20. Normalized void concentration in Cu_2O layer on the samples dipped in 5% hydrogen peroxide and 10 mM BTA solutions with different concentrations of citric acid at pH 7.

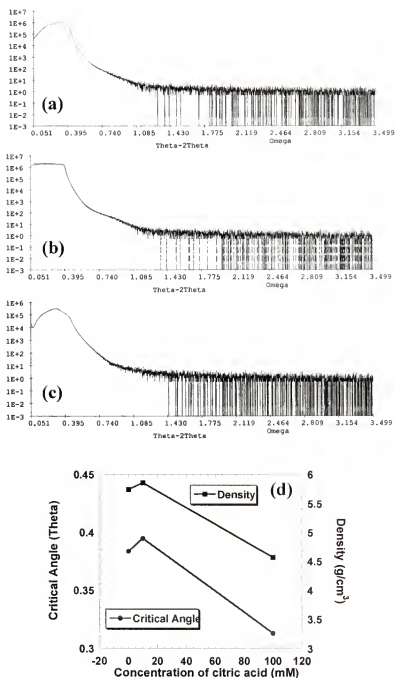


Figure 4-21. XRR measurements ((a), (b), and (c)) and simulations (d) of the chemically modified surface layer on the copper surfaces that were dipped in solution of 5 wt.% hydrogen peroxide, 10 mM BTA, and various concentration of citric acid at pH 7: (a) 0 mM, (b) 10 mM, and (c) 100 mM.

layer was significantly decreased with the concentration of citric acid. It is because the concentration of citric acid affects on the copper dissolution as indicated in Table 4-1. Interestingly, the dissolution rate of copper was not dramatically increased with the addition of citric acid in the solution of hydrogen peroxide and BTA in Table 4-1 as BTA passivates the copper surface in the quasi-static potentiodynamic measurement. However, even though BTA inhibited the copper surface from the chemical attack, the dissolution rate of copper was slightly increased with the concentration of citric acid. It may indicate high dissolution rate of copper in the short time range. Therefore, optimizing the concentration of citric acid will be necessary to achieve better CMP performance by balancing between the passivation and dissolution of the copper surface.

Summary

A systematic study of the chemical interactions on copper chemical mechanical polishing has been carried out to determine the kinetics and thickness of the chemically modified surface layer formed during CMP. The reaction/passivation kinetics and the thickness of the chemically modified surface layer are strongly dependent on the chemistry of CMP slurry in the chemical aspect of CMP, and the thickness of the surface modified layer plays a critical key in the selection of the chemistry and its concentration. Moreover, the reaction/passivation kinetics of the chemically modified surface layer can alter the porosity and density of this layer, resulting in controlling the material removal and defectivity during CMP. Therefore, by proper slurry design of chemicals including pH, the passivation kinetics and thickness of the passive layer can be adjusted to avoid the adverse effects based on the mechanical polishing or chemically polishing such as low removal rate, poor surface finish, etc.

Another issue to understand the chemical interactions – mechanical properties of the chemically modified surface layer – was introduced in the following chapter. The correlation of the copper removal rate and defectivity with the formation kinetics and mechanical properties of the chemically modified surface layer was also presented in Chapter 6.

CHAPTER 5

MECHANICAL PROPERTIES OF THE CHEMICALLY MODIFIED SURFACE LAYER ON THE COPPER SURFACE

Introduction

The kinetics and thickness of the chemically modified surface layer have been investigated in Chapters 3 and 4. The mechanical properties of the chemically modified surface layer are also one of key parameters to understand the metal CMP removal mechanism. As indicated in Zhao's model [Zha02], the mechanical properties of this layer are related to the indent depth of abrasives through the copper surface, controlling the polish rate and the defectivity on CMP. Liu et al. [Liu95] and Tseng et al. [Tse96] suggested that hardness and modulus are the two most important material characteristics affecting the dielectric CMP process. Their results showed a good correlation between the polishing rate of oxide and the reciprocal of the hardness. Luo and Dornfeld [Luo03] also modeled the material removal rate that is inversely proportional to hardness of the layer to $2/3$ power even though their assumptions – dual oxide layer formed during CMP and higher copper removal rate due to higher concentration of oxidizer – were conflicted with the results in Chapter 4. In copper CMP, different chemically modified surface layers can be formed by the combination of the chemical additives as observed in Chapters 3 and 4. Accordingly, the more systematic investigation on the mechanical properties of the surface layer is required. Recently, the alternative CMP processes – abrasive-free polishing (AFP), electro-chemical polishing (ECP), and spin-etch planarization (SEP) – have been investigated to reduce the defectivity (*e.g.*, scratches,

dishing, and erosion) during CMP and to remove the drawbacks (*e.g.*, abrasive contamination and cost) of CMP process [Kon00-a, Kondo00-b, Sat01, Fur99, DeB00]. Especially, AFP manufactured by Hitachi [Kon00-a] has already been introduced to semiconductor manufacturing. The removal mechanism in these alternative polishing methods is controlled by the formation of the softer layer than the oxide layer, which can be removed by lower particle concentration or even CMP pad only without particle. Thus, the mechanical properties of the chemically modified surface layer play more critical roles in the material removal rate, defectivity, planarization, etc. than conventional CMP slurries. However, there are no data on the properties of the chemically modified surface layer due to the lack of the sufficiently sensitive technique on layers of nm-range thickness.

As a consecutive work with regard to the characterization of the chemical interaction on copper CMP, the mechanical properties of the chemically modified surface layer, which is formed by the interaction between the various chemical additives and the copper wafer, were investigated using the nanoindentation. The result obtained would give an insight into the copper CMP removal mechanism. The mechanical properties of this layer were directly measured with light force ($< 100 \mu\text{N}$) due to thickness of this layer and the substrate effect.

Experimental

Nanoindentation

Nanoindentation has recently become a widely used technique to measure the hardness and Young's modulus of thin films [Pha92, Oli92, Saw99, Pan01, Che01, Wol03]. These mechanical properties can be obtained from load-displacement curve without submicron indent depth. A number of papers have discussed the nanoindentation

technique and analysis of load-displacement curves [Pha92, Oli92, Saw99, Che01, Wol03]. The equations used to analyze the hardness, H , and Young's modulus, E , are described as follows:

$$H = \frac{P_{\max}}{A} = c_b \sigma_y \quad (5.1)$$

$$S = \frac{dP}{dh} = \beta \frac{2}{\sqrt{\pi}} \sqrt{A} E_r \quad (5.2)$$

where σ_y is the yield stress, c_b is the constraint factor that depends on indenter shape and material properties (about 3 when $E * \tan(\beta/\sigma_y) > 100$), P is the indentation load, P_{\max} is the maximum indentation load, S is the contact stiffness, h is the displacement, A is the projected contact area, E_r is the reduced modulus, and β is the geometric (or correction) factor that depends on indenter shape. The value of the constant β is 1.000 for circular shape, 1.034 for triangle shape, and 1.012 for square shape of indent. E_r is defined as follows:

$$E_r = \frac{(1 - \nu^2)}{E} + \frac{(1 - \nu_i^2)}{E_i} \quad (5.3)$$

where E and ν are the young's modulus and the poisson's ratio of substrate, and E_i and ν_i are of the properties of a diamond indenter, respectively. Because Young's modulus of diamond ($E = 1140$ GPa) is usually one or two orders of magnitude higher than that of the sample, the reduced modulus is effectively the Young's modulus of the sample.

$S = dp/dh$ is the experimentally measured contact stiffness of the upper portion of the unloading data. Figure 5-1 is an example of a typical indentation load-displacement plot as a result of indentation.

In this experiment, nanoindentation measurements were carried out using a Cube corner diamond indenter (see Figure 5-2(a)) in Triboindenter[®] with TriboScope[®] manufactured by Hysitron. The total included angle of this tip is 90 degrees, and resembles the corner of a cube. Because it has sharper angles and a higher aspect ratio, the radius of curvature can be much smaller than that for a Berkovich tip. Because these are much sharper, their specialty is ultra thin films, where plastic deformation should be kept to a more confined volume (www.hysitron.com). Figure 5-2(b) shows *in situ* image of an indent on the copper sample, dipped in 5% hydrogen peroxide solution at pH 7 for 1 minute, using a Cube corner indenter. The maximum load was 60 μN . A pyramidal shape of an indent was observed.

Figure 5-2(c) is the schematic diagram of the experimental setup. This instrument is a quantitative depth-sensitive nanoindentation. A 1.5 micron thick copper layer (Rms is approximately 2nm) on Ta/SiO₂/Si wafer was used. As a sample, all the copper samples were dipped for 1 minute in the solutions, which were used in Chapter 4. Before dipping in the chemical solution, same pretreatment of the copper surface was carried out except the mechanical polishing. In each sample, the nanoindentations were conducted at 64 separate maximum loads starting from 100 μN to 5 μN with successive 4% decrease. All indentations were performed using a load-time sequence as shown in Figure 5-3. The indenter was loaded during first 10 sec, dwelled for 5 sec, and then unloaded for

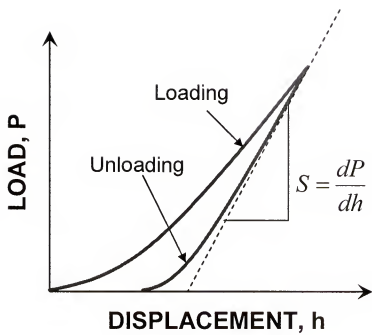
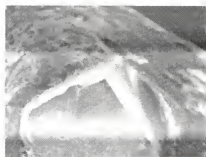
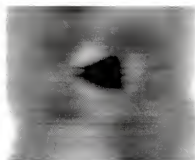


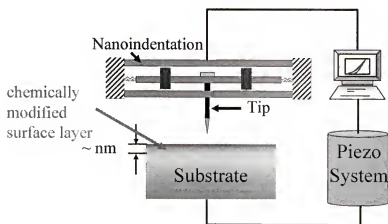
Figure 5-1. Typical indentation load-displacement plot as a result of indentation



(a)



(b)



(c)

Figure 5-2. (a) SEM picture of Cube corner diamond indenter (www.hysitron.com), (b) schematic diagram of the experimental apparatus, and (c) in-situ image (1 by 1 μm) of indent on the copper sample dipped in 5% hydrogen peroxide at pH 7 for 1 minute with Cube corner indenter. The maximum load was 60 μN .

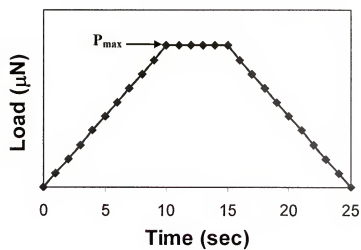


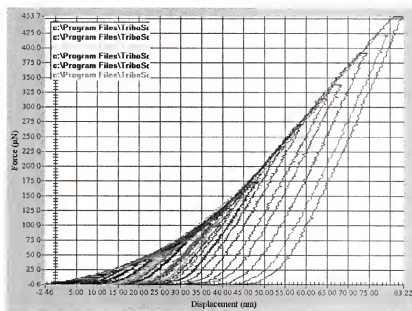
Figure 5-3. Load-time sequence during the nanoindentation experiments.

next 10 seconds. Dwell time allows any time dependent plastic effects (e.g., creep and dislocation) to diminish.

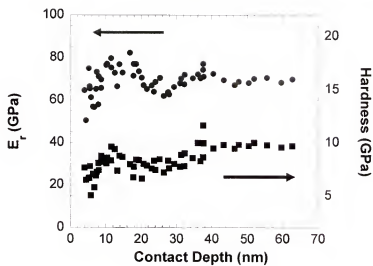
Results

As chemically modified surface layers formed in different chemical environments vary, the mechanical properties of these layers can be diverse. They can affect the CMP performance - for example, if the chemically modified surface layer is hard, low removal rate is expected even though a thicker surface layer is formed. The same chemical effects on the copper surface – the pH effect and the concentration effect of hydrogen peroxide, BTA, and citric acid – were investigated using nanoindentation technology.

At first, amorphous quartz substrate ($E_r = 69.6$ GPa and $H = 9.3$ GPa) was used to confirm the calibrated area function with a Cube corner indenter, which is required to provide the quantitative data of hardness and Young's modulus from load-displacement curves. Figure 5-4(a) shows the load-displacement curves of an amorphous quartz substrate. The calculated values of hardness and Young's modulus are shown in Figure 5-4(b). Since the initial slope of a unload curve is the contact stiffness, the reduced Young's modulus and hardness can be extracted from the initial slope of the unload curve with equation (5.1) and (5.2). From Figure 5-4(b), it was observed that all values of Young's modulus and hardness were identical and equaled to 70.7 GPa and 8.7 GPa, respectively, until the contact depth was less than 9 nm. The mechanical properties of the amorphous quartz started to decrease below the contact depth of 9 nm. It happened due to the truncation of the diamond tip indent [Saw99]. Accordingly, the experimental results obtained below the contact depth of 9 nm were not considered.



(a)



(b)

Figure 5-4. The typical load-displacement curves performed on an amorphous quartz substrate (a) and, as a result, calculated hardness and Young's modulus presented.

pH Effect

At first, selective load-displacement behavior of copper samples subjected on 5% hydrogen peroxide solution at different pHs is shown in Figure 5-5. It shows a scatter of the curves within each sample. This arose from the intrinsic roughness of the surface, as evidenced in Figure 5-6, that is a dominant factor for the data scatter at the light load (< 1 mN) nanoindentation [Fuj02]. The copper surface with the oxide layer has a very rough surface even though the as-received wafer has a smooth surface with Rms of 2 nm. The roughed surface is related to the asperity contact effect; indentation at a local void space induces the contact area a greater value at a given load [Fuj02]. For the purpose of characterizing the mechanical properties of the oxide layer, some curves were excluded from consideration, based on the continuity of the contact stiffness with the curves at 4% higher and 4% lower maximum loads in all the experiment data.

From Figure 5-5, interestingly, the discontinuities (arrows in the figure) of load curves were observed at the contact depth of 10 to 14 nm in all pHs. The initial contact stiffness was also changed at the point of discontinuity. Figure 5-7 also shows clearly that two different regimes exist in Young's modulus and hardness (extracted from Figure 5-5). These mechanical properties abruptly increased in the shallow contact depth, while they decreased slowly in the relatively deeper contact depth. In the result of XPS in Chapter 3, it was found that the oxide layer formed in hydrogen peroxide solution has a dual layer structure. As the cupric oxide has a lower hardness, Mohs scale: 3.5, than the cuprous oxide, 3.75 [Lid98 and www.azminerals.com], it can be indicated that the cupric oxide on top of the sample surface was, at first, depressed before the discontinuity, and then the cuprous oxide was indented. It should be noted that the change of the mechanical properties with the indent depth even in the same oxide layer are due to the substrate

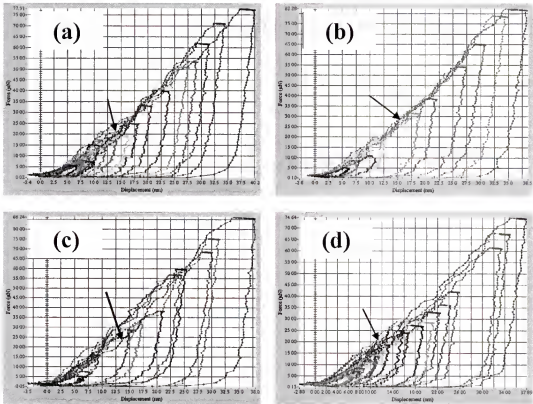


Figure 5-5. Selective load-displacement behavior of copper samples subjected on 5% hydrogen peroxide solution at different pHs: (a) pH 5, (b) pH 6, (c) pH 7, and (d) pH 8. Arrows indicates the discontinuity on the loading curve.

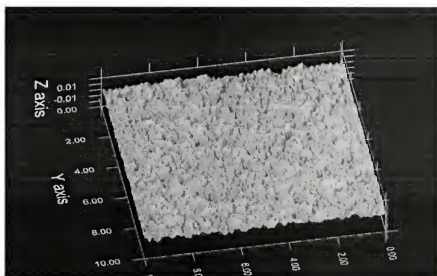


Figure 5-6. *In situ* image of a copper sample, dipped in 5% hydrogen peroxide at pH 7 for 1 min, using the nanoindentation.

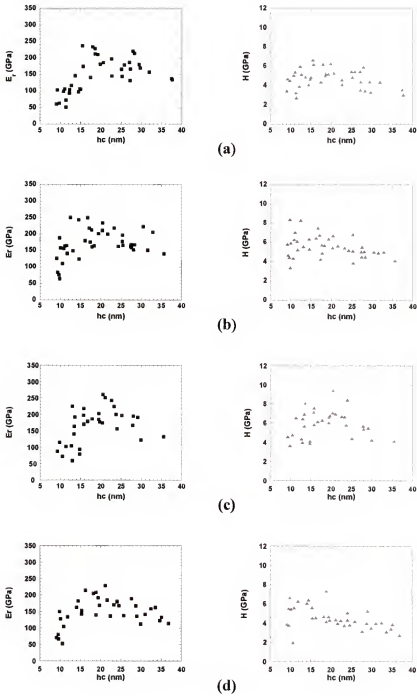
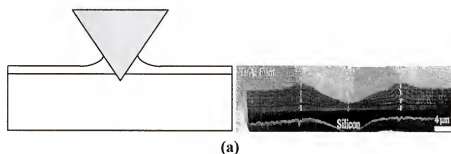
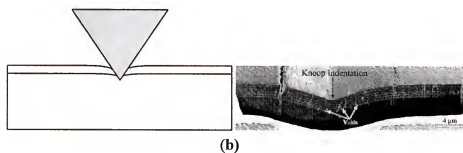


Figure 5-7. The mechanical properties – Young's modulus and hardness – of copper samples, extracted from Figure 5-5 using equation (5.1) and (5.2) as a function of the contact depth and the pHs of 5% hydrogen peroxide dipping solution: (a) pH 5, (b) pH 6, (c) pH 7, and (d) pH8.

effect. In the case of a soft film on a hard substrate, the hard substrate prevents the soft film materials from flowing downwards, and then increases the degree of pile-up as described in Figure 5-8(a) [Tsu99-a]. Chen *et al.* [Che01] suggested that the intrinsic hardness could be obtained from equation (5.2) as long as the indentation depth is less than 50 % of the film thickness based on the experimental results in the case of the soft film on the hard substrate. This is because the plastic deformation zone caused by indentation is much localized. Thus, the substrate effect starts to influence the indentation result when the indentation depth is deeper than one half of the film thickness. In that case, the calculated hardness is a combination of film and substrate properties. Since the substrate is harder than the film, the hardness of the film increases as the diamond indenter is pushed closer to the interface as shown at the shallow contact depth regime in Figure 5-7. On the other hand, in the case of the hard film on the soft substrate, the substrate enhances the sink-in effect as shown in Figure 5-8(b) [Tsu99-b]. Hay and Pharr [Hay98] observed that the surface near the indentation was depressed downward or sank into the material even though it is not in contact with the indenter. This leads to an overestimation of the indentation contact depth and area, resulting in a decrease in the hardness and Young's modulus to the mechanical properties of the substrate. The "sink-in" indent behavior of the hard film on the soft substrate was observed at the relatively deeper contact depth regime in Figure 5-7 due to the fact that hardness of the pristine copper substrate (Mohs scale: 3) is less than that of the cupric oxide. Thus, the mechanical properties of these two layers were obtained from the lowest contact depth (around 9 nm) and the transition point. Figure 5-9 shows the hardness and Young's modulus of the



(a)



(b)

Figure 5-8. Schematic diagrams and SEM pictures of two different indentation behavior due to the substrate effect: (a) soft films on hard substrates (pile-up) and (b) hard films on soft substrates (sink-in) [Tsu99-a, Tsu99-b].

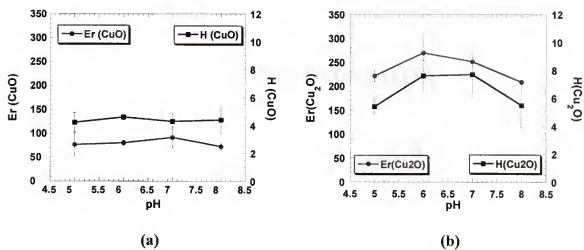


Figure 5-9. The hardness and Young's modulus of CuO and Cu₂O as a function of pH.

oxide layers as a function of pH. The mechanical properties of CuO did not change with pH (Figure 5-9(a)), whereas the mechanical properties of Cu₂O significantly changed with pH (Figure 5-9(b)). As shown in the results of XRR in Chapter 4, the density of Cu₂O increased with pH due to less concentration of voids. Accordingly, it was expected that higher Young's modulus and hardness of Cu₂O would be achieved. The result, however, showed that the mechanical properties were increased and then decreased. It can be explained by the thickness of the layer and the substrate effect. According to Chen *et al.* [Che01] and Tsui *et al.* [Tsu99-b], as the ratio of the indent depth to the film thickness is increased, plastic deformation of the substrate increases sink-in of the film and the substrate effect is very large. Thus, at higher pHs, as the thickness of the oxide layer was decreased with pH, the "sink-in" effect can be dominant even with the shallow indent depth due to relatively high ratio of the indent depth to the film thickness. In addition, since the formation mechanism of CuO is the precipitation from the surface of Cu₂O, the mechanical properties of CuO is not dependent on pH.

The Effect of the Concentration of an Oxidizer

Figure 5-10 presents selective load-displacement behavior of copper samples dipped in solutions with several concentration of hydrogen peroxide solution at pH 7: (a) 2%, (b) 5%, and (c) 10%. The discontinuity in load-displacement curves was observed in all concentration of hydrogen peroxide, indicating the dual oxide structure on the copper surface. The mechanical properties calculated from Figure 5-10 also indicate the dual oxide structure and the substrate effect (Figure 5-11). Interestingly, when 10% hydrogen peroxide was used, the mechanical properties were increased in the shallow contact depth regime as shown in Figure 5-12. It arose from the oxide thickness. As already observed in

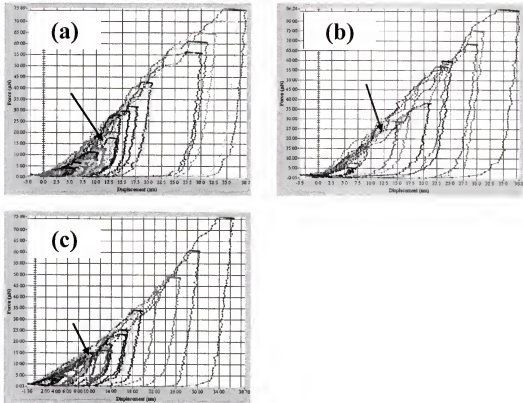


Figure 5-10. Selective load-displacement behavior of copper samples subjected on various concentrations of hydrogen peroxide solution at pH 7: (a) 2%, (b) 5%, and (c) 10%. Arrows indicates the discontinuity on the loading curve.

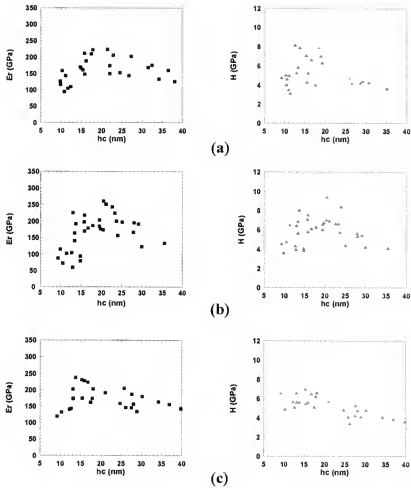


Figure 5-11. The mechanical properties – Young's modulus and hardness – of copper samples, extracted from Figure 5-10 using equation (5.1) and (5.2) as a function of the contact depth and concentration of hydrogen peroxide dipping solution: (a) 2%, (b) 5%, and (c) 10%.

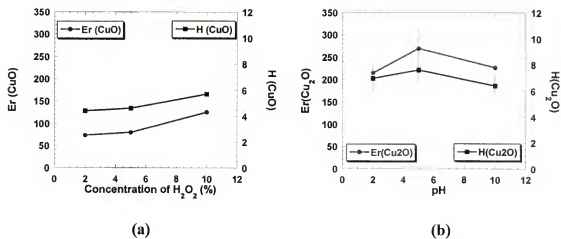


Figure 5-12. The hardness and Young's modulus of CuO and Cu_2O as a function of the concentration of hydrogen peroxide in the solution.

Chapter 4, higher concentration of hydrogen peroxide induces faster passivation kinetics, resulting in thinner oxide layer formed on the copper surface. Due to a very thin oxide layer, the substrate effect in the case of CuO/Cu₂O became larger on the nanoindentation measurements. It resulted in the higher hardness and Young's modulus of CuO than the actual mechanical properties of CuO. On the other hand, in the relatively deeper indent depth, hardness and Young's modulus were reciprocally proportional to the contact depth. As the contact depth increases, the plastic deformation of soft substrate occurs, resulting in lower hardness and Young's modulus just like the case of higher pH.

The penetration depth (δ) of the particle into the surface [Bro81] using Hertzian indentation is as follows:

$$\delta = \frac{3}{4}\phi \left(\frac{P}{2KE} \right)^{\frac{2}{3}} \quad (5.4)$$

where ϕ is the diameter of a spherical particle, P is the pressure, K is the particle fill factor at the surface, and E is the Young's modulus of the polished surface. This equation expresses that the penetration depth of particle, one of the critical factor in the contact removal model, is inversely proportional to the Young's modulus of the polished wafer, especially the chemically modified surface layer. Moreover, Qin [Qin03] developed a CMP removal model including the chemical interaction as well as the mechanical interaction. In his model, the material removal rate in a CMP process is strongly dependent on the mechanical properties (*e.g.*, hardness and Young's modulus) of the polished surface. The detail of this removal model was described in the following chapter. Also, Singh and Lee [Sin03] suggested that the hardness of the layer as well as Young's

modulus plays a critical role in the material removal in the low stressed CMP. Thus, it was expected a lower removal rate as well as few scratches of copper during CMP when higher concentration of hydrogen peroxide is added to the solution of high pH. This expectation is based on the thinner layer formation and the mechanical properties of the chemically modified surface layer (higher density, higher hardness, and higher Young's modulus).

The Effect of the Concentration of BTA

Figure 5-13 presents the load-displacement curves for indentation of copper samples, dipped in hydrogen peroxide based solution at pH 7 with various concentration of BTA: (a) 0 mM, (b) 5 mM, (c) 10 mM, and (d) 20 mM. Figure 5-13(a) shows the discontinuity on the loading curve, as analyzed previously. On the other hand, the loading curves in Figures 5-13(b), (c), and (d) smoothly increased as the maximum load increased (no discontinuity). As the role of BTA was discussed in the previous chapter, BTA is chemically adsorbed on the Cu_2O surface, leading to the passivation on the copper surface as well as the prevention of the precipitation formation of CuO on the Cu_2O surface. As a result, single layer is formed on the copper surface. The discontinuity arising from the presence of CuO could not be observed. Figure 5-14 clearly shows that mechanical properties are inversely proportional to the contact depth. Thus, it was indicated that the sink-in effect was reduced as the contact depth was smaller. Also, it was found that the sink-in effect was not diminished even at the contact depth of 9 nm because the plateau regime was not observed in hardness and Young's modulus results. As the results of Chen et al. [Che01] and Tsui et al. [Tsu99-b] were indicated, the only way to measure quantitative mechanical values of the hard film on the soft substrate is the shallow indentation on the very thick hard film, which is enough not to give the

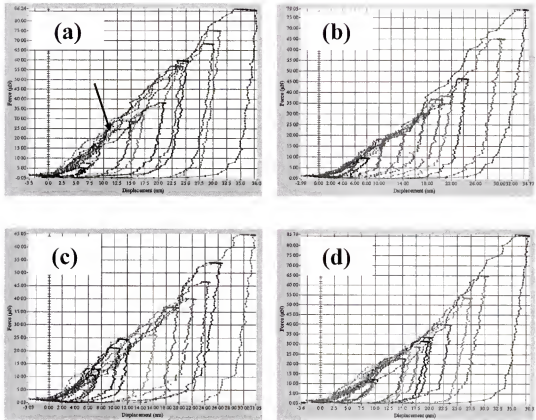


Figure 5-13. Selective load-displacement behavior of copper samples subjected on various concentrations of BTA at 5% hydrogen peroxide solution at pH 7: (a) 0 mM, (b) 5mM, (c) 10 mM, and (d) 20 mM. Arrows indicates the discontinuity on the loading curve.

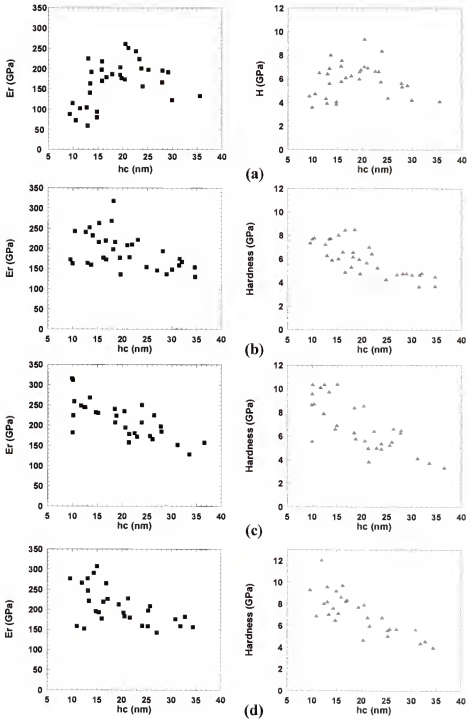


Figure 5-14. The mechanical properties – Young's modulus and hardness – of copper samples, extracted from Figure 5-13 using equation (5.1) and (5.2) as a function of the contact depth and concentration of BTA in dipping solutions: (a) 0 mM, (b) 5 mM, (c) 10 mM, and (d) 20 mM.

plastic deformation on the soft substrate. However, the thickness (38 \AA estimated by electrochemistry and XPS in Chapter 4) of the Cu_2O -BTA layer was too thin to measure the quantitative values from the nanoindentation. Due to this limitation, the qualitative mechanical values were used to compare to others. Hardness and Young's modulus of the surface layer were modified as a function of BTA concentration in the dipping solution as presented in Figure 5-15. At first, when BTA was added in hydrogen peroxide solution, the mechanical properties of a sample were decreased. Interestingly, when the concentration of BTA was increased in the dipping solution, the hardness and Young's modulus of the surface layer increased simultaneously. When the high concentration of BTA is used, the adsorption of BTA on the Cu_2O layer becomes denser. It results in the more effective passivation on the copper surface and higher mechanical properties. Moreover, mechanical properties of copper samples, dipped in 10 mM BTA and 20 mM BTA solutions, were almost identical, indicating that the adsorption of BTA on Cu_2O surface was saturated. As expressed in equation (5.4), the penetration depth of particle into the surface layer is a function of Young's modulus. Thus, it was expected that low concentration of BTA would lead to higher copper removal rate due to the lower hardness, lower Young's modulus as well as lower density, whereas the high concentration BTA may induce the lower removal rate due to the very high Young's modulus and hard surface layer even though the density of the Cu_2O -BTA layer is lower than Cu_2O itself.

The Effect of the Concentration of Citric Acid

As seen in the previous chapters, citric acid tends to dissolve the copper oxide and make the oxide layer less dense. Thus, it was expected that lower hardness as well as lower Young's modulus of the oxide layer on the copper, subjected in citric acid based solution. Figure 5-16 shows the load-displacement curves for indentation of copper

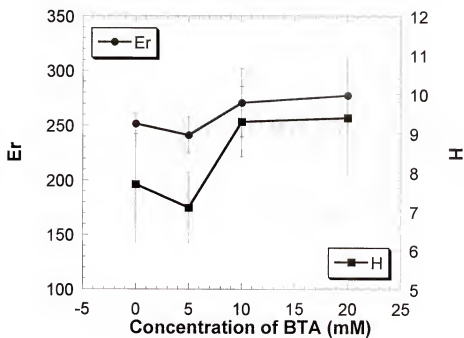


Figure 5-15. Hardness and Young's modulus of the chemically modified surface layer as a function of the concentration of BTA in 5% hydrogen peroxide solution at pH 7.

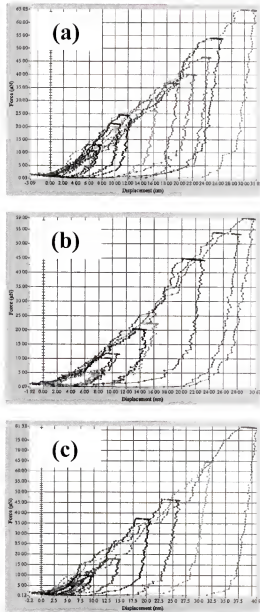


Figure 5-16. Selective load-displacement behavior of copper samples subjected in 5% hydrogen peroxide solution with various concentrations of citric acid at pH 7: (a) 0 mM, (b) 10 mM, and (c) 100 mM

samples, dipped in 5% hydrogen peroxide and 10 mM BTA solution at pH 7 with various concentration of citric acid: (a) 0 mM, (b) 10 mM, and (c) 100 mM. Figure presents that the loading curves in Figures 5-16(a), (b), and (c) smoothly increased without the discontinuity as the maximum load increased. But, the contact stiffness was gradually changed with the maximum load. Also, hardness and Young's modulus of the layer on the copper surface were decreased with the concentration of citric acid as shown in Figure 5-17. More interestingly, the mechanical properties were saturated at the contact depth of 20 to 25 nm, indicating that the thickness of Cu_2O is high enough to remove the substrate effect. Also, due to the etching nature of citric acid, the mechanical properties as well as the density were dramatically decreased with the concentration of citric acid even with BTA (Figure 5-18). This observation indicates that citric acid hinders the adsorption of BTA on the copper oxide surface by dissolving the copper surface. Thus, when citric acid added in the slurry, the copper removal rate would be increased due to lower mechanical properties and thicker layer formation as well as high dissolution rate of copper.

Summary

The nanoindentation technique is a powerful tool for examining the deformation exhibited by various chemically modified surface layers in response to nano-scale surface contacts. The surface mechanical properties of copper presented here were determined by nanoindentation. Experimental results show that the discontinuity on the loading curves were observed on samples, dipped in hydrogen peroxide solution without BTA and hydrogen peroxide and citric acid solution even with BTA. This behavior is due to the dual oxide layer on the copper. Also, it was observed that the role of BTA in the slurry is not only an inhibitor of the chemical attack, but also an inhibitor of the copper removal

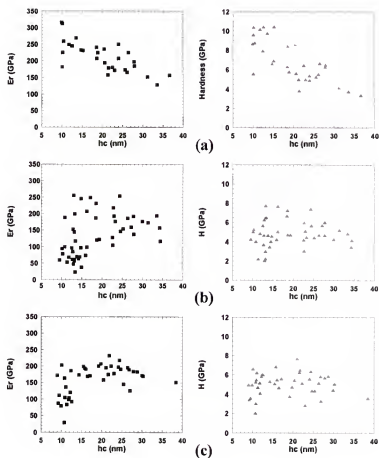


Figure 5-17. The mechanical properties – Young's modulus and hardness – of copper samples, extracted from Figure 5-16 using equation (5.1) and (5.2) as a function of the contact depth and concentration of citric acid in dipping solutions: (a) 0 mM, (b) 10 mM, and (c) 100 mM.

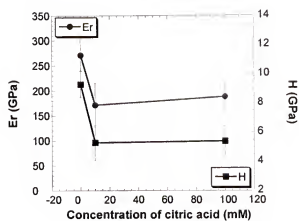


Figure 5-18. The maximum hardness and Young's modulus of the chemically modified surface layer as a function of the concentration of citric acid in 5% hydrogen peroxide and 10 mM BTA solution at pH 7.

due to high hardness and Young's modulus. Since citric acid can control the dissolution rate, the mechanical properties as well as the density of the surface layer, it will play an important role in the low stress CMP and abrasive-free CMP. Its role can be extended to all the complexing agents. Therefore, it was known that the thickness and mechanical properties of the layer are strongly dependent on the balance between the BTA and citric acid activities.

CHAPTER 6 INTERPRETATION OF COPPER CMP PERFORMANCE BASED ON NANO AND MICRO SCALE INTERACTIONS

Introduction

As mentioned in Chapter 2, there is no explicit methodology to delineate the CMP removal mechanism due to the complexity of CMP by multiple involvements of the parameters, concurrent polishing of wide range of materials, and sophisticated chemical effects. Recently, the synergistic effects of mechanical and chemical interactions are formulated into the CMP removal model [Luo01, Fu01, Luo03, Zha02, Zha03]. However, these are regarded as preliminary due to the challenging issues such as the experimental proofs of microscale and nanoscale interactions (the wafer-pad-abrasive contact area, chemical kinetics, mechanical properties of the chemically modified surface layer, molecular bonding energy, etc.).

In previous chapters, the chemical effects, important variables in the CMP removal mechanism, in the nano-scale interactions during CMP were investigated. The roles of the chemical additives were re-defined that are suitable in the short time scheme. The chemically modified surface layers were characterized and their thickness was estimated. In addition, the mechanical properties of the surface layers were characterized using the nanoindentation. Based on all the results, CMP performance can be anticipated as described in Chapters 4 and 5. In this chapter, a copper CMP removal model was delineated, which was based on the relationship of all the parameters that were

investigated. Results and analysis of the model were compared with the experimental results of copper CMP.

Experimental

Copper CMP was conducted on the Struers Rotopol 31 polisher along with IC1000/SUBA IV stacked pads to correlate CMP performance to the results of the electrochemistry and the nanoindentation. The pad was hand-conditioned with a grid-abrade diamond pad conditioner at the beginning and between each polishing run. Copper wafers were used for CMP experiments. These consisted of 1.1 μm copper films with an average surface roughness (Rms) 19.5 nm on 25 nm Ta/SiO₂/Si substrates. Samples (1.5 inch by 1.5 inch) were cleaved from 8-inch wafers. The carrier and the pad speeds were 150 rpm, respectively. The flow rate of slurries was 100 ml/min. Copper wafers were polished under varying polishing pressure from 1.5 psi to 9 psi, under varying size of alumina particle from 40.5 nm (Nanotek[®] manufactured by Nanophase) to 500 nm (AKP-30[®] manufactured by Sumitomo) particles, and under varying the slurry chemistries used in previous chapters. The solid concentration was 3% by weight for all experiments that is commonly used in the commercial slurry (e.g., iCue[®] 5001 manufactured by Cabot Microelectronics). The removal rates were determined by measuring the thickness of samples before and after polishing, using the four-point probe method. The defectivity was observed by the tapping mode in atomic force microscopy (AFM).

Results and Discussion

CMP Removal Model based on the Nano- and Micro-Scale Interactions

As the hydrodynamic lubrication regime was never reached in copper CMP [Lia02] and the chemically modified surface layer is brittle in nature, the copper removal can be understood by the contact-polishing mechanism. Therefore, in this research, the copper

removal in the CMP process is assumed to be primarily due to the mechanical abrasion by the particles included in the slurry. The particles are embedded in the surface of the compliant polishing pad and dragged across the wafer surface by the relative velocity (V) between the wafer and the pad as shown in Figures 1-1. The wafer-pad-particle interaction on the interface between the wafer and the pad is visualized in Figure 6-1. From these figures, the material removal rate (MRR) can be simply defined from the contact mechanics, which is related to material removal by single particle, the number of particles, the linear velocity, and the nominal contact area, as follows:

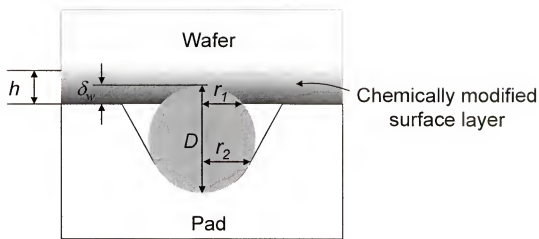
$$MRR \propto \frac{\Delta S \cdot V \cdot N_p}{A} \quad (6.1)$$

where ΔS is the cross-sectional area of the indent in the wafer surface generated by single particle, N_p is the number of particles participating in the material removal, and A is the nominal area of contact between the pad and the wafer.

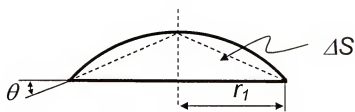
To calculate the removal rate in this model, three important contact variables are considered: contact area between the wafer and the pad, the number of the particles participating in the material removal, and the indentation depth of single particle into the wafer surface.

The contact area between pad and wafer (A_c)

Since the main role of the polishing pad is the delivery of the slurry to the wafer surface, the polishing pad (e.g., IC 1000 pad) has a much rougher surface than the wafer. Also, the pad is easily deformed when load is applied due to its compliant nature. These lead to the change of the contact area between the pad and the wafer when the load



(a)



(b)

Figure 6-1. Schematic of the wafer-pad-particle interaction: (a) the micro-contact system and (b) the cross-sectional area of indentation.

is increased. The contact area with load was usually modeled using Greenwood and Williamson elastic model (GW model) [Gre66] that describes the contact area between a randomly rough surface and a flat surface under a nominal load. According to GW model, it was suggested that the contact area is linearly dependent on the applied pressure. Qin [Qin03] and Basim [Basim02] verified the theoretical calculation using fourier transform infrared spectroscopy/attenuated total internal reflection spectroscopy (FTIR/ATR) technique. The normalized contact area estimated by FTIR/ATR as a function of applied pressure was presented in Figure 6-2 [Qin03]. The contact area was linearly increased with the nominal applied pressure, which is in good agreement with GW model.

In this study, the relation between the contact area and the nominal applied pressure was extracted from a linear fitting line shown in Figure 6-2 because this experimental result can eliminate the theoretical error by assuming the variables. The contact pressure (P_c) on the contact area between the pad and the wafer is related to the applied load (L) and the contact area (A_c):

$$P_c = \frac{L}{A_c} = \frac{100 \cdot L}{0.0334P + 0.0234} \quad (6.2)$$

Figure 6-3 shows the nominal applied pressure dependence on the contact pressure between the pad and the wafer using equation (6.2). The contact pressure has a hyperbolic dependence with the nominal applied pressure. This observation is in contradiction to the assumption used in the other micro-contact models of the material removal. Zhao and Chang [Zha02] and Ahmadi and Xia [Ahm01] used 0.4 times the hardness of the surface layer as a contact pressure between the pad and the wafer, and

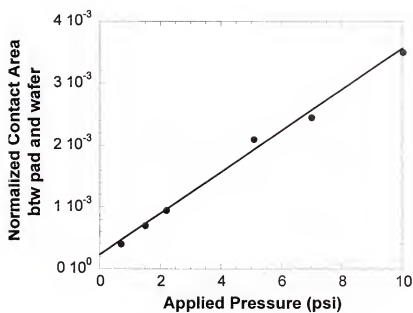


Figure 6-2. The normalized contact area between the pad and the wafer as a function of applied pressure, measured by FTIP/ATP [Qin03].

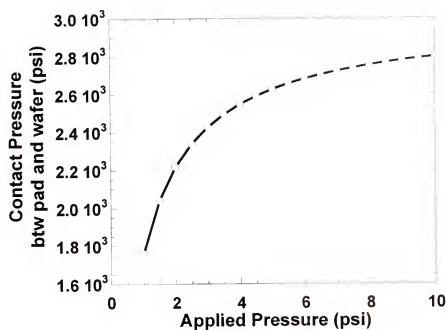


Figure 6-3. The applied pressure dependence on the contact pressure between the pad and the wafer using equation (6.2).

Qin [Qin03] hypothesized that the contact pressure remains constant due to the linear dependence of the contact area with the applied pressure. The increase of the contact pressure has a significant meaning in the CMP removal model because the indentation depth is dependent on the contact pressure, resulting in the different behavior of copper removal. The detail was explained in the following section.

The number of particles participating in the material removal (N_a)

As shown in Equation 6-1, the number of particles (N_a) that is at the interface of the pad and wafer is one of the most critical variables on the material removal. This number can be calculated based on the following three assumptions [Zha02].

1. The particles are uniformly dispersed in the slurry.
2. All the particles are spherical with an average diameter of D .
3. The area density of the particles embedded in the pad is the same as that in the slurry.

When the wafer is pressed down against the pad, the particles can be entrapped at the interface of the pad and the wafer. Therefore, the number of particles participating in the material removal is as a function of the area density of the particles (ρ_A) and the contact area between the pad and the wafer (A_c), which is given as

$$N_a = A_c \cdot \rho_A = A_c \cdot \left(\frac{6 \cdot V_c}{\pi \cdot D^3} \right)^{\frac{2}{3}} \quad (6.3)$$

Equation (6.3) shows that the number of particles is related to the contact area between the pad and the wafer (A_c), particle volume concentration in the slurry (V_c), and the particle size (D).

Indentation depth of single particle into the wafer surface (δ_w)

The contact mechanics in conjunction with the force equilibrium of a particle participating in the wear process is used to determine the indentation depth (δ_w) [Joh85, Zha00, Zha02, Qin03]. When indented by a hard particle, the pad and the wafer experience different modes of deformation because of their very different mechanical properties, which are summarized in Table 6-1. The pad will deform elastically by indentation of particles in a CMP process, whereas the deformation of the wafer associated with the indentation of particles is to be fully plastic in a CMP process [Zha02].

As presented in Figure 6-1, the indentation depth of single particle can be obtained from the force equilibrium of the particle by the pad and the wafer. In the elastic deformation, the contact force (F_{pw}) is related to the contact pressure and the contact area, as follows:

$$F_{pw} = \pi \cdot r_2^2 \cdot P_c \quad (6.4)$$

where r_2 is the indentation radius of a particle in the pad as described in Figure 6-1 and P_c is the contact pressure between the pad and the wafer given by equation (6.2). On the other hand, in the plastic deformation, the contact force (F_{pw}) is dependent on the hardness (H) of the surface layer and the contact area between the particle and the wafer. It is given as

$$F_{pw} = \pi \cdot r_1^2 \cdot H_c \quad (6.5)$$

where r_I is the indent radius of a particle into the wafer and H_e is the effective hardness of the chemically modified surface layer. The term “effective” is used because hardness can be varied with the indentation depth and thickness due to the substrate effect described in Chapter 5. For example, hardness is decreased with the indentation depth when the surface layer is harder than the substrate, whereas hardness is increased with the indentation depth in the system of the soft layer on the hard substrate.

Then, the contact force equilibrium of a particle yields

$$\pi \cdot r_2^2 \cdot P_e = \pi \cdot r_1^2 \cdot H_e \quad (6.6)$$

In a CMP process, the CMP pad should have an optimal property of hardness because it is supposed to hold particles to transmit the contact force between the pad and particles to particles that indent into the wafer. Based on the requirement of the pad property, pad and contact pressure should be sufficiently hard and high respectively to make a value of r_2 to be close to $D/2$ [Qin03]. Thus, the indent radius of a particle in the wafer is given as

$$r_1 = \left(\frac{D}{2} \right) \cdot \left(\frac{P_e}{H_e} \right)^{1/2} \quad (6.7)$$

Referring to Figure 6-1, r_I can be obtained by

$$r_1 = \sqrt{\left(\frac{D}{2} \right)^2 - \left(\frac{D}{2} - \delta_e \right)^2} = \sqrt{\delta_e D - \delta_e^2} \quad (6.8)$$

Since δ_* is much smaller than D , equation (6.8) can be simplified. Thus, the indentation depth of a particle in the wafer can be expressed as follows:

$$\delta_* = \frac{D}{4} \cdot \frac{P_c}{H_c} \quad (6.9)$$

The substrate effect on hardness can be understood with a substrate effect factor, e , which is defined as [Che01]

$$e = \frac{H - H_b}{H_b} \quad (6.10)$$

where H_b is the hardness of a bulk material with the same mechanical properties as the film. The substrate effect factor is the correction factor one needs to take into account when using the relation in equation (5.1), $H = c_b \sigma_y$, to predict the yield stress of the film. The variation of e with σ_f/σ_s is plotted for four different indentation depths in Figure 6-4 [Che01]. σ_f and σ_s denote the yield stress of film and substrate, respectively. It is convenient to define three distinct regimes in this nanoindentation hardness map. Region A is the case of the soft film on the hard substrate. In this regime, the plastic deformation zone can be confined to the film as long as the indentation depth is less than 50% of the film thickness. Region B is the case of the hard film on the soft substrate. In this regime, the plasticity is induced mostly in the substrate with only a small plastic deformation zone in the film. As shown in Figure 6-4, the substrate effect in this regime is almost unavoidable and the error is increasing with the normalized indentation depth (δ_f/h , where h is the film thickness) and the hardness mismatch between the film and substrate

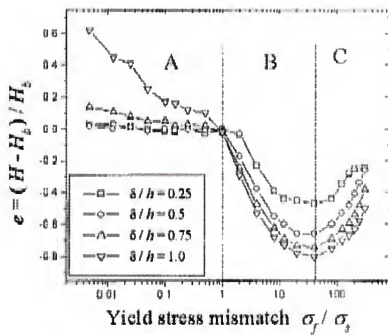


Figure 6-4. The relation between the substrate effect factor e and yield stress mismatch σ_f / σ_s for four different indentation depths, $\delta/h = 0.25, 0.5, 0.75$, and 1 [Che01].

(σ_f/σ_s). Region C is the case of the ultra-hard film on the soft substrate. The substrate is now fully plastic and unable to support the film from underneath. The plate bending effect becomes significant and further reduces the plastic zone in the film. As a result, the error of film hardness measurement becomes smaller with increasing hardness mismatch. Since the hardness of Cu₂O and Cu is 7.7 GPa and 2.7 GPa respectively, the hardness mismatch of Cu₂O formed in the solution of 5% hydrogen peroxide at pH 7 and Cu is 2.85 (that is also the mismatch of the yield stress). Thus, the hardness of layer with the normalized indentation depth can be estimated using the substrate effect factor as shown in Figure 6-5. Figure shows that hardness of the layer can be varied with the indentation depth. The relation between hardness and the normalized indent depth is derived. This relation is modeled by a polynomial fitting, described as

$$H_e = 7.7469 - 4.7155 \cdot \frac{\delta_w}{h} + 1.6558 \cdot \left(\frac{\delta_w}{h} \right)^2 \quad (6.11)$$

Substituting equation (6.11) to equation (6.9) and rearranging yields

$$6.6232 \cdot \frac{\delta_w^3}{h^2} - 18.862 \cdot \frac{\delta_w^2}{h} + 30.988 \cdot \delta_w - 40.5 \cdot D \cdot P_c = 0 \quad (6.12)$$

Equation (6.12) can be used to calculate the indentation depth of the particle into the wafer surface with the knowledge of P_c , which can be calculated from equation (6.2), and the thickness (h) of Cu₂O. The thickness of layer, estimated from the chronoamperometry in Chapter 4, is 1.2 nm in 60 millisecond. Based on this calculation, the indentation depths with the applied pressure and various particle sizes were presented in Figure 6-6.

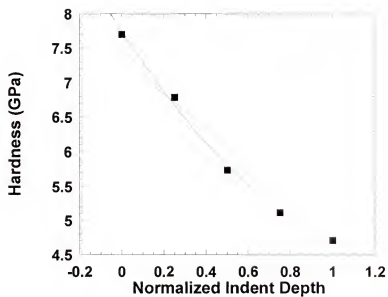


Figure 6-5. The hardness of layer with the normalized indentation depth can be estimated using the substrate effect factor.

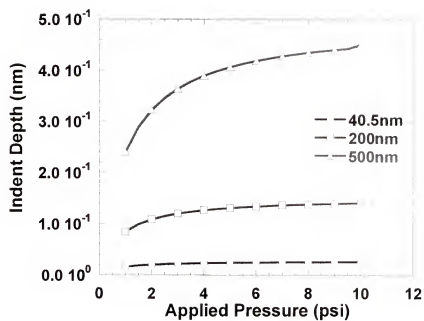


Figure 6-6. The indentation depths with the applied pressure and various particle sizes using equation (6.12)

The applied pressure range is 1 psi to 10 psi, which is in the pressure regime in the CMP process. Interestingly, the indentation depth has a sub-linear dependence with the applied pressure, which was previously expected. This observation is in good agreement with the assumption in the other models [Tse97, Luo01]. The increase of the indent depth became steeper because of the substrate effect. Figure 6-7 presents the load requirement with or without substrate effect. This figure clearly shows that lower load is required to indent the hard layer on the soft substrate than one without the soft substrate effect, especially when the indent depth is greater than the normalized indentation depth of 0.3. This observation also explains the particle size dependence in Figure 6-6. The indentation depth of a larger particle size has strong dependence on the applied pressure because the soft substrate effect is greater in the higher indent depth. Conversely, it can be estimated that higher load is necessary to indent the layer in the case of the soft layer on the hard substrate when the indentation depth is higher than the normalized indentation depth of 0.5. In addition, Figures 6-6 and 6-7 infer that the thickness of layer plays a critical role in the indentation depth. If it is thinner than 1.2 nm, stronger substrate effect will be present in the hardness of the layer, resulting in large dependence on the applied pressure. It should be noted that the penetration of the layer was not concerned in this model because indentation depth is less than the thickness of Cu_2O .

Determination of copper removal rate

As described in equation (6.1), the CMP removal model based on the micro and the nano-scale interactions can be developed to interpret the copper CMP removal mechanism using three valuable contact variables.

At first, the material removal rate by single particle per unit time (MRR_s) can be expressed as follows:

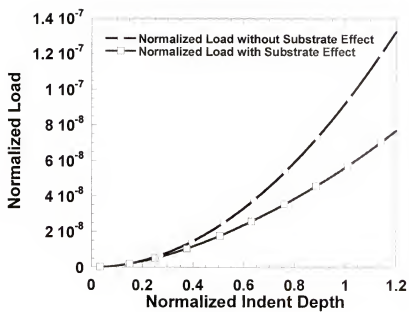


Figure 6-7. The load requirement with or without the soft substrate effect.

$$MRR_i \propto C \cdot \Delta S \cdot V \quad (6.13)$$

where ΔS is the cross-sectional area of indent into the wafer, C is polishing constant that is defined in Ref [Zha02, Rab95] and V is the linear velocity. From Figure 6-1, ΔS with a very small indentation depth can be approximated as a triangle area given by

$$\Delta S \approx \frac{1}{2} \cdot \delta_v \cdot (2 \cdot r_1) = \delta_v \cdot \sqrt{\delta_v \cdot D} \quad (6.14)$$

Substituting equation (6.14) into equation (6.13) yields

$$MRR_i \propto C \cdot \delta_v \cdot \sqrt{\delta_v \cdot D} \cdot V \quad (6.15)$$

Thus, the copper removal rate during CMP can be estimated by substituting equations (6.3) and (6.14) into equation (6.1) as follows:

$$MRR \propto C \cdot \left(\frac{\delta_v}{D} \right)^{\frac{3}{2}} \cdot V_c^{\frac{1}{2}} \cdot \frac{A_s}{A} \cdot V \quad (6.16)$$

where C is the polishing constant that is a fraction of the abraded material that becomes loose wear debris. According to Zhao [Zha03] and Rabinowicz [Rab95], the polishing constant is derived as

$$C = \frac{3}{\pi} \cdot \tan \theta \approx \frac{3}{\pi} \cdot \sqrt{\frac{\delta_v}{D}} \quad (6.17)$$

Equation (6.16) suggested the material removal rate of the chemically modified surface layer. Thus, as mentioned in Chapter 3, the density ratio (ρ_r) of the surface layer and the substrate should be considered in the model. By multiplying ρ_r into the equation (6.16), the material expressed in equation can be converted to the wafer itself. Therefore, the overall material removal rate is given by

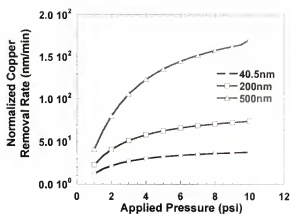
$$MRR = K \cdot \rho_r \cdot \left(\frac{\delta_w}{D} \right)^2 \cdot V_c^{2/3} \cdot \frac{A_c}{A} \cdot V \quad (6.18)$$

where K is the polishing constant. This equation indicates that the removal rate is proportional to velocity and the contact area between the pad and the wafer. It is also proportional to the 2/3 power of the volume concentration of the particle in the slurry. The effects of chemical additives are reflected in the wafer/particle indentation depth and density ratio in terms of the hardness, thickness, and density of the surface layer. The pressure effect also influences the indentation depth and the contact area. It should be noted that the material removal rate is proportional to the square of δ_w/D . Since the indentation depth can be expressed with hardness and thickness of the surface layer, the contact pressure, and particle size in a very complicated equation (6.12), the effect of the indentation depth or the particle size cannot be described individually in the material removal rate.

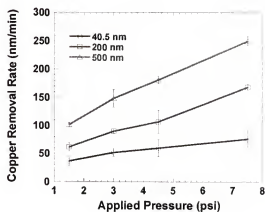
Evaluation of the Model

The copper CMP model based on the micro- and nano-scale interactions developed in this study is used to interpret the copper CMP removal mechanism, which is then compared with experimental data. At first, to justify the model, the pressure effect was

investigated with various particle sizes such as 40.5 nm, 200 nm, and 500 nm. Copper slurry consisted of 5% hydrogen peroxide at pH 7 with 3 wt.% of particle. The values of various parameters in equation (6.18) were specified in the previous chapters: thickness of the surface layer is approximately 1.2 nm in 60 millisecond, the hardness of Cu_2O is around 7.7 GPa, the density of Cu_2O is 5.87 g/cm^3 . With these values, hardness of the surface layer was estimated with the indentation depth using the substrate effect factor, and then the indentation depth was calculated with equation (6.12) along with equation (6.2), which was shown in Figure 6-6. Based on the critical parameters, the copper removal rate was estimated from equation (6.18), which is compared with the experimental results in Figure 6-8. The results of the model (Figure 6-8(a)) show the same trends as the experimental data (Figure 6-8(b)). Interestingly, the model also shows the non-linear behavior of the material removal rate on the pressure dependence that were observed in metal and dielectric CMP [Sta95, Zha99, Ahm01, Qin03, Vie02, Shi98]. Most of them provided one linear line fitting while ignoring the initial removal regime and some used two linear fitting lines for these experimental results. Also, Qin [Qin03] suggested that the non-linear behavior of the removal rate is related to the balance between the indentation depth and the thickness of the surface layer. If the indentation depth is deeper than the thickness, the chemical action can control the overall removal rate, resulting in the lower removal rate. Otherwise, the mechanical action controls the overall removal rate. In this study, as shown in Figure 6-6, the indentation depth of single particle into the wafer is less than the thickness of the surface layer. Thus, the interpretation of the non-linear behavior of removal rate by balance of the indentation depth and the thickness is not appropriate to this study. As mentioned earlier, this model



(a)



(b)

Figure 6-8. Comparison between the removal rates of copper, shown by the model (a) and measured by the CMP experiments.

started from a different viewpoint from other contact models. The contact pressure is a function of the applied pressure. The trend of the removal rate with the applied pressure is very similar to the dependence of the contact pressure on the applied pressure. Based on this analysis, it can be suggested that the non-linear behavior of the material removal rate can be a result from the contact pressure with the applied pressure. It should be pointed out that the slope of the copper removal rate above an applied pressure of 5 psi can be increased due to the substrate effect in the case of the hard layer on the soft substrate. Also, it was observed that the removal rate is proportional to the particle size in copper CMP. However, in tungsten CMP, smaller particle induces the higher removal rate [Bil98]. Unlike $\text{Cu}_2\text{O}/\text{Cu}$ system, tungsten oxide is softer than tungsten itself. Thus, when larger particles are used in tungsten CMP, they may polish the harder layer, resulting in less indentation depth due to the hard substrate effect. The thickness of the tungsten oxide is also very thin because the oxide layer easily passivates the tungsten surface [Bil98]. Therefore, the substrate effect in tungsten CMP can be extremely large. Based on the analysis, it can be suggested that the hard substrate effect results in the higher removal with smaller particle size in tungsten CMP.

Effect of Chemical Interaction on Copper CMP Performance

Figure 6-9 represents the copper removal rate as a function of pH and chemical additives on copper CMP, measured by experiments and calculated by the model together. The polishing pressure was 3 psi and 3 wt.% γ -alumina (40.5 nm) was used in this study. As expected in the previous chapters, the removal rate was decreased with pH. However, the discrepancy in the removal rate was negligible (Figure 6-9(a)). It is because the hardness of the cuprous oxide layer formed at even low pH is too high to be removed by

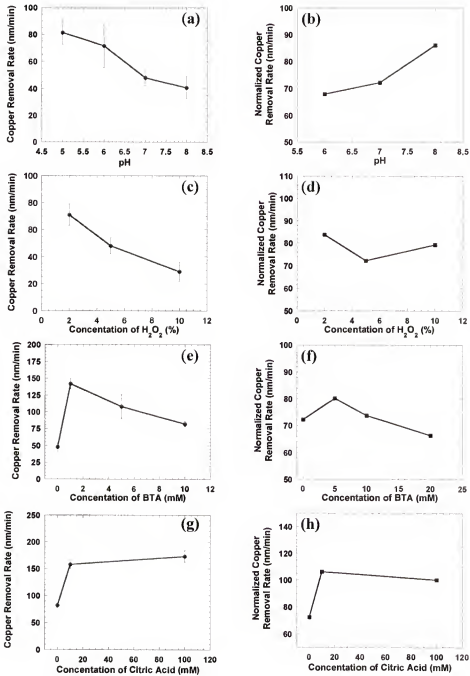


Figure 6-9. Comparison between the experimental removal rate and the theoretical removal rate using the CMP removal model based on the micro- and nano-scale interactions. (a), (c), (e), and (g) present the effect of chemical additives in the copper removal rate and (b), (d), (f), and (h) shows the theoretical values obtained using the model.

nanosized γ -alumina abrasives. However, the removal rate obtained using the model shows the opposite trend (Figure 6-9(b)), resulting from the soft substrate effect. As discussed in Chapter 5, the soft substrate effect became stronger when the surface layer is thinner. Thus, the error from the hardness of the surface layer resulted in higher removal rate at the higher pH. As H_2O_2 concentration was decreased (Figure 6-9(c)); BTA concentration was decreased (Figure 6-9(e)); or citric acid concentration was increased (Figure 6-9(g)), a higher copper removal rates were observed. Decrease in the copper removal rate with BTA can result from Cu_2O -BTA layer formation on the copper surface. As discussed in previous chapters, Cu_2O -BTA layer has higher hardness than Cu_2O layer, and easily passivates the copper surface, resulting in very thin layer (*e.g.*, thickness of 0.45 nm in 60 millisecond when 5 wt.% hydrogen peroxide and 20 mM BTA were added in the solution). When the concentration of BTA increased, the hardness of the layer was increased, resulting in the lower removal rate. It is in good agreement with the result of the model (Figure 6-9(f)). On the other hand, when the high concentration of H_2O_2 was used, the harder and thinner Cu_2O was formed, resulting in the lower removal rate. However, in the result of the model, the removal rate was increased at higher concentration of hydrogen peroxide because the surface layer is too thin to measure the proper property of the surface layer due to the soft substrate effect (Figure 6-9(d)). When citric acid was added in the solution of hydrogen peroxide and BTA, the copper removal rate was increased. It was expected due to the lower hardness and thicker thickness of the surface layer.

From the results, it was known that the chemical additives play important roles in the copper CMP removal rate. Their relations give a basic idea of the slurry design. The

thickness should be thin, which can be achieved by the passivation of the copper surface. Simultaneously, the hardness of the surface layer should be lower to increase the removal rate of copper without compromising the passivity of the copper surface. These results also simulated using our CMP removal model with the physical and mechanical properties of the surface layer estimated in the previous chapters. The results of the model were corresponding to the experimental in the case of less substrate effect observed. Since this model is very sensitive to the hardness of the surface layer, the proper values of the layer hardness are required. Finally, this model can be used as a tool to anticipate the CMP performance for the slurry design along with the experimental observations of the micro- and nano interactions.

Summary

A comprehensive CMP removal model based on the micro- and nano-scale interactions has been developed to interpret the material removal mechanism in CMP process. This model is based on the contact mechanics, abrasive wear, and chemical interactions with copper surface. Thus, it represents as an extension of earlier models that were reported by Zhao and Chang [Zha02] and Qin [Qin03]. Moreover, the analysis of the chemical interactions such as the kinetics of the layer formation, thickness of the surface layer, and the physical and mechanical properties of the surface layer measured in the previous chapters are necessary to eliminate several assumptions from this model. In addition, this model takes into account the pressure dependence on the contact pressure between the pad and the wafer and the soft substrate effect on the hardness of the surface layer. Based on all the measured important variables, even though the equation of the material removal rate is very similar to a model presented by Zhao and Chang, its result showed quite different trends of the material removal rate. With this model, the non-

linear behavior of the material removal rate can also be interpreted without using two different fitting lines. It was found in all the results that the pressure dependence on the contact pressure between the pad and the wafer induces the non-linear behavior of the material removal rate. The effect of the particle size on the material removal rate can be varied by the substrate effect and the thickness of the surface layer.

The comparison between the experimental data and the analysis of the model in the effect of the chemical additives on the CMP performance reveals some insights into the principle of the slurry design. The removal rate is very sensitive to chemical additives used in the slurry that control the thickness and hardness of the surface layer as well as the dissolution of the surface layer or bare metal. Therefore, the optimal CMP performance can be achieved by controlling the balance of the passivation of the copper surface, controlled by the corrosion inhibitor, and the hardness of the surface layer, governed by the complexing agent.

CHAPTER 7

CONCLUSION

The following conclusions are drawn from this research.

1. By performing a systematic investigation of the potentiodynamic measurements and x-ray photoelectron spectroscopy, the basic roles of the chemical additives were verified. Hydrogen peroxide oxidizes the copper surface, resulting in the formation of cuprous oxide layer. Then, cupric oxide is precipitated on the surface of the cuprous oxide resulting in the poor passivation. Hence a corrosion inhibitor is required for the copper CMP. As BTA was added in the solution, the dissolution rate decreased due to the adsorption of BTA on the cuprous oxide surface. Moreover, the adsorption of BTA prevented the precipitation of cupric oxide on the cuprous oxide. However, when citric acid was added into hydrogen peroxide and BTA based solution, the dissolution rate became a function of the citric acid concentration in the solution. The surface layer was also different from the one that was formed without the use of citric acid. The results of XPS show that thick cuprous oxide layer and cupric oxide layer existed on the surface. Higher dissolution rate may enhance the kinetics of the precipitation of cupric oxide on the surface.

2. The kinetics and thickness of the chemically modified surface layer was investigated using *in situ* electrochemistry. The concentration of chemical additives has a great impact on the kinetics and thickness of the layer. Hydrogen peroxide induces a relatively fast passivation rate with the concentration. It indicates the lower copper removal rate with an increase in the concentration of hydrogen peroxide. When BTA was

added into hydrogen peroxide based solution, the passivation kinetics due to the formation of the layer was not changed at low concentration, whereas it exponentially increased and then saturated with an increase in the concentration of BTA. However, the passivation kinetics even with very low concentration of BTA showed a significantly different behavior in the long time regime. The trend is similar to the observation in the potentiodynamic measurements. Since removal mechanisms in a CMP process occur in less than one second, we can deduce that the copper surface could be passivated with at least 10 mM BTA during CMP. As citric acid was introduced in the solution, the reaction kinetics was enhanced due to the higher dissolution rate. In addition, the results of XRR and VASE indicate that the density and porosity of the chemically modified surface layer are related to the dissolution rate of copper and the type of the layer. For example, as citric acid reacts with copper/copper oxide and forms a copper complex, porosity in the layer was increased. From all the results, the role of the chemical additives was re-defined to be suitable in the short time regime.

3. The nanoindentation technique was applied to characterize the mechanical properties – hardness and Young's modulus – of the chemically modified surface layer. The results show that two different substrate effects were presented as a function of the maximum load, indicating that the relatively soft cupric oxide on the top of the cuprous oxide was formed on the copper surface in hydrogen peroxide based solution. Interestingly, the adsorption of BTA on the cuprous oxide layer enhances the mechanical properties. As the particle penetration depth is inversely proportional to the Young's modulus, the lower removal rate with an increase in the concentration of BTA was expected during CMP. Moreover, addition of citric acid reduces both hardness and

Young's modulus. Thus, we can conclude that an optimal balance between the complexing agent and the corrosion inhibitor plays a critical role in slurry design for better CMP performance.

4. A comprehensive CMP removal model based on the micro- and nano-scale interactions has been developed to explain our CMP results. The model is based on (i) the analysis of the chemical interactions (such as the kinetics of the layer formation, thickness of the surface layer, and the physical and mechanical properties of the surface layer) to eliminate several assumptions, (ii) the applied pressure dependence on the contact pressure between the pad and the wafer, and (iii) the soft substrate effect on the hardness of the surface layer. Using this model it was found that the applied pressure dependence on the contact pressure between the pad and the wafer induces a non-linear behavior of increasing material removal rate as a function of applied pressure. It represents an extension of earlier models that were reported by Zhao and Chang [Zha02] and Qin [Qin03]. This model can also explain the effect of the particle size on the material removal rate, which can be varied by the substrate effect and the thickness of the surface layer. The effect of the chemical additives on the CMP performance was determined by the comparison between the experimental data and the analysis of the model, which can provide an insight into the principle of the slurry design.

Thus, we can conclude that the transient behavior of copper in less than one second is the most important parameter to provide us an insight into copper CMP removal mechanism and the principle of the slurry design. Therefore, the above-mentioned conclusions give us a possible solution for the optimal slurry design along with a better understanding of CMP removal mechanism.

LIST OF REFERENCES

- Ahm01 Ahmadi G., and Xia X. (2001). *J. Electrochem. Soc.*, **148**, G99
- Alt72 Altura, D., and Nobe, K. (1972). *Corrosion*, **28**, 345
- Bas02 Basim, G. B. (2002). Ph. D. Dissertation, University of Florida
- Bey99 Beyer, K. D. (1999). *IBM Micronews*, **5**, 40
- Bie00 Biemann, M., Mahajan, U., Singh, R. K., Agarwal, P., Mischler, S., Rosset, E., and Landolt, D. (2000). *Materials Research Society Symposium – Proceedings*, **566**, 97
- Bie98 Biemann, M. (1998). Master Thesis, University of Florida
- Bie99 Biemann, M., Mahajan, U., and Singh, R.K. (1999). *Electrochem. Solid-State Lett.* **2**, 401
- Bla69 Black, J. R. (1969). *IEEE Trans. Electron Devices*, **ED-16**, 338
- Bro81 Brown, N.J., Baker, P.C., and Maney, R.T. (1981). *Proc. SPIE*, **306**, 42
- Bru92 Brundle, C. R., Evans, C. A., Jr., and Wilson, S. (1992). “*Encyclopedia of Materials Characterization: Surfaces, Interfaces, Thin Films*”, Butterworth-Heinemann, Boston
- Bur91 Burke, P.A. (1991). *VMIC Conference*, **1112**, 379
- Car01 Cardien, K. C., and Feller, D. A. (2001). U.S. Patent 6,178,585 B1
- Car90 Carr, J. W. (1990). U.S. Patent 4,954,142
- Car95 Carpio, R., Farkas, J., and Jairath, R. (1995). *Thin Solid Films*, **266**, 238
- Che01 Chen, X., and Vlassak, J.J. (2001). *J. Mater. Res.*, **16**, 2974
- Chi99 Chiang, S.-K., and Lassen, C. L. (1999). *Solid State Technol.*, **42**, 42
- Cun00 Cunningham, J. A. (2000). *Semiconductor International*, **23**, 95
- Dan81 Dang, R. L. M., and Shigyo, N. (1981). *IEEE Electron Devices Lett.*, **EDL-2**, 196

- DeB00 DeBear, D. S., Levert, J. A., and Mukherjee, S. P. (2000). *Solid State Technology*, **43**, 53
- Den74 Dennard, D.H., Gaensslen, F. H., Yu, H., Rideout, V. L., Bassous, E., and LeBlank, A. R. (1974). *IEEE J. Solid-State Circuits*, **SC-9**, 256
- Der92 Deroubaix, G., and Marcus, P. (1992). *Surf. Interface. Anal.*, **18**, 39
- Elb98 Elbel, N., Neureither, B., Ebersberger, B., and Lahnor, P. J. (1998). *J. Electrochem. Soc.* **145**, 1659
- Fis96 Fisher, A. C. (1996). “*Electrode Dynamics*”, Oxford University Press
- Fra98 Frankovic, R. and Bernstein, G. H. (1998). *IEEE Transactions on Electron Devices*, **43**, 2233
- Fu01 Fu, G., Chandra, A., Guha, S., and Subhash, G. (2001). *IEEE Trans. Semiconduct. Manuf.*, **14**, 406
- Fuj02 Fujisawa, N., Awain, M.V., James, N.L., Tarrant, R.N., Woodard, J.C., and McKenzie, D.R. (2002). *J. Mater. Res.*, **17**, 861
- Fur99 Fury, M., Levert, J., Mukherjee, S., and DeBear, D. (1999). *Electrochem. Soc. Proceeding*, Hawaii
- Gre66 Greenwood, J., and Williams, J. (1966). *Proc. R. Soc. Lon. Ser.-A*, **295**, 300
- Gru00 Grumbine, S. K., Streinz, C. C., and Mueller, B. L. (2000). U.S. Patent 6,068,787
- Han02 Hanazono, M., Amanokura, J., and Kamigata, Y. (2002). *Material Research Society Bulletin*, **27**, 772
- Her01 Hernandez, J., Wrschka, P., and Oehrlein, G. S. (2001). *J. Electrochem. Soc.*, **148**, G389
- ITR02 International Technology Roadmap for Semiconductors
<http://public.itrs.net/Files/2002Update/Home.pdf> (2002)
- Jac98 Jacson, R., Broadbent, E., Cacouris, T., Harrus, A., Biberger, M., Patton, E., and Walsh, T. (1998). *Solid State Technology*, **41**, 49
- Joh85 Johnson, K.L. (1985). “*Contact Mechanics*”, Cambridge University Press, New York
- Joh99 Johs, B., Woollam, J. A., Herzinger, C. M., Hilfiker, J. N., Synowicki, R., and Bungay, C. (1999). *SPIE Proceedings*, **CR72**, 59
- Kau00-a Kaufman, V. B., and Wang, S. (2000). U.S. Patent 6,039,891

- Kau00-b Kaufman, V. B., Kistler, R. C., and Wang, S. (2000). U.S. Patent 6,126,853
- Kau00-c Kaufman, V. B., Kistler, R. C., and Wang, S. (2000). U.S. Patent 6,063,306
- Kau91 Kaufmann, F.B., Thompson, D. B., Broadie, R. E., Jaso, M. A., Githrie, W. L., Pearson, D. J., and Small, M. B. (1991). *J. Electrochem. Soc.*, **138**, 3460
- Kim74 Kim, K. S. (1974). *J. Electron Spectrosc. and Related Phenomena*, **3**, 217
- Kne96 Kneer, E.A., Raghunath, C., Jeon, J.S., and Raghavan, S. (1996). *J. Electrochem. Soc.*, **143**, 4095
- Kne97 Kneer, E.A., Raghunath, C., Mathew, V., Raghavan, S., and Jeon, J.S. (1997). *J. Electrochem. Soc.*, **144**, 3041
- Kon00-a Kondo, S., Sakuma, N., Homma, Y., Goto, Y., Ohashi, N., Yamaguchi, H., and Owada, N. (2000). *J. Electrochem. Soc.*, **147**, 3907
- Kon00-b Kondo, S., Homma, Y., Sakuma, N., Takeda, K., and Hinode, K. (2000). U.S. Patent 6,117,775
- Kuo00 Kuo, H., and Tsai, W. (2000). *J. Electrochem. Soc.*, **147**, 149
- Kuo00 Kuo, H., and Tsai, W. (2000). *J. Electrochem. Soc.*, **147**, 2136
- Lan92 Landis, H., Burke, P., Cote, W., Hill, W., Hoffman, C., Kaanta, C., Koburger, C., Lange, W., Leach, M., and Luce, S. (1992). *Thin Solid Films*, **220**, 1
- Lar99 Larsen-Basse, J., and Liang, H. (1999). *Wear*, **233–235**, 647
- Lee00 Lee, S.-M., Mahajan, U., Chen, Z., and Singh, R. K. (2000). *Proceeding of Material Research Society spring meeting, Material Research Society*, San Francisco, **613**, E7.8.1
- Lee02 Lee, S.-M., Choi, W., Craciun, V., Jung, S.-H., and Singh, R.K. (2002). in *Chemical-Mechanical Planarization*, edited by S.V. Babu, R.K. Singh, M.R. Oliver, and N. Hayasaka (Mater. Res. Soc. Symp. Proc., Warrendale, PA)
- Lee99 Lee, S.-M., Chen, Z., Mahajan, U., and Singh, R. K. (1999). *ECS Meeting Abstracts*, **MA 99-2**, 1256
- Lia02 Liang, H., and Xu, G. H. (2002). *Scripta Materialia*, **46**, 343
- Lid98 Lide, D. R. (1998). “*Handbook of Chemistry and Physics*”, 78th ed., CRC, NY
- Liu95 Liu, C.-W., Dia, B.-T., and Yeh, C.-F. (1995). *J. Electrochem. Soc.*, **142**, 3098
- Liu96 Liu, C.-W., Dai, B., Tseng, W., and Yeh, C. (1996). *J. Electrochem. Soc.*, **143**, 716

- Liu99 Liu, R., Pai, C.-S., and Martinez, E. (1999). *Solid-State Electronics*, **43**, 1003
- Luo01 Luo, J., and Dornfeld, D.A. (2001). *IEEE Trans. Semiconduct. Manuf.*, **14**, 112
- Luo03 Luo, J., and Dornfeld, D.A. (2003). *IEEE Trans. Semiconduct. Manuf.*, **16**, 45
- Luo98 Luo, Q., Ramarajan, S., and Babu, S.V. (1998). *Thin Solid Films*, **335**, 160
- Mah98 Mahajan, S., and Sree Harsha, K. S. (1998). “*Principles of Growth and Processing of Semiconductors*”, WCB/McGraw-Hill, Boston
- Mah99 Mahajan, U., Biemann, M., and Singh, R. K. (1999). *Electrochem. Solid-State Lett.*, **2**, 80
- Mai01 Maier, G. (2001). *Prog. Polym. Sci.*, **26**, 3
- Mil69 Miller, B. (1969). *J. Electrochem. Soc.*, **116**, 1675
- Mil95 Millet, B., Fiaud, C., Hinnen, C., and Sutter, E. M. M. (1995). *Corr. Sci.*, **37**, 1903
- Moo65 Moore, G. E. (1965). *Electronics*, **38**, April
- Moo99 Moon, Y. (1999). Ph. D. Dissertation, University of California at Berkeley
- Mou95 Moulder, J. F., Stickle, W. F., Sobol, P. E., and Bomben, K. D. (1995). “*Handbook of X-ray Photoelectron Spectroscopy*”, Physical Electronics, MN
- Mue99 Mueller, B. L., Streinz, C. C., and Grumbine, S. K. (1999). U.S. Patent 5,958,288
- Mur00 Murarka, S. P., Verner, I. V., and Gutmann, R. J. (2000). “*Copper-fundamental mechanisms for microelectronic applications*”, John Wiley, New York
- Mur93 Murarka, S. P. (1993). “*Metallization: theory and practice for VLSI and ULSI*”, Butterworth-Heinemann, Boston, 100
- Mur96 Murarka, S. P. (1996). *Solid State Technol.*, **3**, 83
- Noy76 Noyota, T. and Poling, G. (1976). *Corrosion*, **32**, 216
- Ogl75 Ogle, I. and Poling, G. (1975). *Can. Metall. Q.*, **14**, 37
- Ole93 Olsen, J., and Moghadam, F. (1993). “*Planarization Techniques, in Multilevel Metallization for Integrated Circuits*”, eds. Wilson S.R., Tracy C.J., and Freeman J.L., Noyes Publications, Park Ridge, NJ
- Oli92 Oliver, W.C., and Pharr, G.M. (1992). *J. Mater. Res.*, **7**, 1564
- Pan01 Pang, M., and Bahr, D. F. (2001). *J. Mater. Res.*, **16**, 2634

- Pet81 Peterson, W. M., and Wong, R. V. (1981). "EG&G Princeton Applied Research", American Laboratory
- Pet98 Peters, L. (1998). *Semiconductor International*, **21**, 15
- Pha92 Pharr, G.M., Oliver, W.C., and Brotzen, F.R. (1992). *J. Mater. Res.*, **7**, 613
- Pou74 Pourbaix, M. (1974). "Atlas of Electrochemical Equilibria in Aqueous Solution", NACE, Houston, TX
- Pre27 Preston, F. (1927). *J. Soc. Glass Technol.*, **112**, 14
- Qin03 Qin, K. (2003). Ph. D. Dissertation, University of Florida
- Run94 Runnels, S.R., and Eyman, L.M. (1994). *J. Electrochem. Soc.*, **141**, 1698
- Rus02 Russell, C. H. (2002). *Mat. Res. Symp. Proc.*, **716**, B1.3.1
- Rut95 Rutten, M., Feeney, P., Cheek, R., and Landers, W., *Semiconductor Int.*, **August**, 123 (1995)
- Rya95 Ryan, J. G., Geffken, R. M., Poulin, N. R., and Paraszczyk, J. R. (1995). *IBM J. Res. Dev.*, **39**, 371
- Sat01 Sato, S., Yasuda, Z., Ishihara, M., Komai, N., Ohtorii, H., Yoshio, A., Segawa, Y., Horikoshi, H., Ohoka, Y., Tai, K., Takahashi, S., and Nogami, T.. *IEEE International Electron Devices Meeting*, 84
- Saw99 Sawa, T., Akiyama, Y., Shimamoto, A., and Tanaka, K. (1999). *J. Mater. Res.*, **14**, 2228
- Shi98 Shi, F.G., and Zhao, B. (1998). *Appl. Phys. A*, **67**, 249
- Sho90 Shon-Roy, L. (2000). *Solid State Technol.*, **43**, 67
- Sin02 Singh, R. K., Lee, S.-M., Choi, K.-S., Basim, D. B., Choi, W., Chen, Z., and Moudgil, B. M. (2002). *Material Research Society Bulletin*, **27**, 752
- Sin03 Singh, R. K., and Lee, S.-M. (2003). *Proceeding of CMP-MIC 2003*, 128
- Sin98 Singer, P. (1998). *Semiconductor International*, **June**, 90
- Spe85 Speckmann, H.-D., Lohrengel, M. M., Schlitz, J. W., and Strehblow, H.-H. (1985). *Ber. Bunsenges. Phys. Chem.*, **89**, 392
- Sta95 Stavreva, Z., Zeidler, D., Plotner M., and Drescher K. (1995). *App. Surf. Sci.*, **91**, 192

- Ste95 Steigerwald, J. M., Murarka, S. P., Ho, J., Gutmann, R. J., and Duquette, D. J. (1995). *J. Vac. Sci. Tech. B*, **13**, 2215
- Ste97 Steigerwald, J. M., Murarka, S. P., and Gutmann, R. J. (1997). “*Chemical Mechanical Planarization of Microelectronic Materials*”, John Wiley & Sons, New York
- Ste98 Stein, D.J., Hetherington, D.L., Guilinger, T., and Cecchi, J.L. (1998). *J. Electrochem. Soc.*, **145**, 3190
- Ste99-a Stein, D.J., Cecchi, J.L., and Hetherington, D.L. (1999). *J. Mat. Res.*, **14**, 3695
- Ste99-b Stein, D.J., Hetherington, D.L., and Cecchi, J.L. (1999). *J. Electrochem. Soc.*, **146**, 1934
- Ste99-c Stein, D.J., Hetherington, D.L., and Cecchi, J.L. (1999). *J. Electrochem. Soc.*, **146**, 376
- Sun99 Sundararajan, S., Thakurta, D.G., Schwendeman, D.W., Murarka, S.P., and Gill, W.N. (1999). *J. Electrochem. Soc.*, **146**, 761
- Tam02 Tamilmani, S., Huang, W., Raghavan, S., and Small, R. (2002). *J. Electrochem. Soc.*, **149**, G638
- Tic99 Tichy, J., Levert, J.A., Shan, L., and Danyluk, S. (1999). *J. Electrochem. Soc.*, **146**, 1523
- Tse96 Tseng, W.-T., Liu, C.-W., Dia, B.-T., and Yeh, C.-F. (1996). *Thin Solid Films*, **290-291**, 458
- Tse97 Tseng, W.-T. and Wang, Y.-L. (1997). *J. Electrochem. Soc.*, **144**, L15
- Tse99 Tseng, W.-T., Chin, J.-H., and Kang, L.-C. (1999). *J. Electrochem. Soc.*, **146**, 1952
- Tsu99-a Tsui, T. Y., Vlassak, J., and Nix, W. D. (1999). *J. Mater. Res.*, **14**, 2196
- Tsu99-b Tsui, T. Y., Vlassak, J., and Nix, W. D. (1999). *J. Mater. Res.*, **14**, 2204
- Uhl85 Uhlig, H.H., and Revie, R.W. (1985). “*Corrosion and Corrosion Control*”, John Wiley & Sons, NY
- Vai80 Vaidya, S., Sheng, T. T., and Sinha, A. K. (1980). *Appl. Phys. Lett.*, **36**, 464
- Vie01 Viet, N. H. (2001). Ph.D. Dissertation, Universiteit Twente, Netherlands
- Wag81 Wagner, C. D., Davis, L. E., Zeller, M. V., Taylor, J. A., Raymond, R. H., and Gale, L. H. (1981). *Surf. Interface Anal.*, **3**, 211
- War91 Warnock, J. (1991). *J. Electrochem. Soc.*, **138**, 2398

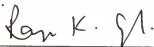
- Wat99 Watts, D., Bajaj, R., Das, S., Farkas, J., Dang, C., Freeman, M., Saravia, J. A., Gomez, J., and Cook, L. B. (1999). U.S. Patent 5,897,375
- Wes85 Weste, N., and Eshraghian, K. (1985), "*Principals of CMOS Design*", Addison-Wesley Pub. Co., MA
- Wil93 Wilson, S. R., Tracy, C. J., and Freeman, J. L. Jr. (1993). "*Handbook of Multilevel Metallization for Integrated Circuits*", Noyes Publications, New Jersey
- Wol03 Wolf, B. and Richter, A. (2003). *New J. Phys.*, **5**, 15
- Woo99 Woollam, J. A., Johs, B., Herzinger, C. M., Hilfiker, J. N., Synowicki, R., and Bungay, C. (1999), *SPIE Proceedings*, **CR72**, 29
- Yu93 Yu, Y., Yu, C.C., and Orlowski, M. (1993). *IEEE IEDM*, 865
- Yu94 Yu, Y., Yu, C.C., and Orlowski, M. (1994). *IEEE NUPADV*, **499**, 29
- Zha00 Zhao, Y., Maietta, D.M., and Chang, L. (2000). *J. of Tribology*, **122**, 86
- Zha02 Zhao, Y., and Chang, L. (2002). *Wear*, **252**, 220
- Zha03 Zhao, Y., Chang, L., and Kim, S. H. (2003). *Wear*, **254**, 332
- Zha99 Zhao, B., and Shi, F.G. (1999). *Electrochem. and Solid-State Lett.*, **2**, 145

BIOGRAPHICAL SKETCH

Seung-Mahn Lee was born on December 11, 1969, in Seoul, Korea. He attended Korean University, Seoul, Korea, and earned a Bachelor of Science degree in metallurgical engineering on February 1992. In the Fall of 1992, he enrolled the graduate program in the same department at Korean University and received his Master of Science degree in August 1994.

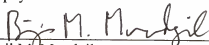
He came to the United States to improve his English and study the electronic materials in English Language Institute at the University of Florida in the summer 1996. In the Fall 1997, he enrolled in the Ph. D. program in the Department of Materials Science and Engineering at the University of Florida. In January 1998, he joined Dr. Singh's research group. His current research focuses on study of mechanisms of chemical-mechanical planarization including *in situ* electrochemistry, kinetics of surface layer formation during chemical mechanical planarization of metal films. His work has led to development of novel slurries for polishing of copper and refractory layers. He is the author of 10 papers and has filed 2 US patents during his graduate research.

I certify that I have read this study and that in my opinion it conforms to acceptable standards of scholarly presentation and is fully adequate, in scope and quality, as a dissertation for the degree of Doctor of Philosophy.



Rajiv K. Singh, Chairman
Professor of Materials Science and
Engineering

I certify that I have read this study and that in my opinion it conforms to acceptable standards of scholarly presentation and is fully adequate, in scope and quality, as a dissertation for the degree of Doctor of Philosophy.



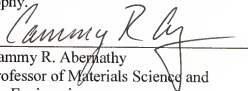
Brij M. Moudgil
Professor of Materials Science and
Engineering

I certify that I have read this study and that in my opinion it conforms to acceptable standards of scholarly presentation and is fully adequate, in scope and quality, as a dissertation for the degree of Doctor of Philosophy.



Stephen J. Pearton
Professor of Materials Science and
Engineering

I certify that I have read this study and that in my opinion it conforms to acceptable standards of scholarly presentation and is fully adequate, in scope and quality, as a dissertation for the degree of Doctor of Philosophy.



Cammy R. Abernathy
Professor of Materials Science and
Engineering

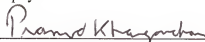
I certify that I have read this study and that in my opinion it conforms to acceptable standards of scholarly presentation and is fully adequate, in scope and quality, as a dissertation for the degree of Doctor of Philosophy.



Dinesh O. Shah
Professor of Chemical Engineering

This dissertation was submitted to the Graduate Faculty of the College of Engineering and to the Graduate School and was accepted as partial fulfillment of the requirements for the degree of Doctor of Philosophy.

August' 2003



Pramod P. Khargonekar
Dean, College of Engineering

Winfred M. Phillips
Dean, Graduate School